Copyright

by

Gauri Vibhakar Karve

2005

The Dissertation Committee for Gauri Vibhakar Karve Certifies that this is the approved version of the following dissertation:

Avalanche Photodiodes As Single Photon Detectors

Committee:

Joe C. Campbell, Supervisor

Archie Holmes, Jr.

Sanjay Banerjee

Ananth Dodabalapur

Donald Bethune

Avalanche Photodiodes As Single Photon Detectors

by

Gauri Vibhakar Karve, B.S., M.S.

Dissertation

Presented to the Faculty of the Graduate School of

The University of Texas at Austin

in Partial Fulfillment

of the Requirements

for the Degree of

Doctor of Philosophy

The University of Texas at Austin

May 2005

Dedicated

To

my parents

Acknowledgements

My supervisor, Dr. Joe Campbell, has been the most important person in guiding this research work. I appreciate his trust in me when this research started off as a new project in the group. I could not have succeeded in this project without his keen insight. He has taught me to be an independent and confident researcher by giving me the freedom to explore. He has always been very encouraging to new ideas. I have learned not only the science and engineering of detectors under his guidance, but also the importance of conducting ethical and meaningful research. I want to thank him from the bottom of my heart for giving me this opportunity to work with him.

I want to thank Dr. Archie Holmes for his constant support throughout my PhD. His optimism towards life is unparalleled. His warm smile and friendliness have always been assuring. I would also like to thank to Dr. Banerjee, Dr. Dodabalapur and Dr. Bethune for serving on my dissertation committee. Dr. Banerjee kindly allowed me to use the wire bonder in his group. Thanks to Dr. Dodabalapur for allowing me to use the low temperature probe station.

My special thanks go to my fellow group members Feng Ma, Shuling Wang, Xiaowei Li, Xiaoguang Zheng, Ning Li, Ariane Beck, Ning Duan, Xiangyi Guo, Minguo Liu, Zhihong Huang, Ning Tan, Xiaofeng Zhang, Jean Hsu, Zhang Lijuan, Ning Kong, Drs. Geoff Kinsey, Chuck Collins, Jungwoo Oh, Zhengmao Ye, Stephane Demigual, Hao Chen and Sebastian Csutak for their friendliness. I am very proud to be a part of such an

Most importantly, I want to acknowledge my family for being there for me. I want to thank my mother and father for believing in me. My sister, my brother, my brother-in-law and my nephew have always been very supportive through all these years. One person without whose support and encouragement my Ph.D. would not have been realized is my husband, Srikanth. His warm and charming friendship made it easier for me to go through the graduate school. I have found a true and a lifelong friend in him. You are all the "wind beneath my wings".

I have realized that every one of us has a wealth of knowledge. It is not the Ph.D. or any other degree that makes a person knowledgeable. It is the perception of life and willingness to learn and grow that defines a truly knowledgeable person. I want to thank everyone I have interacted with for making my learning experience enjoyable.

Avalanche Photodiodes As Single Photon Detectors

Publication No._____

Gauri Vibhakar Karve, Ph.D.

The University of Texas at Austin, 2005

Supervisor: Joe C. Campbell

Photodiodes capable of detecting very weak intensities of light, down to single photon levels, have been investigated for a long time. Single photon detectors have numerous applications, including quantum cryptography, three-dimensional imaging, atmospheric monitoring, and time resolved spectroscopy. Conventionally, photo-multiplier tubes have been the detectors of choice for low intensity light applications. However, due to their limitations such as high operating voltages, bulkiness, and limited sensitivity in the infrared, alternative solutions are sought. Avalanche photodiodes (APDs) operated above their breakdown voltage, can achieve single photon sensitivity. APDs were fabricated for single photon detection at wavelengths ranging from ultraviolet to infrared. Linear mode characterization experiments such as contact resistance and current-voltage were performed to determine the viability of a detector as a photon counter. Single photon detectors are often operated at low temperatures to minimize the dark noise. The temperature dependence of forward and reverse characteristics of the APDs was studied. A cryogenic system was established and calibrated for characterization of photodetectors at very low levels of illumination. The effect of

various experimental parameters such as temperature, excess voltage, and discriminator threshold on Geiger mode APD performance was studied. Single photon detection at 1.54 µm was demonstrated using a separate-absorption-charge-multiplication avalanche photodetector with an $In_{0.52}Al_{0.48}As$ multiplication layer. Various dark count generation mechanisms were modeled to understand the temperature dependence of dark counts in the $In_{0.53}Ga_{0.47}As/In_{0.52}Al_{0.48}As$ APDs. The experimental observations were explained using band-to-band tunneling in the multiplication layer as the dominant dark count mechanism. Based on the modeling and experimental results, design guidelines for single photon counting avalanche diodes are suggested. An APD structure with thicker $In_{0.52}Al_{0.48}As$ multiplication layer and punchthrough voltage close to the breakdown voltage was designed. In addition, SiC and GaAs based APDs were evaluated as photon detectors in the ultraviolet and near infrared regions, respectively. Single photon counting at 325nm was achieved using 4H-SiC APDs. Although MBE grown GaAs/AlGaAs APDs with high quantum efficiencies and low dark currents showed promise for single photon counting at 830nm, further experiments are needed to understand their inability to function as single photon detectors.

Table of Contents

List of Figures

xvii

Chapter 1   Avalanche Photodiodes for Single Photon Counting

Single photon counting is a powerful measurement technique for detection of weak intensities of light. Single photon detectors find applications in many areas like astronomy, biochemistry and telecommunications. Section 1.1 of this chapter discusses the applications and current state of available photomultiplier tube (PMT) and avalanche photodiode (APD) based single photon counters. A photodiode or a PMT detects light levels by converting them into current or voltage. This is the analog mode of detection. When the intensity of light becomes very low, the incident photons arrive as separate bursts of energy. At such low levels if the average separation between incoming photons is longer than the time resolution of the detector, response is generated for individual photons. For very low light levels, such digital detection of photons is better than analog signal measurement for high detection efficiency, low noise, and better stability. The principle of operation of APD as single photon counter is explained in section 1.2. Section 1.3 describes the motivation for the research presented in this thesis. Organization of the thesis is presented in section 1.4.

1.1   SINGLE PHOTON COUNTING DETECTORS

Photon counters are widely used in ultra-sensitive detection and spectroscopy involving single molecule detection [1-1]. In astronomy, use of single photon counters enables detection of weak incoming optical radiation [1-2]. In biochemistry, weak fluorescent studies and investigation of DNA reactions are possible with the use of single photon counters [1-3]. Recently, photon counting infrared detectors have received increased attention due to the emergence of applications such as quantum cryptography, optical network testing, three-dimensional imaging, study of recombination kinetics in

1

Indium based semiconductors, optical time domain reflectometry (OTDR), etc [1-4, 1-5, 1-6, 1-7]. 1.3 μm and 1.55 μm wavelengths are of special interest due to the low loss and small dispersion of optical fibers at these wavelengths. 1.55 μm is the eye-safe wavelength and thus attractive in applications such as atmospheric monitoring, eye-safe range finding, etc [1-8]. This wavelength is also favorable for quantum key distribution because optical fibers exhibit minimum loss at 1.55 μm (0.2dB/km). Novel applications such as non-destructive IC debugging and failure analysis tools have also been developed using single photon counters [1-9].

Conventionally, photo-multiplier tubes (PMTs) have been the detectors of choice for low light-level applications. They have been available commercially since 1960. PMT operation is based on the photoelectric effect [1-10]. A PMT typically consists of a photocathode, focusing electrodes, an electron multiplier, and an anode. A photon absorbed by the photocathode is converted into an electron. It passes through a series of dynodes under the action of electric and magnetic fields and gets multiplied by secondary emission. The current is then collected by the anode. PMTs have very low dark current, especially with cooled cathodes, where spurious electron emission at the photo cathode is minimized. PMTs exhibit very high gain and have large detection area. Currently PMTs operating from ultraviolet (UV), to infrared (IR) spectral range are available commercially [1-11]. However, PMTs are bulky and they need high operating voltages (~100s of volts). They are sensitive to magnetic fields by design. Their sensitivity in the IR region is limited by availability of suitable photocathode materials that have required photon-to-electron conversion efficiency and low spurious electron emission rates. IR sensitive PMTs are available from Hamamatsu Company. They use a cooled InGaAs photo cathode (R3809U-69), which exhibits 1% detection efficiency at 1500nm.

APDs are extensively used in long haul telecommunications systems. The internal gain of APDs makes them preferable over p-i-n detectors (PINs). Avalanche photodiodes (APDs) can achieve single photon detection sensitivity due to their internal gain. APDs used as single photon detectors are referred to as single photon avalanche diodes (SPADs) [1-12]. SPADs have several advantages over PMTs. They are compact, have lower operating voltages and also cost less. They are good candidates for fabricating arrays of single photon counting APDs, thus enabling applications such as 3-D LIDAR imaging, spatially resolved detection of fluorescence decay, etc [1-15], [1-16]. Most importantly, their IR detection efficiencies are far superior to PMTs, which makes them very attractive at wavelengths of interest for optical communications. Single photon detection with APDs can be achieved by two ways. The APD can be operated close to, but not exceeding the breakdown voltage with a trans-impedance amplifier to boost the output signal level. Alternately, the APD can be operated above breakdown voltage in the bi-stable mode. This mode of operation is referred to as the Geiger mode [1-13], [1-14].

Silicon (Si) APDs operated in Geiger mode achieve very high detection efficiencies and low dark count rates in the visible range [1-17], [1-18]. A lot of research has been done in the past fifteen years in optimizing their structure and the operation of Geiger mode electronics. Single photon counting modules using Si APDs have been commercialized by Perkin Elmer and more recently by Optoelectronic Components [1-19], [1-20]. State of the art Si photon counters exhibit detection efficiencies > 45% (at 532nm) with dark count rates <300 counts per second at room temperature [1-20]. Use of standard CMOS processing for Si APDs has opened up the possibility of integrating

detection electronics with the detectors [1-21]. Arrays of single photon counting Si APDs have also been demonstrated by several groups [1-22], [1-23], [1-24].

The band gap of Si is 1.12 eV, which limits its operating wavelength to < 1.1 μm. Hence different solutions are sought for applications extending to wavelengths in the IR range. Germanium APDs can be operated as single photon detectors at longer wavelengths. Ge SPADs have exhibited detection efficiencies as high as 15% at 1.3 μm [1-25], [1-26]. However, Ge detectors are plagued with high dark count rates. Hence they have to be cooled to ~77 K to reduce the dark counts to an acceptable level. At low temperatures their responsivity is blue shifted to $\lambda \leq 1.45$ μm. Longer wavelength operation can be achieved, but at reduced detection efficiency. For example, a liquid nitrogen cooled Ge APD operating in active gated mode has been shown to exhibit photon counting efficiency of 1% at 1.54 μm [1-27]. Higher detection efficiencies at 1.55 μm can be achieved using InGaAs or InGaAsP as the absorbing material.

Photon counting using an InGaAs absorber APD was first demonstrated in 1984 [1-14]. Since then, Separate-Absorption-Charge-Multiplication (SACM) APDs using $In_{0.53}Ga_{0.47}As$ as the absorbing layer and InP as the multiplication layer have been studied widely as single-photon counters [1-28], [1-29]. Detection efficiency of 20% at low dark count probability of 10^{-6} per bias pulse has been demonstrated at 220 K using an $In_{0.53}Ga_{0.47}As$/InP APD manufactured by Epitaxx Ltd. (EPM239) [1-30]. Although most of these studies have used commercially available APDs that were designed for fiber optic transmission, recently there have been some efforts in designing InGaAs or InGaAsP APDs for single photon counting applications [1-31], [1-32], [1-33]. The process technology for III-V semiconductors and Ge is not as mature as that for Si.

Hence, generation-recombination centers and trap densities are much higher in these materials. High dark counts and high trap related enhancement of dark counts (afterpulsing) are some of the major issues in IR photon counting.

Silicon has superior multiplication properties compared to III-V semiconductors. Hence, efforts for combining the good multiplication properties of Si with the high absorption coefficient of InGaAs or Ge are also in progress. A wafer bonded APD with Si multiplication layer and InGaAs absorber has been shown to photon count with an efficiency of 33% at 1.5 μm with dark count probability of 10^{-3} [1-34]. Room temperature photon counting at 1.2 μm using a Si/SiGe absorption layer APD has been demonstrated as well [1-35].

Detection of weak UV light has numerous applications such as biological agent detection, non-line-of-sight communications, etc. Currently PMTs are the detectors of choice for UV radiation. However, due to limitations such as high operating voltage, bulkiness, etc., alternative solutions are sought. Silicon has very high absorption coefficient in the UV region. Hence most of the incident UV photons get absorbed close to its surface. Due to high surface recombination of photo-generated electron-hole pairs, these carriers are lost before being collected. High quantum efficiency UV-enhanced Si photodiodes have been demonstrated [1-36]. GaN-based APDs for single photon counting has also been investigated [1-37]. However, GaN APD yield is very low due to poor material quality. SiC based APDs exhibit high gain, low dark current, and low noise [1-38]. Single photon counting using SiC APDs has been recently demonstrated [1-39]. Single photon counting in the visible has also been demonstrated using GaP and GaAs

APDs [1-40]. In this study, GaP and GaAs APDs operated in Geiger mode were shown to exhibit single photon sensitivity from X-ray to near IR region.

1.2 APD AS A PHOTON COUNTER

The electric field in the depletion layer of an APD is engineered to be high. At high electric fields, an electron or a hole drifting through the depletion layer can gain enough energy to create secondary electron-hole pairs (ehps) by the process of impact ionization [1-41]. Operation of an APD below breakdown voltage (V_{br}) is referred to as linear mode operation. In this mode, an APD acts as a current amplifier, linearly amplifying the electrical response of incident photons. Operation of an APD above its V_{br} is fundamentally different. Above V_{br}, an APD acts as a trigger circuit. Due to the trigger nature of a photon counting APD, which is similar to a Geiger-Muller counter of nuclear radiation, this mode of operation is also referred to as the Geiger-mode operation. In the Geiger mode an APD sustains the high bias across the depletion layer as long as there are no free carriers in the depletion layer. This is the 'off' state of the Geiger mode APD. As soon as even one carrier enters the depletion layer, it can create secondary ehps by impact ionization. Due to the high electric fields above V_{br}, the multiplication process is self-sustaining with a finite breakdown probability and a macroscopic current pulse is produced in response to a single carrier in the depletion layer. This is the 'on' state of the Geiger mode APD. Note that due to the trigger circuit property, gain cannot be defined above breakdown. Use of an SPAD to sense single photons is possible if the probability of dark carrier generation in an APD can be reduced sufficiently. This is the operating principle of a single photon counting APD.

6

For the case of SPADs or even PMTs, use of the word 'photon counting' is misleading. An SPAD can detect the presence of one or more photons at the input. But it cannot resolve the number of incident photons. An SPAD performs single photon detection not single photon counting. Therefore it is a threshold detector unless designed specifically for resolving the photon number at the input. For counting number of photons at the input, instead of using a discriminator at the output to convert a current pulse into a standardized digital form, total charge in a pulse is measured [1-42].

Experiments involving single photon detection can be loosely divided into two categories. When the detector is used to sense the presence of photons at the input, it is referred to as photon counting. Dark count probability and detection efficiency are generally used as figures of merit in such experiments. Experiments where the SPAD is used to determine the arrival time of a photon are referred to as photon timing experiments [1-43]. In such experiments, the rising edge of the current pulse marks the photon arrival time if the pulse is photo-generated. The detector operated in this mode is characterized by timing jitter, photon detection efficiency and dark count rate. Requirements for a single photon detector and the accompanying electronics depend on the application. For example, in an application such as time resolved photoluminescence, timing resolution is very critical. In quantum cryptography, achieving a lower dark count rate is more crucial than good timing resolution. Further, the arrival time of a photon is well known in quantum cryptography and hence gated mode operation of an SPAD is used to reduce the dark count rate.

1.3 MOTIVATION AND OBJECTIVES

Applications for single photon counters are ever growing. As shown in section 1.2, the performance of SPADs in the infrared region significantly lags behind that of Si SPADs in the visible region. One reason for this is the lack of maturity in III-V growth and process technology. Further, very little emphasis has been given so far to designing APDs specifically for single photon detection applications in the IR regime. Most of the photon counting experiments for IR wavelengths have used commercial APDs, which were designed for linear mode operation. One of the goals of this research project was to understand the design principles for infrared SPADs. In order to pursue this, an experimental set-up for single photon detection in IR was established. Study of single photon detection performance of a telecommunication photodetector of a known structure was used as a reference for better single photon detector designs. An APD with InAlAs multiplication layer was chosen for this purpose. The dark count rate of this detector was characterized in the Geiger mode. Using the known structure of the APD, a suitable model was developed to explain the observed dark count rate in this device. Knowing the dark count generation mechanism helps in modifying the design suitably. Photon counting experiments at other wavelengths were also conducted. AlGaAs APDs as photon counters at 830nm and SiC APDs for UV photon counting were studied.

1.4   ORGANIZATION OF THE THESIS

The primary focus of my work in this project was single photon detection in the IR region. Chapter 2 describes the experimental set up that was established to characterize detectors as single photon counters. Chapter 3 describes the typical structure of an SACM APD. This structure is used widely in linear mode applications as well as Geiger mode operation of APDs. Various processing steps involved in fabricating devices

are also described along with the linear mode characterization. Various operating parameters greatly influence performance of a single photon detector. In chapter 4, operation of an InGaAs/InAlAs APD is used to illustrate the optimization of experimental parameters in a photon counting experiment. For single photon counting applications, the photodetector is almost always cooled to low temperatures to achieve a lower dark count rate. It is necessary to understand the effect of temperature on APD behavior. The temperature dependence of breakdown voltage, dark current and punchthrough voltage is discussed in chapter 5. Chapter 6 analyzes the origin of dark counts in a single photon counting APD. Based on the results of this modeling, modifications in the APD structure for single photon counting are suggested. SiC and GaAs based avalanche photodiodes have the potential for single photon detection in uv and near IR region. Chapter 7 describes single photon detection results using SiC APDs. Experiments involving GaAs/Al$_{0.6}$Ga$_{0.4}$As APDs for photon counting at 830nm are also described. Chapter 8 discusses future directions for continuing this work and its potential.

References:

[1-1] L-Q. Li and L. M. Davis, "Single photon avalanche diode foe single molecule detection", *Rev. Sci. Instrum.*, vol. 64, no. 6, pp. 1524-1529 (1993).

[1-2] Siegmund, O.H.W, "Advances in microchannel plate detectors for UV/visible astronomy", *Nuclear Instruments & Methods in Physics Research, Section A (Accelerators, Spectrometers, Detectors and Associated Equipment)*, vol. 525, no.1-2, pp. 12-16 (2004).

[1-3] S. Cova, M. Ghioni and I. Rech, "Photon counting and timing detector modules for single-molecule spectroscopy and DNA analysis", *Proceedings of IEEE LEOS Annual Conference*, vol. 1, pp. 70-72 (2004).

[1-4] W. P. Risk, and D. S. Bethune, "Quantum cryptography using autocompensating fiber-optic interferometers," *Optics and Photonics news*, vol. 13, no. 7, pp. 26 (2002).

[1-5] B. F. Levine, C. G. Bethea, and J. Campbell, "1.52 μm room temperature photon counting optical time domain reflectometer," *Electron. Lett.*, vol. 21, pp. 194-196 (1985).

[1-6] A. Lacaita, F. Zappa, S. Cova, and P. Lovati, "Single-photon detection beyond 1 μm: performance of commercially available InGaAs/InP detectors," *Appl. Optics*, vol. 35, no. 16, pp. 2986-2996 (1996).

[1-7] J. M. Smith, P. A. Hiskett, I. Gontijo, L. Purves and G. S. Buller, "A picosecond time-resolved photoluminescence microscope with detection at wavelength greater than 1500nm", *Review Sci. Intrum.*, vol. 72, no. 5, pp. 2325-2329 (2001).

[1-8] Sang Lee, H., Hwang, I.H., Spinhirne, J.D., and Scott, V.S, **"Micro pulse lidar for aerosol and cloud measurement"**, *Advances in* Atmospheric *Remote Sensing with Lidar. Selected Papers of the 18th International Laser Radar Conference (ILRC). Berlin, Germany: Springer-Verlag*, pp. 7-10 (1996).

[1-9] Credence Systems Co.; 1421 California Circle Milpitas, CA 95035. (www.credence.com).

[1-10] D. Halliday and R. Resnick, *Physics: Part II*, Willey Eastern Limited, 1995.

[1-11] Hamamtsu Co., 360 Foothill Rd, Bridgewater, NJ 08807. (www.hamamatsu.com).

[1-12] B. F. Levine, C. G. Bethea, and J. C. Campbell, "Near room temperature 1.3 μm single photon counting with a InGaAs avalanche photodiode," *Electron. Lett.*, vol. 21, pp. 194-195 (1985).

[1-13] X. Sun and F. M. Davidson, "Photon counting with silicon avalanche photodiodes", *J. Lightwave Tech.*, vol. 10, no. 8, pp. 1023-1032 (1992).

[1-14] B. F. Levine, C. G. Bethea, and J. C. Campbell, "Near room temperature 1.3 μm single photon counting with a InGaAs avalanche photodiode," *Electron. Lett.*, vol. 20, no. 14, pp. 596-597, (1984).

[1-15] K. A. McIntosh, J. P. Donnelly, D. C. Oakley, and A. Napoleone, "Development of Geiger-mode APD arrays for 1.06 μm", *Proceedings of IEEE LEOS Annual Conference*, vol. 2, pp. 760-761 (2002).

[1-16] A. Rochas, M. Gosch, A. Serov, and P. A. Besse, "First fully integrated 2-D array of single-photon detectors in standard CMOS technology", *IEEE Photonics Technology Letters*, vol.15, no.7, pp. 963-965 (2003).

[1-17] H. Dautet, P. Deschamps, B. Dion, A. D. MacGregor, D. MacSween, R. J. McIntyre, C. Trottier, and P. W. Webb, "Photon counting techniques with silicon avalanche photodiodes," *Appl. Optics*, vol. 32, no. 21, pp. 3894 (1993).

[1-18] A. Lacaita, M. Ghioni, and S. Cova, "Double epitaxy improves single-photon avalanche diode performance," *Electron. Lett.*, vol. 25, pp. 841-843, (1989).

[1-19] Perkin Elmer Optoelectronics; 44370 Christy Street, Fremont, CA 94538-3180, USA (http://perkinelmer.com).

[1-20] Optoelectronic components; 28 Des Lilas, Kirkland, QC H9J 4A7.

[1-21] A. Rochas, M. Gani, B. Furrer, P. A. Besse and R. S. Popovic, "Single photon detector fabricated in a complimentary metal-oxide-semiconductor high voltage technology", *Review of Sc. Intrum.*, Vol. 74, no. 7, pp. 3263-3270 (2003).

[1-22] F. Zappa, S. Tisa, S. Cova, P. Maccagnani, D. Bonaccini, G. Bonanno, M. Belluso and R. Ronacella, "Pulsing technologies: Single-photon avalanche photodiode arrays", *SPIE*, vol. 5490 (2004).

[1-23] J.C. Jackson, D. Phelan, A. P. Morrison, R. M. Redfern and A. Mathewson, "Toward integrated single photon counting microarrays", *Opt. Engn*. Vol. 42, no. 1, pp. 112-118 (2003).

[1-24] R. M. Heinrichs, B. F. Aull, R. M. Marino, D. G. Fouche, A. K. McIntosh, J. J. Zayhowski, T. Stephens, M. E. O'Brian and M. A. Albota, "Three-dimensional laser radar with APD arrays", *Proc. SPIE*, vol. 4377, pp. 106-116 (2001).

[1-25] A. Lacaita, P. A. Francese, F. Zappa and S. Cova, "Single-photon detection beyond 1 μm: performance of commercially available germanium photodiodes," *Appl. Optics*, vol. 33, no. 30, pp. 6902-6918 (1994).

[1-26] B. F. Levine and C. C. Bethea, "10-MHz single photon counting at 1.3 μm", *Appl. Phys. Lett.*, vol. 44, pp. 581-583 (1984).

[1-27] L. Duraffourg, J. M. Merolla, J. P. Goedgebuer, N. Butterlin, and W. T. Rhodes, "Photon counting in the 1540-nm wavelength region with a germanium avalanche photodiode," *IEEE J. Quantum Electron.*, vol. 37, no. 1, pp. 75-79, (2001).

[1-28] P. A. Hiskett, G. S. Buller, A. Y. Loudon, J. M. Smith, I. Gontjo, A. C. Walker, P. D. Townsend, and M. J. Robertson, "Performance and design of InGaAs/InP photodiodes for single photon counting at 1.55 μm," *Appl. Optics*, vol. 39, no. 36, pp. 6818-6829 (2000).

[1-29] J. G. Rarity, T. E. Wall, K. D. Ridley, P. C. M. Owens, and P. R. Tapster, "Single-photon counting for the 1300-1600-nm range by use of Peltier-cooled and

passively quenched InGaAs avalanche photodiodes," *Appl. Optics*, vol. 39, no. 36, pp. 6746-6753 (2000).

[1-30] D. S. Bethune, W. P. Risk and G. W. Pabst, "A high performance integrated single-photon detector for telecom wavelengths," *J. Modern Optics,* vol. 51, no. 9-10, pp. 1359-1368 (2004).

[1-31] K. K. Forsyth, and J. C. Dries, "Variations in the photon-counting performance of InGaAs/InP avalanche photodiodes", *Proceedings of IEEE LEOS Annual Conference*, vol. 2, pp. 777 (2003).

[1-32] Karve, G.; Zheng X.; Zhang X.; Li X.; Li N.; Wang S.; Ma F.; Holmes, A., Jr.; Campbell, J.C.; Kinsey G.S.; Boisvert J.C.; Isshiki T.D.; Sudharsanan R.; Bethune D.S.; Risk W.P., "Geiger mode operation of an $In_{0.53}Ga_{0.47}As-In_{0.52}Al_{0.48}As$ avalanche photodiode", *IEEE Journal of Quantum Electronics*, vol. 39, pp. 1281 (2003).

[1-33] K. A. McIntosh, J. P. Donnelly, D. C. Oakley, A. Napoleon, S. D. Calawa, L. J. Mahoney, K. M. Molvar, E. K. Duerr, S. H. Groves, and D. C. Shaver, "InGaAsP/InP avalanche photodiodes for photon counting at 1.06 μm," *Appl. Phys. Lett.*, vol. 81, no. 14, pp. 2505-2507, Sep. 2002.

[1-34] Y. Kang, Y-H. Lo, M. Bitter, S. Kristjansson, Z. Pan and A. Puchard, "InGaAs-on-Si single photon avalanche photodetectors", *Appl. Phys. Lett.*, vol. 85, no. 10, pp.1668-1670, 2004.

[1-35] A. Y. Loudon, P. A. Hiskett, and G. S. Buller," Enhancement of the infrared detection efficiency of silicon photon-counting avalanche photodiodes by use of silicon germanium absorbing layers", *Optics Letters*, vol.27, no.4, pp. 219-21 (2002).

[1-36] A. M. Saad, "High quantum efficiency of uv-enhanced silicon photodiodes", *Can. J. Phys.,* vol. 80, pp. 1601-1608 (2002).

[1-37] S. Verghese, K.A. McIntosh, R.J. Molnar, L.J. Mahoney, R.L. Aggarwal, M.W. Geis, K.M. Molvar, E.K. Duerr, and I. MeIngailis, "GaN Avalanche Photodiodes Operating in Linear-Gain Mode and Geiger Mode," *IEEE Trans. Electron Devices*, vol. 48 n.3, pp.502-511 (2001).

[1-38] F.Yan, C.Qin, J.H.Zhao, M.Weiner, B.K.Ng, J.P.R.David, and R.C.Tozer, "Low-noise visible-blind UV avalanche photodiodes with edge terminated by 2° positive bevel," *Electon. Lett.*, vol. 38, pp. 335-336 (2002).

[1-39] A.L. Beck, G. Karve, S. Wang, J. Ming, X. Guo, and J.C. Campbell, "Geiger Mode Operation of Ultraviolet 4H-SiC Avalanche Photodiodes," *IEEE Electron. Lett.*, accepted for publication.

[1-40] I. Prochazka, K. Hamal and B. Soplo, "Achievements in single photon detector and their applications", .*J. Modern Optics*, vol. 51, no. 9-10, pp. 1289-1312 (2004).

[1-41] S. M. Sze, *Physics of semiconductors*, Wiley-interscience publication, 2nd edition.

[1-42] E. Waks, K. Inoue, W. D. Oliver, E. Diamanti and Y. Yamamoto, "High-efficiency photon-number detection for quantum information processing", *IEEE J. of selected topics in Quan. Electron.*, vol. 9, no. 6, pp. 1502-1511 (2003).

[1-43] F. Zappa, A. Lacaita, S. Cova and P. Webb, "Nanosecond single-photon timing with InGaAs/InP photodiodes", *Optics Lett.*, vol. 19, no. 11, pp. 846-848 (1994).

Chapter 2   Experimental Set-up for Single Photon Detection

Single photon sensitivity can be achieved in an APD by operating it above its breakdown voltage (V_{br}). This mode of operation is referred to as the Geiger mode, after Geiger-Muller counters used in nuclear radiation detection. In this mode, any photo-generated or thermally generated carrier or carrier pair in the depletion region can generate a huge current pulse that can be detected by a simple comparator at the output. This avalanche current is self-sustaining unless properly quenched. The photons that fall on the detector during the avalanche breakdown fail to produce a distinguishable output pulse and thus are undetected. Hence, to detect a subsequent photon, the avalanche current must be quenched as soon as possible by lowering the detector bias below V_{br}. The APD bias is then restored to the quiescent value after a short dead time. The amount of charge passing through the detector also affects the probability of carrier trapping and thus after-pulsing. This is another reason to keep the duration of current through the device as short as possible. The operating circuit (quenching circuit) used in a photon counting application must perform all these tasks, namely: (i) sense the rise of the avalanche current, (ii) produce a standard pulse at the output corresponding to an avalanche, (iii) reset the APD bias below V_{br} thus limiting the current through the device, and (iv) restore the APD bias to the required value thus getting it ready to detect next photon. Performance of a single photon detector is strongly dependent on the choice of the quenching technique and design of the quenching circuit. There are three commonly used techniques, passive, active and gated quenching. A good discussion on various quenching schemes is presented by Cova, et. al. in reference [2-1]. Section 2.1 of this chapter discusses passive quenching technique. The gated mode quenching technique was implemented in our lab. It is explained in section 2.2.

14

2.1   PASSIVE QUENCHING

In passive quenching mode, the APD is reverse biased above its breakdown voltage through a large load resistor (R_L). Figure 2.1 shows the electrical bias diagram of an APD operated in this mode. As shown in the figure, output voltage is measured across a 50Ω resistor and sensed with a comparator. The discriminator threshold, which is set at the comparator decides which pulses represent an avalanche breakdown event. Each pulse is counted by an electronic counter. Upon detection of an event, the avalanche current ($I_{detector}$) in the circuit increases the voltage drop across the load resistor by $R_L * I_{detector}$, thus lowering the APD bias below breakdown. The reduction in APD bias causes the multiplication factor to drop significantly, which quenches the avalanche current. The load resistor, R_L, must be large enough to reduce the APD bias sufficiently below breakdown. The APD bias subsequently rises above the breakdown voltage with a time constant, which is determined by the value of the load resistor (R_L), the APD capacitance (C_d) and stray capacitance (C_s).
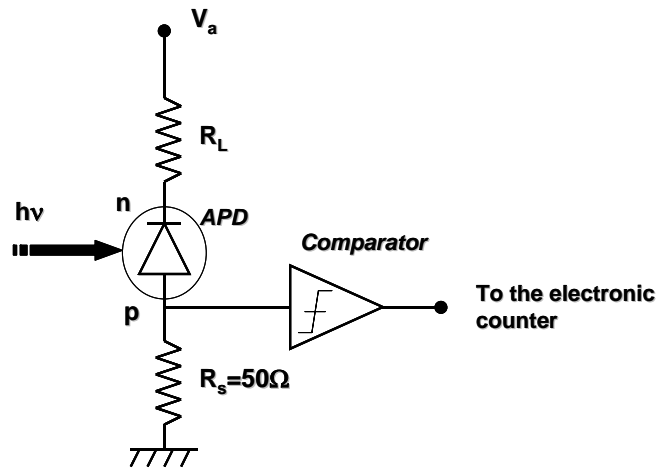
Figure 2.1:   Schematic of passive quenching circuit.

15

Though the passive quenching technique is simple to implement, it has following drawbacks.

2.1.1. **Dead time**: As mentioned earlier, a photon arriving within the duration of avalanche current is not detected at the output. Further, during the voltage recovery, the APD bias rises slowly above V_{br} and hence probability of breakdown (P_{br}) also rises slowly to its final value. Any photon incident during this time produces a smaller current pulse and hence may not be detected. This causes loss of counts at high-count rates. Thus the detector is insensitive to any photon arriving in the time interval from the onset of the avalanche to the APD bias reset. This is the dead time of the system. It can be taken into account by applying the following correction to the measured dark counts.

$$N_c = \frac{N_m}{1 - N_m \cdot T_d} \tag{2.1}$$

where, N_c are the corrected dark counts per second, N_m are the measured dark counts per second and T_d is the system dead time.

When applying a large excess bias, it is necessary to use a large load resistor to ensure quenching after an avalanche event. The large value of the load resistor increases the dead time of the system. The dead time is typically hundreds of nanoseconds to microseconds. A large value of the dead time limits the maximum count rate that can be handled without significant error.

In a passive counting system, the dead time depends not only on the values of R_L, C_d, and C_s, but also on the relative height of the discriminator threshold and that of the normal output pulse. Hence it is not a very well defined number, thus making it hard to account for error due to dead time.

16

2.1.2. **Recharge time**: When the voltage drop across R$_L$ increases, the APD bias drops below the breakdown voltage with a time constant, $T_q = (C_s + C_d) \cdot R_d$, where R$_d$ is the diode resistance. Its value is typically a few nanoseconds. The large current flowing through the device during this time causes increased charge trapping by defect centers. Hence trap-assisted dark counts (after-pulses) pose a significant problem in passive quenching. One way to solve this is to enforce an electronic dead time externally. The bias across the APD is held below V$_{br}$ for a certain time after detection of an event. The charge carriers released from trapping centers during this time are thus prevented from causing a detectable avalanche [2-1].

Other quenching methods are active quenching and gated quenching. The active quenching technique was conceived and developed at the Politecnico di Milano by Dr. S. Cova and co-workers [2-2]. In this technique, an external feedback loop is used to sense the rise of an avalanche pulse and pull the APD bias below breakdown. The bias is restored above breakdown after a fixed time. Another quenching technique, gated quenching is discussed in the next section.

2.2   GATED QUENCHING

In gated mode, the APD is dc biased just below V$_{br}$. The bias is taken above V$_{br}$ by applying an ac pulse. The duration of the ac pulse is kept short so that the current passes through the APD only for a short time. The end of the gate pulse quenches the avalanche current. This method is particularly useful in applications such as quantum cryptography where the arrival time of the photon is known.

A photon counting system utilizing gated mode quenching was established. Figure 2.2 shows a schematic of the experimental set up. The device was biased below

17

V_{br} with a dc power supply. It was pulse-biased above breakdown through capacitor, C_g. The voltage pulse was applied to the APD through the differentiator of capacitors $(C_g+C_d+C_s)$ and resistor R_L. C_d is the APD capacitance and C_s is the stray capacitance. The value of C_g must be chosen much higher than (C_d+C_s) so that most of the pulse voltage drops across the APD. Typically C_s and C_d are or the order of a few pF and so C_g of 100 nF was chosen in the circuit. In the experiments, an ac pulse width of 2ns was used. The APD can be biased at a repetition rate of 1Hz to 300 MHz. In this study the repetition rate was limited to 700kHz due to the limitation imposed by the electronic counter.

Sharp rise and fall times of the applied pulse bias produce capacitive transients at the output. These transients can be much stronger than the avalanche signal, thus making it hard to detect the true signal. For a long ac pulse width and less sharp rise and fall times, a low pass filter can be used at the output to smooth the response. For very short ac pulses (Eg. 2ns) used in these experiments, it is more effective to cancel the transients using a matched pair of 50 Ω coaxial cables [2-3]. The operation and benefits of the transient cancellation cables can be found in appendix I.
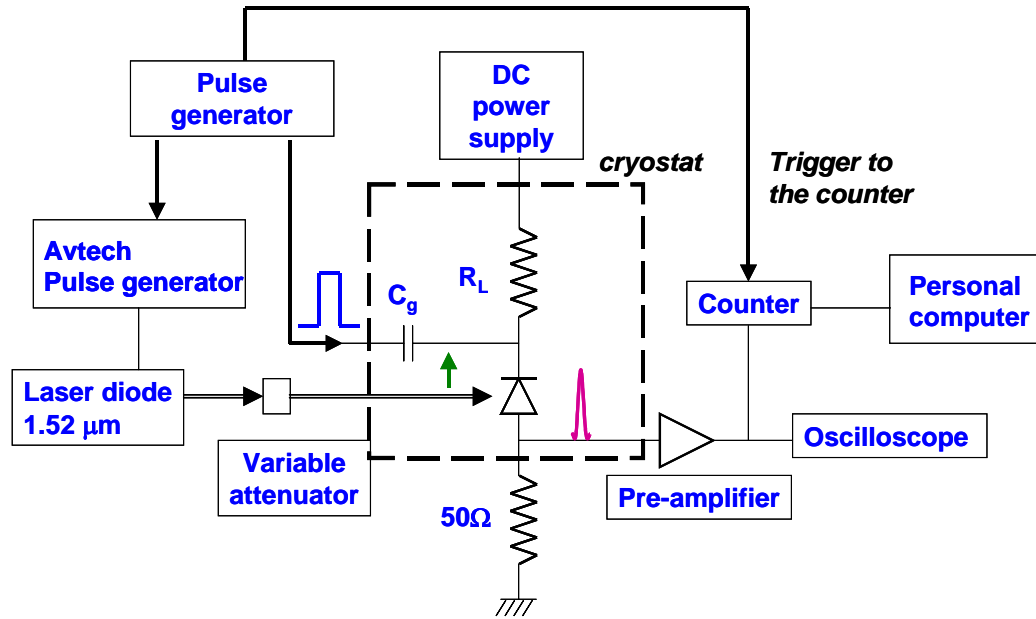
Figure 2.2:   Schematic of the experimental set-up for gated mode photon counting.

In photon counting experiments, it is necessary to operate the detector at low temperature to reduce the dark noise. Hence the device, the quenching circuit, and the transient cancellation cables were mounted inside a continuous-flow cryostat (Janis Research Co.). The cryostat electrical feedthroughs were modified to accommodate SMA connectors. All the cables in the experiment were kept as short as possible. Also note that for this configuration of the photon counting experiments, both the APD terminals are floating.

APDs with an $In_{0.53}Ga_{0.47}As$ absorber were illuminated either with 1.3μm or 1.52μm light. The light sources were a laser diode that produced 370 ps optical pulses at 1.52μm/1.3μm. To produce short pulses of light, the laser diode was triggered by a high performance Avtech pulser (AVP-AV-HV2-B-P). Since the pulse width of the laser pulse was measured using a 1GHz oscilloscope, the actual width of the laser pulse may be even

shorter than the observed 370ps. Light was attenuated to single photon level using a calibrated variable optical attenuator by JDS Uniphase. The number distribution of photons in a laser source is Poissonian and at the single photon level the mean number of photons/pulse should be interpreted as follows [2-4]. Let $\bar{n}$ be the average number of photons in a pulse. $\bar{n} = 0.4$, for example, means that there is a 40% probability that a randomly sampled optical pulse will contain a photon. It does not exclude the possibility of having more than one photon in a pulse. Figure 2.3 shows the probability of having n photons in a pulse containing average number of photons 0.1, 0.5, 1 and 5. The average photon number should be kept as low as possible to avoid two or more photons in a pulse. Calculation of average number of photons/pulse for a given average laser power is described in Appendix II.
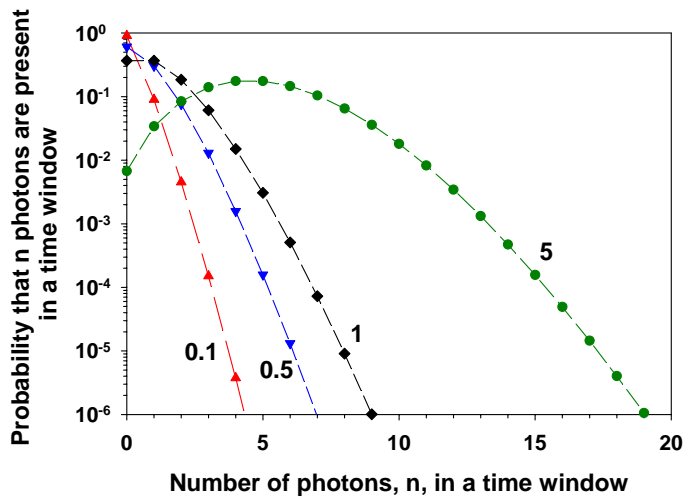
Figure 2.3: Poisson statistics applied to number of photons in a pulse. $\bar{n}$ is indicated next to each curve.

Output current pulses were amplified using a preamplifier, discriminated and counted using a photon counter (Stanford Research Systems, SR400). The detection gate

20

of the counter was 5 ns. Integration time for a measurement is decided by number of triggers for which counts are collected.

In gated mode, the delay between the ac pulse bias and the incident photon and between the output pulse and the detection gate must be well synchronized. The pulse generator, (Agilent technologies, Inc., 81110A), was used as the system clock for the experiment. It pulse biased the detector and also generated a trigger signal for the laser diode photon source and the electronic counter at the APD output. Synchronization in the system was achieved in two steps. First, the delay between the output pulse and the gate was adjusted with the photon source off. Adjustment was done by viewing the discriminated output and the position of detection gate on the oscilloscope. For more accurate adjustment, however, dark counts were measured as a function of detection gate delay for various excess voltage and discriminator threshold values. Figure 2.4 shows the plot of dark counts as a function of detection gate delay. The first and the last peaks are due to the transients discussed above. The peak in the center is the APD response. The width of the peak in the center is determined by the detection gate width. After the positions of the electrical gate and the output pulse were fixed, the delay in the optical channel was scanned to maximize photo counts. Figure 2.5 shows the plot of total counts and dark counts as a function of delay in the optical channel. The data was taken at fixed temperature and excess bias.
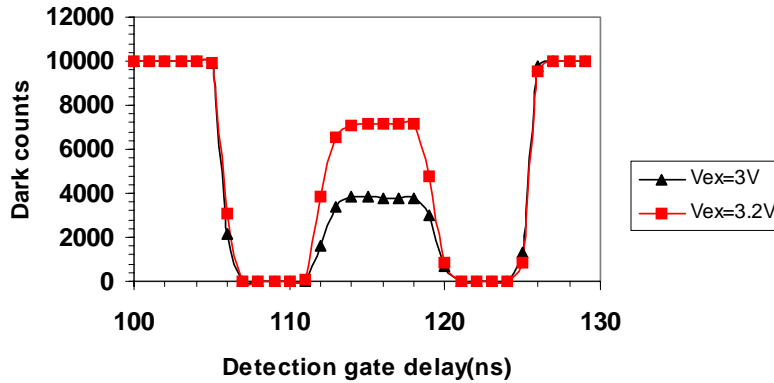
Figure 2.4: Adjustment of detection gate position. Parameters used were as follows. T=295K, repetition rate = 10kHz, pulse width =2ns and discriminator threshold = 5mV. Data at two different excess biases is shown.
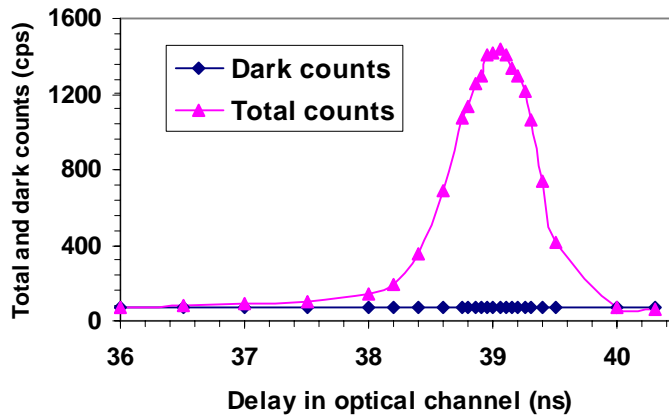
Figure 2.5: Adjustment of delay between optical and electrical pulse. Parameters used are as follows. T=175K, excess bias = 0.7V, repetition rate = 10kHz, pulse width =2ns, optical pulse width = 370ps and the mean number of photons/pulse = 6.

An avalanche process is statistical in nature. At a given excess bias, there is a distribution of multiplication factor around an average value. Use of discriminator threshold in a photon counting experiment reduces the effect of this uncertainty.

22

However, the number of detection events per second is statistically distributed around an average value. Hence, for a given set of experimental conditions, data must be averaged over a sufficient number of measurements, as shown in Figure 2.6. Due to these statistical fluctuations, the photo counts corresponding to incoming photons must be greater than or comparable to the standard deviation in the collected counts.
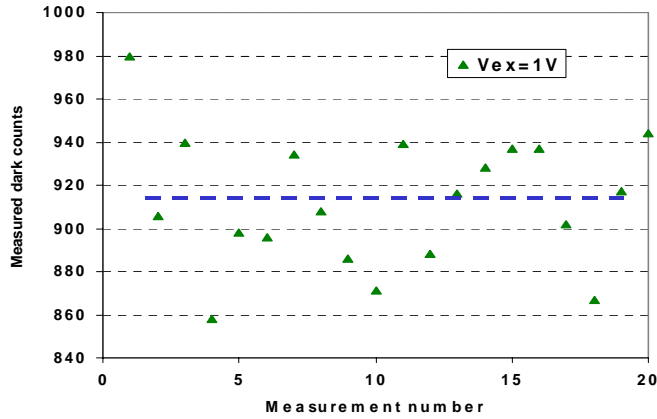
Figure 2.6:   Statistical distribution of counts about the average value. Parameters used are: $In_{0.52}Al_{0.48}As/In_{0.53}Ga_{0.47}As$ APD, T=295K, repetition rate = 10kHz and pulse width =2ns.

Note that in gated mode photon counting using a small bias pulse, at most one event can be detected in each pulse. Hence the maximum counts that can be accumulated in one second is equal to the repetition rate.

Once the overlap between optical-electrical signal and between the detection gate-output was ensured, counts were collected in dark and in the presence of single photons. The photon detection efficiency was calculated by taking into account the Poissonian statistics of the incident photon number using the relation [2-5]

$$P_{total} = 1 - (1 - P_{dark}) \cdot e^{-\bar{n} \cdot SPDE} . \tag{2.2}$$

23

P_{total} is the total probability of detecting an event, P_{dark} is the dark count probability, $\bar{n}$ is the average number of photons per pulse and SPDE is single photon detection efficiency.

P_{total} and P_{dark} are defined as follows.

$$P_{total} = \frac{N_{dark} + N_{light}}{f_s \cdot t} \qquad (2.3)$$

$$\text{and } P_{dark} = \frac{N_{dark}}{f_s \cdot t} \qquad (2.4)$$

Here, N_{dark} is the measured dark counts per detection gate, N_{light} is the measured light counts per detection gate, f_s is the gate repetition rate and t is the integration time.

The photon detection efficiency in the Geiger mode is a product of external quantum efficiency and breakdown probability, that is, the probability that a photo-generated carrier initiates an avalanche that continues to grow until quenched by an external circuit. More discussion on breakdown probability can be found in Chapter 3.

In an experiment, excess bias, temperature and discriminator threshold determine the dark count rate and the single photon detection efficiency. At fixed dark count rate, varying the number of photons incident on the detector changes the total probability of event detection (P_{total}). Equation (2.2) can be used to fit the experimental data to a single value of SPDE. Figure 2.7 shows such a plot of the experimental data and the fit.
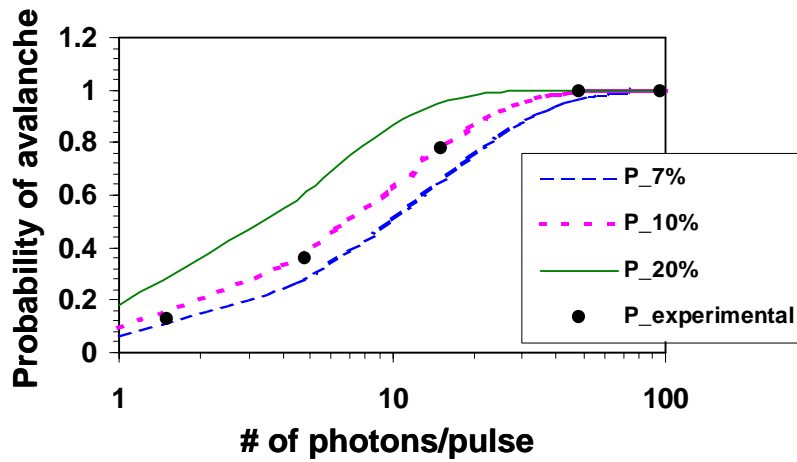
Figure 2.7: Fit of the experimental P_{total} to a single value of SPDE. Parameters used: repetition rate = 10kHz, dark count probability = 10^{-4}.

In order to calibrate the set-up, experiments were first performed on a commercial APD for which photon counting results have been published [2-6]. Note that the number of counts per second at the output corresponds to the number of detectable events in an experiment. This number is a function not only of the detector used, but also of the values of the load resistor, the discriminator threshold, etc. Hence photo and dark counts obtained in different experiments should be compared with care. As shown in Figure 2.8, the dependence of dark counts on excess bias is a function of discriminator setting.
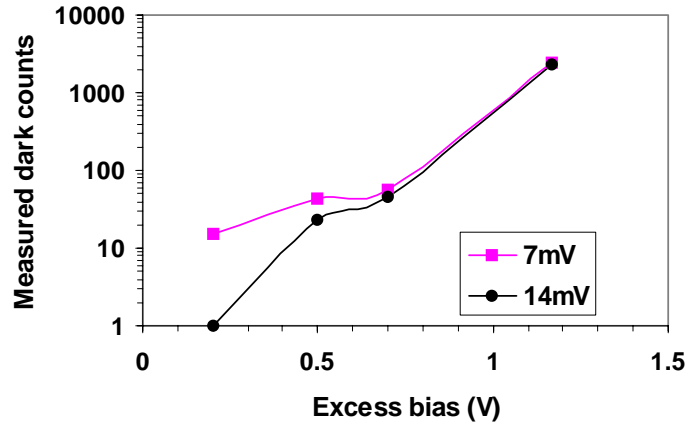
Figure 2.8:   Measured dark counts versus excess bias for discriminator setting of 7mV and 14mV. Other experimental parameters were: T=115K, repetition rate = 10kHz, pulse width =2ns.

Hence a dark count probability versus single photon detection efficiency plot was used to compare measurements on different set-ups. Plotting the probability of registering a dark count versus single photon detection efficiency is a convenient way to express single photon counting performance. For a given device and operating temperature each point on the graph indicates a particular value of excess bias (voltage above V_{br}). In Figure 2.9, the photon counting performance of a commercial detector (EPM239, JDS Uniphase) published in the literature is plotted along with measurements in our set-up. Device operating conditions were identical in both the measurements. It can be seen that there is a good agreement between the two sets of measurements. Dark count probability of 10^{-4} means that 1 out of 10^4 detected counts will be a false count.
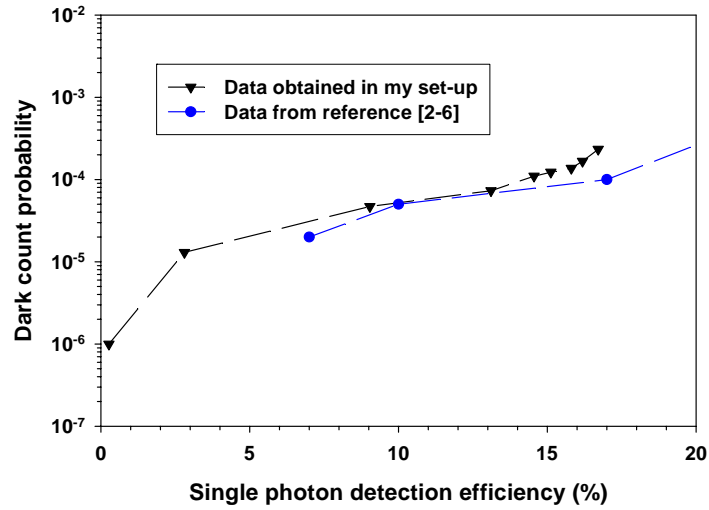
Figure 2.9:   Comparison between data obtained for EPM239 in my set-up and the reported data in reference [2-6]. In both cases, T~200K, repetition rate = 10kHz, bias pulse width = 2ns, optical pulse width = 370ps.
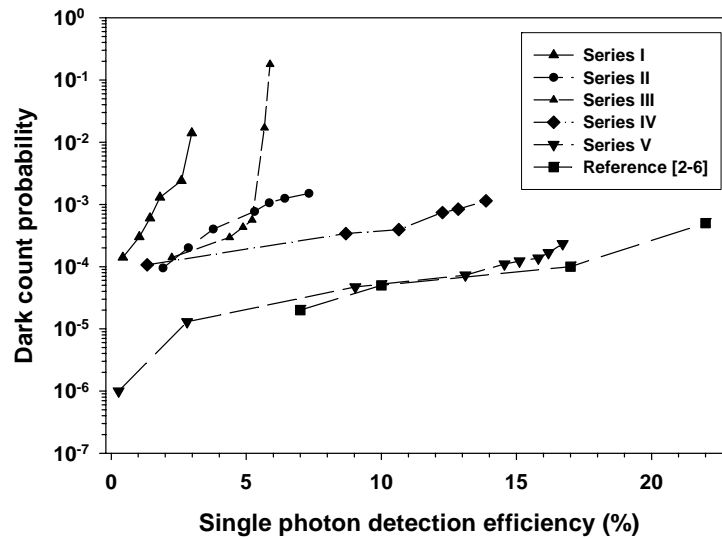
Figure 2.10:   Improvement obtained in the performance of EPM239 by improving coupling efficiency and heat sink. Operating conditions in all measurements: T=175K, repetition rate = 10kHz, bias pulse width = 2ns, optical pulse width = 370ps.

The performance of any given device, even under the same operating parameters, depends strongly on the quality of heat sink and the optical coupling efficiency. Figure 2.10 shows the effect of these two on the performance of EPM239, for a fixed set of operating conditions. The improvement in detection efficiency from series I to series V was obtained by improving optical coupling efficiency and using a better heat sink. Coupling efficiency was improved by tuning the optics. The heat sink was improved by using copper mounts instead of aluminum mounts and also by fitting them snugly with the device package.

Note that the use of equation (2.2) for estimation of SPDE in a single photon counting detector assumes that single photon counting is a Poisson process. A Poisson process by definition means that the successive events are uncorrelated. However, that is not strictly true for photon counting, as detection of an event at the output reduces the probability of detection for the next event. More research is needed in understanding the statistics of single photon counting avalanche diodes.

To conclude, this chapter describes passive and gated mode quenching techniques of single photon counting. A detailed description of the set-up in our lab along with the calibration data for a commercial detector is given. The importance of different experimental parameters is discussed.

References:

[2-1] S. Cova, M. Ghioni, A. Lacaita, C. Samori, and F. Zappa, "Avalanche photodiodes and quenching circuits for single-photon detection," *Appl. Optics,* vol. 35, no. 12, pp. 1956-1976 (1996).

[2-2] S.Cova, A.Longoni and A. Andreoni, "Towards picosecond resolution with single-photon avalanche diodes", *Rev. of Sc. Instrum.*, vol. 52, pp. 408-412 (1981).

[2-3] D. S. Bethune, and W. P. Risk, "An autocompensating fiber-optic quantum cryptography system based on polarization splitting of light," *IEEE J. Quantum Electron.*, vol. 36, no. 3, pp. 340-347 (2000).

[2-4] B A. E. Saleh and M. C. Teich, *Fundamentals of photonics*, Wiley Interscience publication, 1991.

[2-5] B. F. Levine, C. G. Bethea, and J. C. Campbell, "Near room temperature 1.3 μm single photon counting with a InGaAs avalanche photodiode," *Electron. Lett.*, vol. 20, no. 14, pp. 596-597, (1984).

[2-6] D. Stucki, G. Ribordy, A. Stefanov, H. Zbinden, J. G. Rarity, and T. Wall, "Photon counting for quantum key distribution with Peltier cooled InGaAs/InP APDs," *J. Modern Optics*, vol. 48, no. 13, pp. 1967-1981 (2001).

Chapter 3   Design, Device Processing and Linear Mode Characterization of Avalanche Photodiodes

All the current APDs used in the telecommunications industry utilize separate-absorption-charge-multiplication (SACM) structures. The electric field in an SACM structure is tailored to achieve the desired gain while keeping tunneling dark current in the absorber low. For single photon counting applications, where it is critical to maintain low dark current level, SACM APDs are expected to perform better than homojunction APDs. This chapter discusses the structure of a typical InGaAs/InAlAs SACM APD, critical steps involved in the device fabrication and their linear mode properties. Section 3.1 explains the advantages of SACM devices over homojunction devices for III-V APDs. The main features of the SACM structure are explained with the help of its electric field profile. APDs using the $In_{0.53}Ga_{0.47}As/In_{0.52}Al_{0.48}As$ material system were used in my experiments. Section 3.2 discusses the reason for this choice of material system. Important processing steps involved in fabricating mesa photodiodes and device packaging are described in section 3.3. Basic experiments to determine the usability of a detector as a photon counter are discussed in section 3.4. These tests include contact resistance, current-voltage, capacitance-voltage and quantum efficiency measurements of the diode operated in the linear mode. Although the experiments described here were performed using detectors at 1.5μm, the device design guidelines and measurement techniques are applicable for detectors working at other wavelengths as well.

3.1   HETEROJUNCTION AVALANCHE PHOTODIODES

A photodetector is an electronic eye that can be made sensitive to a chosen wavelength range. The simplest photodiode structure is a pn junction formed in a material

sensitive to the wavelength of interest. In practice, photodiodes with p-i-n (PIN) structure are preferred. Use of a wider depletion region leads to smaller junction capacitance and thus faster response time, as well as increased responsivity in a PIN device. Very low dark current InGaAs PIN photodiodes with a peak responsivity of 0.8 A/W at 1.5 μm, operating at speeds up to 10GHz are available commercially [3-1], [3-2]. The use of homojunction semiconductor diodes works well for PIN photodiodes, which do not exhibit gain and hence work at lower operating voltages. For the case of avalanche photodiodes, however, the electric field required to achieve impact ionization in the depletion layer is very high (~ hundreds of kV/cm). At such high electric fields, tunneling in the InGaAs depletion layer leads to very high dark current. This problem can be overcome by separating the absorption layer from the multiplication layer using a hetero-junction device. A simplified schematic diagram of such a device, the electric field profile, and the equilibrium band diagram are shown in Figure 3.1. In this structure, the electric field in the multiplication layer (M) is maintained at a high value to get the desired multiplication, whereas the field in the absorber (A) is kept below the tunneling electric field. A non-zero electric field in the absorber ensures that the photo-generated carriers drift to the multiplication layer instead of diffusing in order to maintain high operating speeds. A field control layer known as the charge layer (C) is used to tailor the electric field profile in the device. This structure is referred to as a separate-absorption-charge-multiplication (SACM) APD. Another advantage of the SACM structure is single carrier injection in the multiplication layer, which results in lower excess noise [3-3]. This concept has been applied to Si photodetectors to make reach-through APDs. In III-V semiconductors, a low dark current and high gain heterostructure InGaAsP/InP APD was first demonstrated in 1979 [3-4]. Since then a lot of research has been done in optimizing the heterostructure APD design [3-5], [3-6].

31
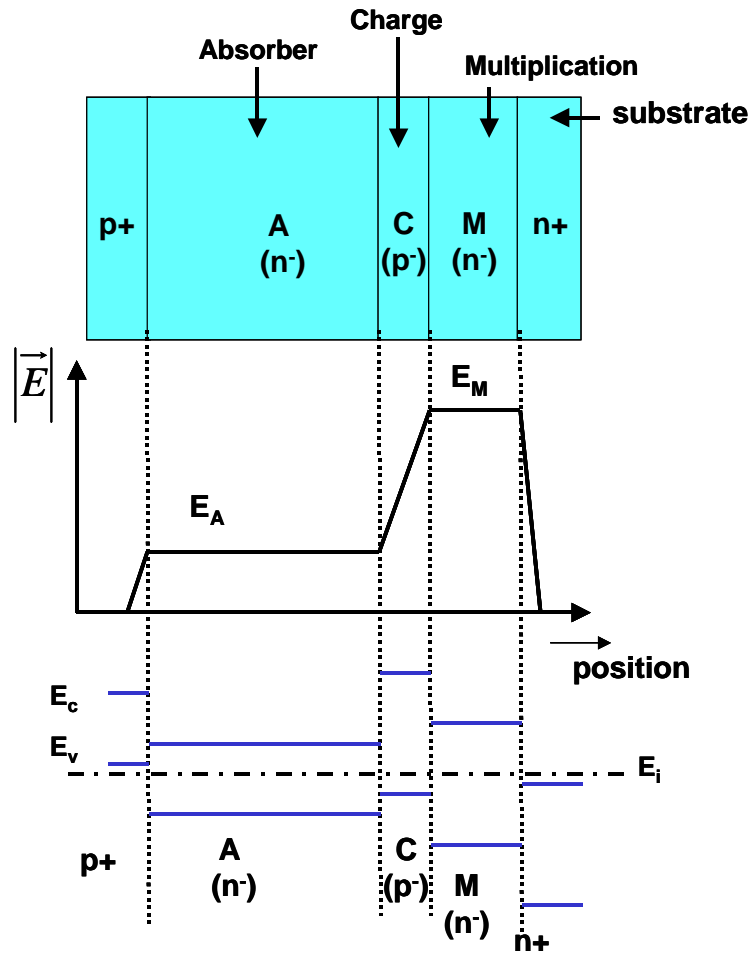
Figure 3.1: Simplified schematic, electric field profile, and the equilibrium energy band diagram for an SACM APD.

p+: InGaAs 9×10^{18,} 50nm
p+: InAlAs 5×10^{18}, 300nm
i: InGaAlAs Transition, 50nm
i: InGaAs, 1000nm
i: InGaAlAs Transition, 50nm
i: InAlAs Spacer, 50nm
p: InAlAs , , 3×10^{17,} 200nm
i: InAlAs , 400nm
n+: InAlAs , 5×10^{18}, 100nm
n+: InP, 5×10^{18}, 500nm
n+ InP Substrate

Absorber → (pointing to *i*: InGaAs, 1000nm)

Charge layer → (pointing to *p*: InAlAs, 3×10^{17}, 200nm)

Multiplication region → (pointing to *i*: InAlAs, 400nm)
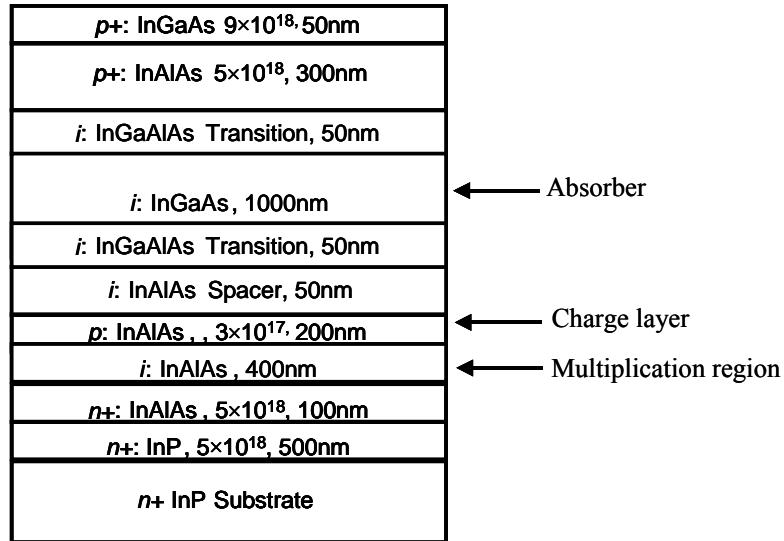
Figure 3.2:   Schematic of an In$_{0.53}$Ga$_{0.47}$As/In$_{0.52}$Al$_{0.48}$As APD.

The schematic of an SACM APD utilizing In$_{0.53}$Ga$_{0.47}$As absorber and In$_{0.52}$Al$_{0.48}$As multiplication layer is shown in Figure 3.2. The field control layer or charge layer is formed in In$_{0.52}$Al$_{0.48}$As as well. The lattice mismatch between In$_{0.53}$Ga$_{0.47}$As and InP is <0.2% and that between In$_{0.52}$Al$_{0.48}$As and InP is <0.1%. In In$_{0.52}$Al$_{0.48}$As, electrons have higher ionization probability than holes. Hence multiplication by seed electrons is preferred for low noise operation. This is achieved by using a top p contact for the device. The photo-generated electrons and holes in the absorber drift to the multiplication layer and to the p contact, respectively. For devices with an InP multiplication layer, on the other hand, avalanche initiation by holes is preferred and hence an n-i-p structure is used. Figure 3.3 shows the calculated electric field for the device shown in Figure 3.2 at two different applied biases.
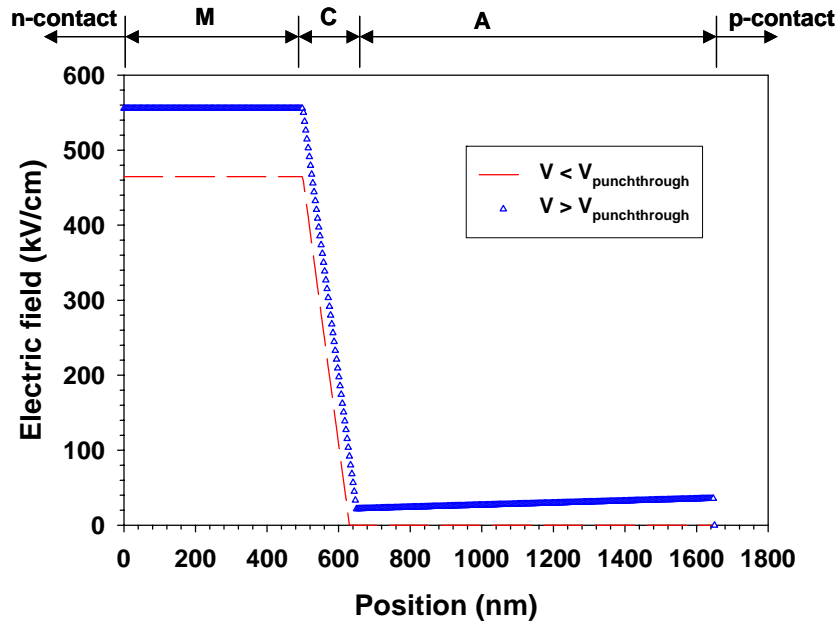
Figure 3.3:   Calculated electric field profile for structure shown in Figure 3.2.
M: multiplication layer, C: charge layer and A: absorber layer.

As the applied reverse bias voltage to the device increases, the charge layer gets depleted first. At voltage > $V_{punchthrough}$, the depletion layer begins to extend to the n$^-$ In$_{0.53}$Ga$_{0.47}$As absorber layer. Any photo-generated carrier in the absorber drifts through the absorber instead of diffusing through it. Thus the detector operates with high detection efficiency only for voltages above $V_{punchthrough}$. At sufficiently high voltages, the electric field in the multiplication layer causes carrier multiplication. The voltage at which the device exhibits gain depends on the electron and hole ionization coefficients for the multiplication layer. At even higher bias, the electric field exceeds the breakdown field in the multiplication layer, the avalanche gain becomes infinite, and a self-sustaining current flows through the device. In practice, the current is limited by the diode space-charge resistance and/or external circuit resistance.

The punchthrough voltage is determined by the integrated charge in the charge layer and in the multiplication layer. Thickness and doping of the charge layer determine the electric field at the $In_{0.53}Ga_{0.47}As$-$In_{0.52}Al_{0.48}As$ heterointerface at breakdown. It has been shown that the electric field at this heterointerface must be less than 200kV/cm for low tunneling leakage current and more than 100kV/cm for high bandwidth and quantum efficiency [3-7]. For the same charge density in the charge layer, the field in the absorber is lower for smaller doping in the charge layer. For a given punchthrough, the thickness of this layer should be minimized keeping the total charge density constant.

Both the absorption and multiplication layers are undoped. This maintains a uniform electric field in the layers. Doping in the multiplication layer should be kept low to reduce the probability of tunneling. The unintentionally doped absorber makes the depletion of this layer easier and leads to higher carrier velocities. Structures grown using MBE or MOCVD exhibit a background n doping of $\approx 10^{15}$ /cm^3 in both InGaAs and InAlAs. This background doping causes a small slope in the electric field in these two layers as shown in Figure 3.3.

An important feature of the band profile of the heterojunction APD is the band edge discontinuity between InGaAs and InAlAs. This band discontinuity causes carrier trapping at the heterointerface and reduces the bandwidth. Hence intermediate band gap quaternary layers of InGaAlAs, known as grading layers, are introduced between InGaAs and InAlAs [3-8], [3-9].

The substrate used is either n type (for $In_{0.52}Al_{0.48}As$ multiplication layer) or p type (InP multiplication layer) or a semi-insulating InP wafer. A semi-insulating substrate

is preferred in high-speed applications as it exhibits lower parasitic capacitance between p and n pads. For any choice of substrate, an InP buffer layer is usually used between the substrate and the multiplication layer. Use of the buffer layer moves the imperfections at the substrate-epi layer to a region of zero electric field.

3.2   CHOICE OF SPAD MATERIAL SYSTEM

3.2.1   Absorption layer

Choice of the absorber material is dictated solely by the absorption coefficient of the material at the wavelength of interest. For operation at $\lambda > 1$ μm, Germanium, $In_{0.53}Ga_{0.47}As$ or InGaAsP based devices are used. The band gap of Germanium (Ge) is 0.66eV, which corresponds to a cut off wavelength of 1.8 μm at room temperature. However Germanium APDs operated as single photon counters are plagued with a very high dark count rate. Hence they have to be cooled to ~77 K to reduce dark counts to an acceptable level. At low temperatures the detector responsivity is blue shifted to $\lambda \leq 1.45$ μm [3-10]. Longer wavelength operation can still be achieved with Ge APDs, but at reduced detection efficiency. For example, a liquid nitrogen cooled Ge APD operating in active gated mode has been shown to exhibit photon counting efficiency of 1% at 1.54 μm [3-11]. Higher detection efficiencies at 1.55 μm can be achieved using $In_{0.53}Ga_{0.47}As$ as the absorbing material. Figure 3.4 shows the absorption coefficient for $In_{0.53}Ga_{0.47}As$ at various temperatures [3-12]. Even at 77K, its cut off wavelength is > 1.52 μm.
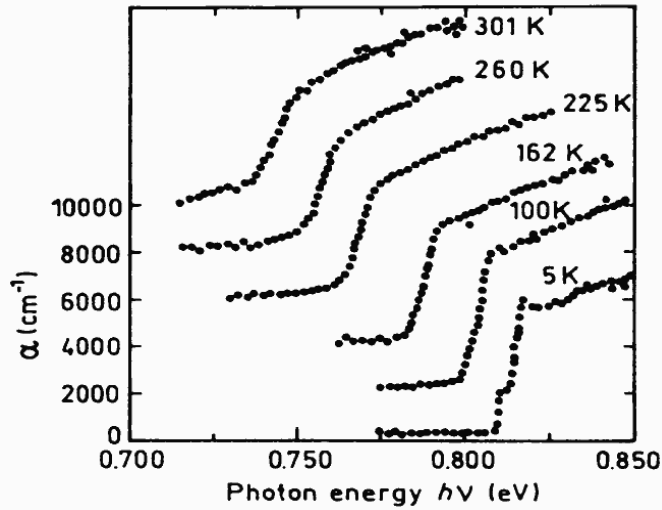
Figure 3.4:   Absorption coefficient as a function of photon energy for In$_{0.53}$Ga$_{0.47}$As at various temperatures. Reference [2-9].

InGaAsP lattice matched to InP is another choice for the absorber. The larger band gap of InGaAsP implies reduced tunneling related dark current. However, diodes using In$_{0.53}$Ga$_{0.47}$As absorber are sensitive over a broader spectral range than InGaAsP diodes, and hence are more attractive.

3.2.2   Multiplication layer

In an APD, a high electric field is required in the multiplication layer to achieve impact ionization. Hence a material with large band gap and large tunneling electric field is preferred for the multiplication layer. Most of the telecommunication APDs use InP as the multiplication layer. The reason is the ease of fabricating planar APD structures. We have used In$_{0.52}$Al$_{0.48}$As lattice matched to an InP substrate as the multiplication layer. In$_{0.52}$Al$_{0.48}$As was chosen for its better breakdown characteristics over InP, as explained in the following paragraph.

37

Photon detection efficiency in Geiger mode is a product of external quantum efficiency and breakdown probability (P_{br}). P_{br} is the probability that a photo-generated carrier initiates an avalanche that continues to grow until quenched by an external circuit. P_{br} is close to zero at the breakdown voltage (V_{br}) and it increases monotonically for voltages above V_{br}, eventually approaching a limit close to 1. A steep increase in breakdown probability above V_{br} ensures that any incoming photon generates a measurable response, thus leading to high detection efficiency [3-13]. It has been shown by McIntyre that the rate of increase of breakdown probability at voltages above V_{br} is higher in a semiconductor with a higher ratio of electron to hole ionization coefficients, *k* [3-14]. This ratio is ~0.5 for InP, where as it is ~0.3 for $In_{0.52}Al_{0.48}As$ [3-15], [3-16]. Breakdown probabilities for InP and $In_{0.52}Al_{0.48}As$ calculated by Wang et.al. confirm this characteristic [3-17]. In this work, McIntyre's history-dependent analytical impact ionization model was used to study breakdown characteristics in GaAs, InP and $In_{0.52}Al_{0.48}As$ of various thickness. Figure 3.5 summarizes the conclusions of this study. For a given relative excess voltage, $In_{0.52}Al_{0.48}As$ shows a breakdown probability higher than InP of same thickness.

APDs incorporating an $In_{0.53}Ga_{0.47}As$ absorber and an $In_{0.52}Al_{0.48}As$ multiplication layer, lattice matched to an InP substrate, have demonstrated a high quantum efficiency, high gain-bandwidth product and low excess noise factor [3-18], [3-19]. Geiger mode operation for $In_{0.52}Al_{0.48}As$ multiplication layer APDs has also been demonstrated [3-20], [3-21].
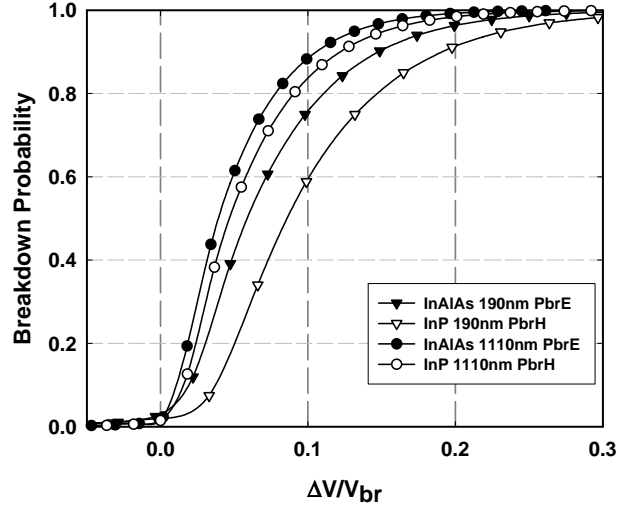
Figure 3.5: Comparison of breakdown probabilities between $In_{0.52}Al_{0.48}As$ (electron injection, solid symbols) and InP (hole injection, open symbols). Triangles are for thin 190nm devices and circles are for thick 1110nm devices. $\Delta V/Vbr$ is the relative excess bias above breakdown. Reference [3-17].

3.3   DEVICE PROCESSING

The complexity in device fabrication depends on the measurements to be performed with them. For evaluating the epitaxial wafer quality, noise and quantum efficiency measurements, large area devices without contact pads are fabricated. For photon counting measurements, however, it is necessary to use devices with smaller diameter to reduce the capacitance and with contact pads for ease of packaging. An excellent description of both large and small diameter device fabrication can be found in reference [3-22]. In this section, the critical processing steps are highlighted with special attention to device packaging for photon counting experiments.

3.3.1 P contact formation

P contacts are formed using standard lift-off technique. For obtaining a uniform field distribution across the mesa, ring contacts were used. A sacrificial SiO_2 layer was first deposited on the wafer for easy lift-off of small patterns. The contact pattern was then defined using a positive photoresist AZ5214 and Karl Suss contact mask aligner. After developing, buffered oxide etch was used to open contact areas in the oxide. Metal was deposited using electron beam (e-beam) evaporation. Cr (400 Å)/Au (1000 Å) or Ti (200 Å)/Pt (250 Å)/Au (1000 Å) were used to form ohmic p-type contacts on p-InGaAs. Selection of the metal for making ohmic contacts depends on the electron affinity of the p semiconductor and the metal work function [3-23]. A very heavily doped p InGaAs cap layer is usually grown to ensure fabrication of low resistance ohmic contacts. While using Pt, a thin layer of Ti was deposited to increase contact adhesion strength. The contacts were annealed at 420°C for 20sec using Rapid Thermal Annealing (RTA) to reduce contact resistance.

3.3.2 Mesa etch and passivation

Mesa formation is essential for isolating devices from each other. Mesas can be formed either by wet chemical etching or dry reactive ion etching. Wet etching of InAlAs APDs has been thoroughly studied. InAlAs and InGaAs were etched using H_3PO_4: H_2O_2: H_2O in the ratio of 1:1:10 by volume. This concentration gives an etch rate of ~ 0.4 μm/min. The solution was mixed thoroughly to get a uniform etch rate. A step profiler (Alpha-step 500) was used during the etch process to calibrate the etch rate. Due to the isotropic nature of wet etching, the mesa has a slope with the top having a smaller diameter than the base. While designing the mask, enough space should be left between the p-contact and mesa edge to account for the difference in diameters. After etching, the

surface of the semiconductor is left exposed. This creates chemically active dangling bonds and surface states, which lead to an increased leakage current and long term reliability issues. Therefore the mesa sidewalls must be passivated. Various materials have been studied as passivation materials [3-24]. We used plasma enhanced chemical vapor deposition (PECVD) deposited SiO_2 as a passivation layer. To reduce surface contamination, the wafer was loaded in the PECVD chamber immediately after mesa etching. For top illuminated devices, the thickness of SiO_2 was chosen such that it acted as a coarse antireflection coating. The thickness of SiO_2 (t_{AR}) needed to eliminate reflection is approximately given by

$$t_{AR} = \frac{\lambda}{4 \cdot n}$$ (3.1)

where λ is the wavelength of incident light and n is the refractive index of SiO_2 at λ. At 1.5μm, roughly 2400 °A of SiO_2 forms a good antireflection coating.

3.3.3 N contact formation

AuGe (400 Å)/ Ni (200 Å)/ Au (1000 Å) was used as the n contact metal on InAlAs. It was deposited using e-beam evaporation. Standard lift-off in acetone was used in this case as well. The contacts were annealed at 420 °C for 20 seconds.

3.3.4 Contact pads

For high speed and low temperature measurements, devices with large contact pads are preferred. Very thick (> 1μm) gold metal pads are required for reliable wire bonding. Such thick contact pads were deposited using electroplating. In order to reduce the parasitic capacitance, the pads were deposited on SiO_2. Poor adhesion of the metal pads to the oxide layer during wire bonding is a major concern. Hence special care must

be taken during the contact pad formation. Standard AZ5214 photoresist was used to pattern the pads. While developing the pattern, the wafer was dipped in the developer for 10-15 second after completing developing. This ensures that all the developed photoresist gets washed away from small feature areas. To remove any residual photoresist, a 2 minute O_2 plasma clean was done prior to depositing gold. Figure 3.6 shows a picture of a completely processed device.
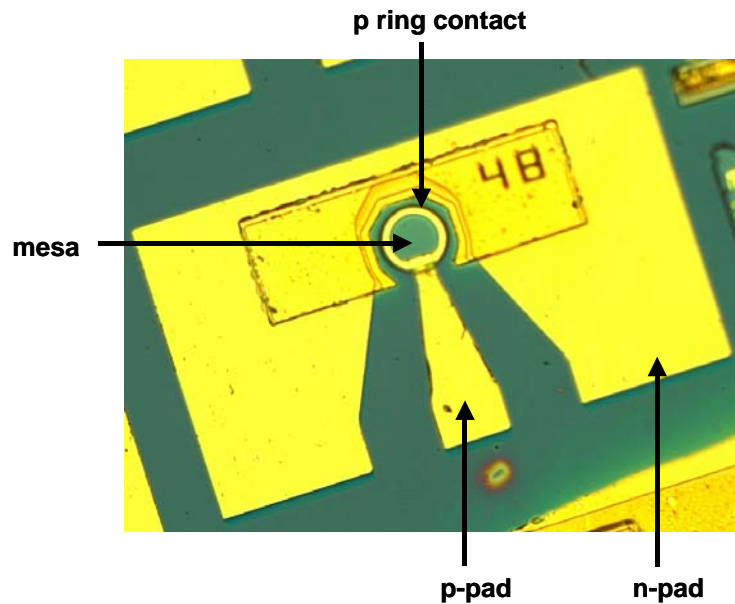
Figure 3.6:   Optical microscope image of a completely processed device.

3.3.5   Packaging

For low temperature characterization of the devices, individual dies were packaged on TO cans and mounted inside the cryostat. In order to get a good thermal contact, very thin Aluminum nitride (AlN) pads were used between the TO can case and the device. AlN was also used to electrically isolate the die from the body of the can, which was grounded during the experiments. Gold ball bonding (Model number 7700E,

Westbond, Inc.[3-25]) was used to wire bond the p and n contact pads of the device to the TO header leads. All bonding experiments were done at room temperature. The diameter of the gold wire was 25 μm, which gave a 75μm diameter footprint for a ball bond and 50x75 μm footprint for a wedge bond. Smaller diameter wire can be used for achieving smaller footprint. However, the wire must be thick enough to handle the maximum current that will be passed through it.

3.4   CHARACTERIZATION IN LINEAR MODE

3.4.1   Contact resistance

The specific contact resistance was measured for p and n contacts using Transmission Line Model (TLM) [3-26]. Specific contact resistance of ~ 10^{-5} $\Omega.cm^2$ and 10^{-6} $\Omega.cm^2$ was obtained for Ti/Pt/Au (p) and AuGe/Ni/Au (n) contacts, respectively.

3.4.2   Current-voltage and multiplication

Current (I) – voltage (V) characteristics for all the devices were measured to determine the material quality of the wafer. This was done using a semiconductor parameter analyzer (HP 4145, Agilent technologies). Figure 3.7 shows the dark current and photocurrent characteristics of a 160μm diameter InGaAs/InAlAs device, under 1.55μm illumination. For this device, at voltages below 20V, photo carriers generated in InGaAs diffuse to the multiplication layer and get collected. Hence the photo response is low. At punchthrough voltage of 20V, the depletion layer reaches the InGaAs layer and the photo-generated carriers in the absorber can drift to the multiplication layer. This increases the carrier collection efficiency, and causes a step in the photocurrent. To achieve maximum efficiency, an APD should be operated above its punchthrough

voltage. At even higher biases, the device exhibits gain and a room temperature breakdown voltage of 33V. Gain (M) at voltage V is defined as

$$M(V) = \frac{I_{total}(V) - I_{dark}(V)}{I_{M=1}} \tag{3.2}$$

where, I_{total} (V) and I_{dark} (V) are the total and dark currents at voltage V, $I_{M=1}$ is the photocurrent just above punch through at unity gain. For devices with high punchthrough voltage, the electric field in the multiplication layer may be enough to cause multiplication at punchthrough. This non-unity gain must be taken into account while calculating the gain curve. The gain – voltage characteristics for the above device are shown in Figure 3.7.
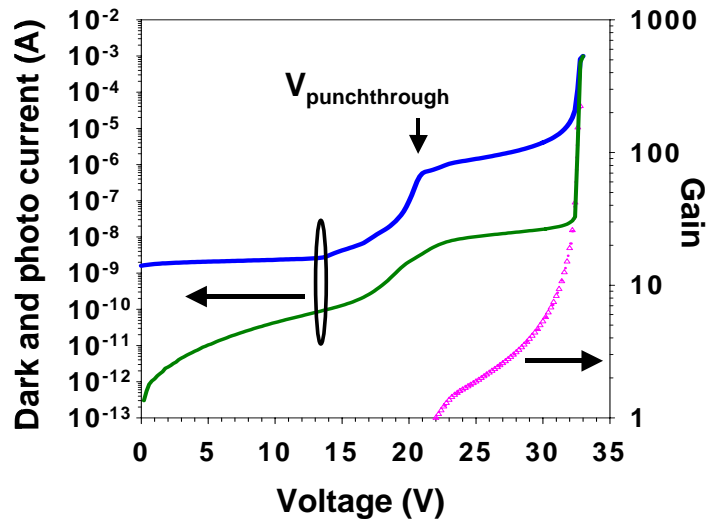
Figure 3.7: Gain and IV for an SACM APD. Structure is shown in Figure 3.2.

Total dark current in a detector is the sum of bulk leakage (I_{bulk}) and surface leakage ($I_{surface}$) currents,

$$I_{total} = I_{bulk} + I_{surface}. \tag{3.3}$$

For an avalanche detector, it can be expressed as follows.

$$I_{total} = M \cdot I_{M=1} + I_{surface} \tag{3.4}$$

44

Equation (3.4) assumes that the surface leakage current is not multiplied. It can be extracted by plotting I_{total} as a function of M as shown in Figure 3.8.
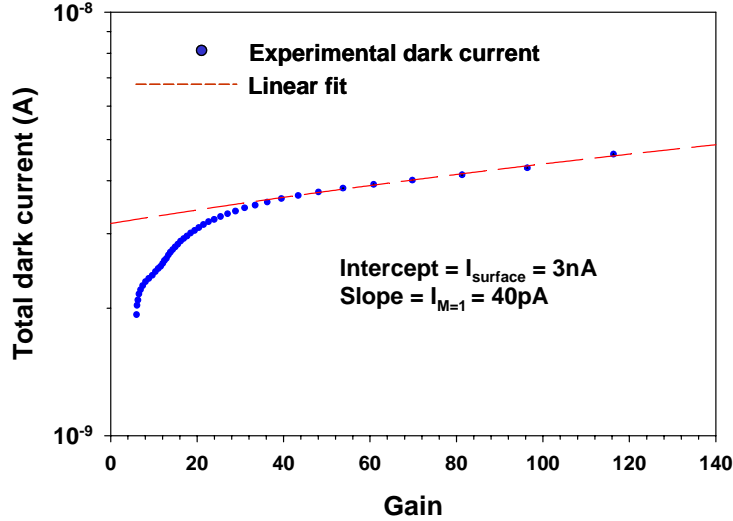
Figure 3.8: Extraction of surface leakage current in an APD. Active area diameter = 40 μm.

3.4.3 Capacitance-voltage characteristics

The capacitance (C) of the device was measured using an LCR meter (HP4275B, Agilent technologies). Figure 3.9 shows CV characteristics for an SACM APD. This device had a 400 nm-thick multiplication layer, a 1000 nm absorber and an integrated charge density of 3×10^{12} /cm^2 in the charge layer. The expected value of punchthrough voltage is ~ 20V. At voltages above punchthrough, the InGaAs layer begins to deplete. This results in a decrease in capacitance as shown in the figure. CV measurements are useful in confirming the punchthrough voltage of a device.
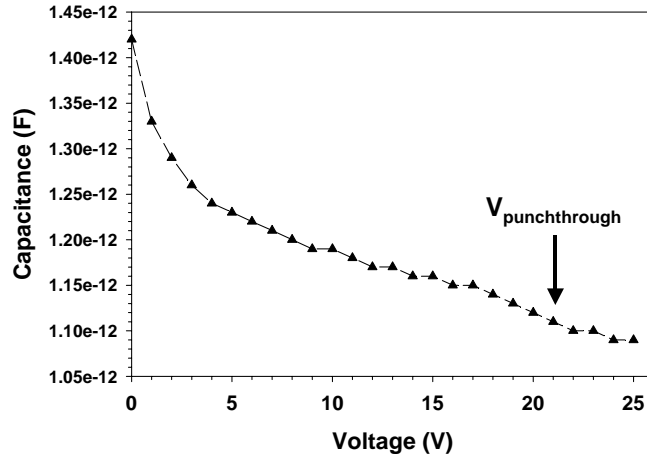
Figure 3.9:   Capacitance-voltage for an SACM APD. T = 295K.

3.4.4   Quantum efficiency

The external quantum efficiency (η) of a photodiode is given by the expression

$$\eta = (1-R)(1-e^{-\alpha \cdot L}) \tag{3.6}$$

Where, R is the fraction of incident light lost due to reflection, α is the absorption coefficient at wavelength λ and L is the thickness of the absorber. The higher the quantum efficiency the better is the chance of detecting a single photon. In these measurements light from a Xenon lamp was passed through a grating spectrometer and then focused on the device. For accurate measurements, the spot size must be smaller than the device active area. Photocurrent was measured as a function of wavelength using lock-in detection. The absolute value of the room temperature quantum efficiency was obtained by using a calibrated Germanium or InGaAs PIN detector. Figure 3.10 shows measured quantum efficiency as a function of wavelength for an 80μm diameter InGaAs/InAlAs device. The detector has 41% quantum efficiency at 1.55 μm just above punchthrough. At 1.5 μm, α is 0.67 μm^{-1}, for the $In_{0.53}Ga_{0.47}As$ material used in this

46

device. A thicker absorber will increase the quantum efficiency. However, a thicker absorber will also result in large generation-recombination current in the InGaAs and reduced bandwidth.
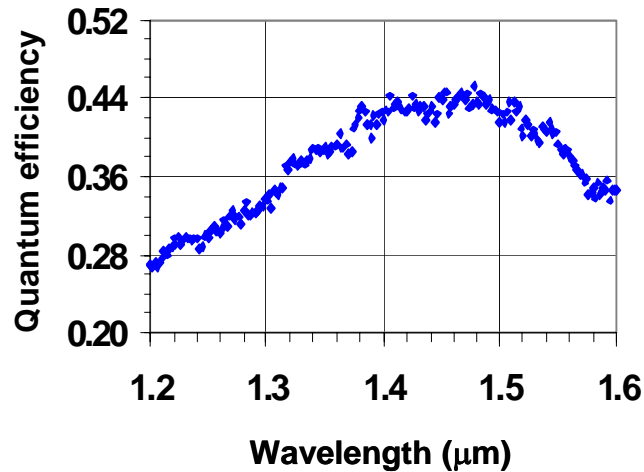
Figure 3.10: Quantum efficiency of a 80μm diameter InGaAs/InAlAs device as a function of wavelength at 295K.

In summary, this chapter discusses the structure of a typical SACM APD used in single photon counting. Critical steps in processing of mesa photodiodes are highlighted. Initial tests including IV, CV and quantum efficiency characterization to determine usability of a detector as a single photon counter are described and their relevance explained.

References:

[3-1] Perkin Elmer Optoelectronics; 44370 Christy Street, Fremont, CA 94538-3180, USA (http://perkinelmer.com).

[3-2] Sensors unlimited Inc.; 3490 Route 1, Building 12, Princeton, NJ 08540 USA (www.sensorsinc.com).

[3-3] S. Wang, "Low Noise Avalanche Photodiodes with An Impact-Ionization-Engineered Multiplication Region", Ph.D. dissertation, (University of Texas at Austin, Austin, TX, 2002).

[3-4] K. Nishida, K. Taguchi and Y. Matsumoto, "InGaAsP heterostructure avalanche photodiode with high avalanche gain," *Appl. Phys. Lett.*, vol. 35, pp. 251-253 (1979).

[3-5] Y. Liu, S. R. Forrest, J. Hladky, M. J. Lange, G. H. Olsen and D. E.Ackley, "A planar InP/InGaAs avalanche photodiode with floating guard ring and double diffused junction", *J. of lightwave tech.*, vol. 10, no. 2, pp. 182-193 (1992).

[3-6] C. L. F. Ma, M. J. Deen, L. E. Tarof and J. Yu, "Modelling breakdown voltage and its temperature dependence in SAGCM InP/InGaAs avalanche photodiode", *IEDM*, pp. 583-586 (1994).

[3-7] S. R. Forrest, R. G. Smith and O. K. Kim, *IEEE J. Quantum Electron.*, vol. QE-18, pp. 2040-2048 (1982).

[3-8] S. R. Forrest, O. K. Kim and R. G. Smith, "Optical response time of $In_{0.47}Ga_{0.53}As/InP$ avalanche photodiodes", *Appl. Phys. Lett.*, vol. 41, pp. 91-95 (1982).

[3-9] S. R. Forrest, R. G. Smith and O. K. Kim, "Performance of $In_{0.47}Ga_{0.53}As/InP$ avalanche photodiodes", *J. Quantum Electron.*, vol. QE-18, no. 12, pp. 2040-2047 (1982).

[3-10] S. Fancey, "Single photon avalanche diodes for time resolved photoluminescence measurements in the near infra-red", Ph.D. dissertation (Heriot-Watt University, Edinburgh, UK, 1996).

[3-11] L. Duraffourg, J. M. Merolla, J. P. Goedgebuer, N. Butterlin, and W. T. Rhodes, "Photon counting in the 1540-nm wavelength region with a germanium avalanche photodiode," *IEEE J. Quantum Electron.*, vol. 37, no. 1, pp. 75-79 (2001).

[3-12] E. Zielinski, H. Schweizer, K. Streubel, H. Eisele and G. Weimann, *J. Appl. Phys.*, vol. 59, no. 6, pp. 2196-2204 (1986).

[3-13] M. M. Hayat, U. Sakoglu, O-H Kwon, S. Wang, J. C. Campbell, B. E. A. Saleh, and M. C. Teich, "Breakdown probabilities for thin heterostructure avalanche photodiodes," *IEEE J. Quantum Electron.*, vol. 39, no. 1, pp. 179-185 (2003).

[3-14] R. J. McIntyre, "A new look at impact ionization-Part I: A theory of gain, noise, breakdown probability, and frequency response," *IEEE Trans. Electron. Devices*, vol. 46, no. 8, pp. 1623-1631 (1999).

48

[3-15] M. A. Saleh, M. M. Hayat, P. P. Sotirelis, A. L. Holmes, J. C. Campbell, B. A. E. Saleh, and M. C. Teich, "Impact-ionization and noise characteristics of thin III-V avalanche photodiodes", *Trans. Electron. Devices*, vol. 48, no. 12, pp. 2722-2731 (2001).

[3-16] C. Lenox, H. Nie, P. Yuan, G. Kinsey, A. L. Holmes Jr., B. G. Streetman, and J. C. Campbell, "Resonant-cavity InGaAs-InAlAs avalanche photodiodes with gain-bandwidth product of 290 GHz," *IEEE Photon. Tech. Lett.*, vol. 11, no. 9, pp. 1162-1164 (1999).

[3-17] Wang S., Ma F., Li X., Karve G., Zheng X., and Campbell, J.C., "Analysis of breakdown probabilities in avalanche photodiodes using a history-dependent analytical model", *Applied Physics Letters*, vol. 82, pp. 1971 (2003).

[3-18] G.S. Kinsey, J. C. Campbell, and A. G. Dentai, "Waveguide avalanche photodiode operating at 1.55 μm with a gain-bandwidth product of 320 GHz," *IEEE Photon. Tech. Lett.*, vol. 13,no. 8, pp. 842-844 (2001).

[3-19] H. Nie, K. A. Anselm, C. Lenox, P. Yuan, C. Hu, G. Kinsey, B. G. Streetman, and J. C. Campbell, "Resonant-cavity separate absorption, charge and multiplication avalanche photodiodes with high-speed and high gain-bandwidth product, " *IEEE Photon. Tech. Lett*, vol. 10, no. 3, pp. 409-411 (1998).

[3-20] Karve G., Zheng X., Zhang X., Li X., Li N., Wang S., Ma F., Holmes A. Jr., Campbell J.C., Kinsey G.S., Boisvert J.C., Isshiki T.D., Sudharsanan R., Bethune D.S., and Risk W.P., "Geiger mode operation of an $In_{0.53}Ga_{0.47}As$-$In_{0.52}Al_{0.48}As$ avalanche photodiode", *IEEE Journal of Quantum Electronics*, vol. 39, pp. 1281 (2003).

[3-21] J. Boisvert, G. S. Kinsey, D. McAlister, T. Isshiki, R. Sudharsanan, and M. Krainak, "Large area InAlAs/InGaAs single photon counting avalanche photodiodes", *Proc. SPIE*, vol. 5412, pp.126-136 (2004).

[3-22] X. Zheng, "Long-wavelength, high-speed avalanche photodiodes and APD arrays", Ph.D. dissertation (University of Texas at Austin, Austin, TX, 2004).

[3-23] S. Banerjee, B. Streetman, *Solid state electronic devices*, Prentice-Hall, Englewood Cliffs, NJ, 3rd edition 1990.

[3-24] H. S. Kim, J. H. Choi, H. M. Bang, Y. Jee, S.W. Yun, J.Bur, M. D. Kim and A. G. Choo, "Dark current reduction in APD with BCB passivation", *Electron. Lett.*, vol. 37, no. 7, pp. 455-457 (2001).

[3-25] Westbond Inc.; 1551 Gene Autry Way, Anaheim, CA 92805 (www.westbond.com).

[3-26] Ting Li, "Gallium Nitride and Aluminum Nitride based ultraviolet photodetectors" Ph.D. dissertation (University of Texas at Austin, Austin, TX, 2000).

Chapter 4   Parameter Optimization for Single Photon Counting

Efficient detection of weak intensity infrared signals can be achieved by avalanche photodiodes with $In_{0.53}Ga_{0.47}As$ absorption layer [4-1], [4-2]. Performance of a detector as a single photon counter depends very strongly on the experimental conditions such as temperature, excess voltage, etc. The effect of some important experimental parameters is discussed in this chapter. The optimization process is illustrated using data from an $In_{0.53}Ga_{0.47}As/In_{0.52}Al_{0.48}As$ single photon avalanche diode (SPAD). The parameters discussed in this chapter are: bias pulse width, repetition rate, excess voltage (ac and dc bias), temperature and discriminator threshold.

The device under test was an SACM APD with a 1 μm-thick $In_{0.53}Ga_{0.47}As$ absorbing layer and 400nm-thick $In_{0.52}Al_{0.48}As$ multiplication layer. The schematic of the detector is shown in Figure 4.1. The structure was grown on n^+ substrate using metal-organic chemical vapor phase deposition (MOCVD). Top-illuminated mesa devices were fabricated using standard photolithography, lift-off, wet chemical etching and SiO_2 passivation. Ti/Pt/Au and AuGe/Ni/Au were used as the p-contact and n-contact, respectively. Details of the structure and the processing can be found in Chapter 3. Performance of this detector in linear regime is also discussed in Chapter 3. For single-photon detection, the detector was operated in gated quenching mode. The experimental set up is described in Chapter 2. All data presented in this chapter were taken for a 40 μm diameter device operated at 10kHz gate frequency with 2ns-wide pulse of 2V amplitude.

```
┌─────────────────────────────────────────┐
│        p+: InGaAs  9×10¹⁸, 50nm           │
├─────────────────────────────────────────┤
│        p+: InAlAs  5×10¹⁸, 300nm          │
├─────────────────────────────────────────┤
│      i: InGaAlAs  Transition, 50nm        │
├─────────────────────────────────────────┤
│                                           │
│         i: InGaAs , 1000nm                │  ←──── Absorber
├─────────────────────────────────────────┤
│      i: InGaAlAs  Transition, 50nm        │
├─────────────────────────────────────────┤
│        i: InAlAs  Spacer, 50nm            │
├─────────────────────────────────────────┤
│      p: InAlAs , , 3×10¹⁷, 200nm          │  ←──── Charge layer
├─────────────────────────────────────────┤
│         i: InAlAs , 400nm                 │  ←──── Multiplication region
├─────────────────────────────────────────┤
│      n+: InAlAs , 5×10¹⁸, 100nm           │
├─────────────────────────────────────────┤
│      n+: InP , 5×10¹⁸, 500nm              │
├─────────────────────────────────────────┤
│                                           │
│         n+ InP Substrate                  │
│                                           │
└─────────────────────────────────────────┘
```
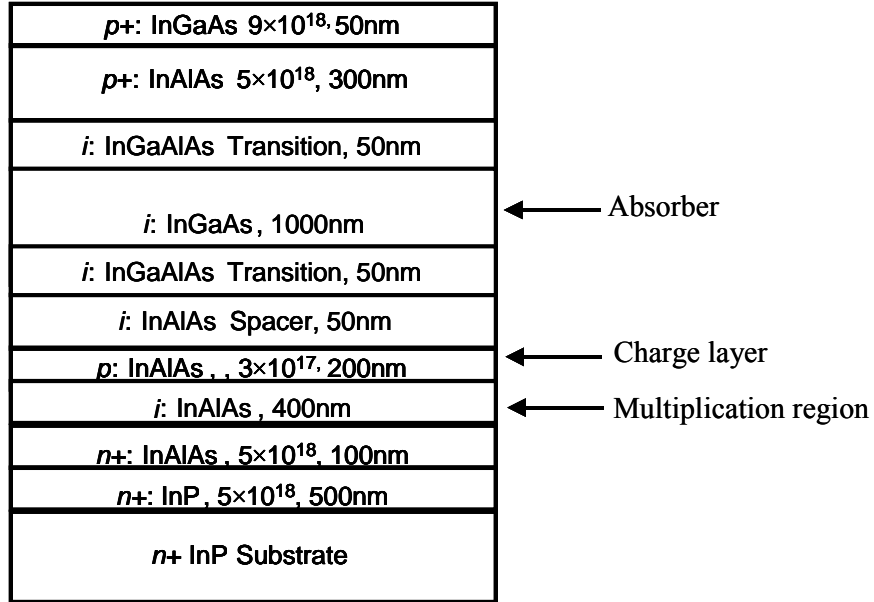
Figure 4.1:   Schematic of $In_{0.53}Ga_{0.47}As/In_{0.52}Al_{0.48}As$ APD.

4.1   EXCESS BIAS

Excess bias (V_{excess}) is defined as the voltage above breakdown (V_{br}) that the detector is operated at in the Geiger mode.

$$V_{excess} = V_{applied} - V_{br}(T) \tag{4.1}$$

where, $V_{applied}$ is the applied bias and $V_{br}(T)$ is the breakdown voltage at temperature T. In gated mode, the device is dc biased below breakdown at V_{dc}. An ac bias (V_{ac}) takes it above breakdown. Hence V_{excess} is given as $V_{excess} = V_{dc} + V_{ac} - V_{br}(T)$. Different values of V_{excess} are obtained by varying V_{dc}, keeping V_{ac} constant. It can be seen that the value of excess bias depends on V_{br}. At a given temperature, V_{br} is defined as the voltage at which the APD gain becomes infinite. In practice, V_{br} is defined as the voltage at which dark current crosses a certain threshold value, typically 100 μA.

At a given temperature, as the excess bias increases so does the probability of breakdown (see Chapter 3). Hence probability of both photon detection and dark carrier detection increases as shown in Figure 4.2. The effect of excess bias can also be seen by plotting noise equivalent power (NEP) as a function of excess bias. Noise equivalent power is defined as the minimum signal power required at the input to achieve a signal to noise ratio of 1. The smaller the achievable NEP, the better is the detector performance. NEP is defined as follows.

$$NEP = \frac{h \cdot \nu}{SPDE} \cdot \left[\frac{N_{dark}}{t} \right]^{1/2} \tag{4.2}$$

where, ν is the frequency of the optical pulse, SPDE is the single photon detection efficiency, N_{dark} is the number of dark counts per second and t is the integration time.

N_{dark} used in equation (4.2) refers to the dark counts rate in number/second, which is the number of dark counts measured when the detector has a cumulative bias above breakdown voltage for 1 second. For a detector operated in the gated mode, the measured dark counts are converted into the dark count rate by dividing the measured dark counts by the time for which the detector bias is held above breakdown voltage.

$$N_{dark} = \frac{M_{d,measured}}{\tau_{ac} \cdot n_s} \tag{4.3}$$

where, N_{dark} is the number of dark counts per second, $M_{d,measured}$ is the number of measured dark counts, τ_{ac} is the pulse width and n_s is the number of bias pulses in one second.
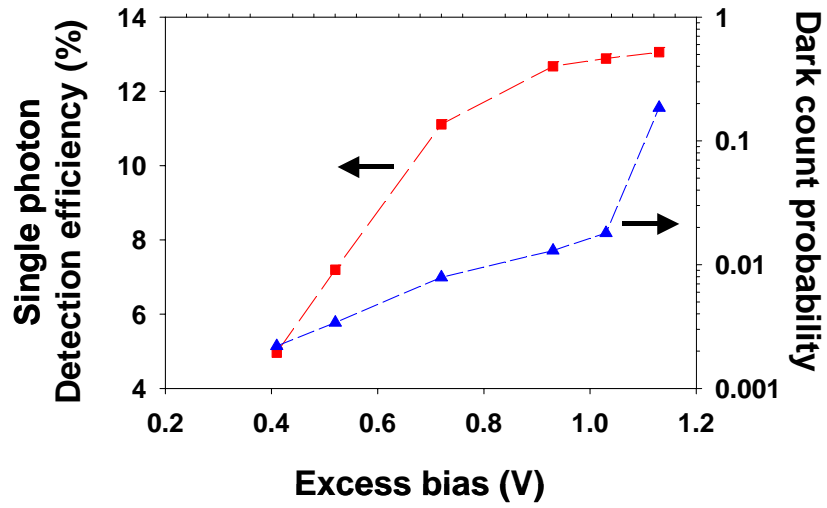
Figure 4.2: Dependence of photon detection efficiency and dark count probability on excess bias. T = 200K.
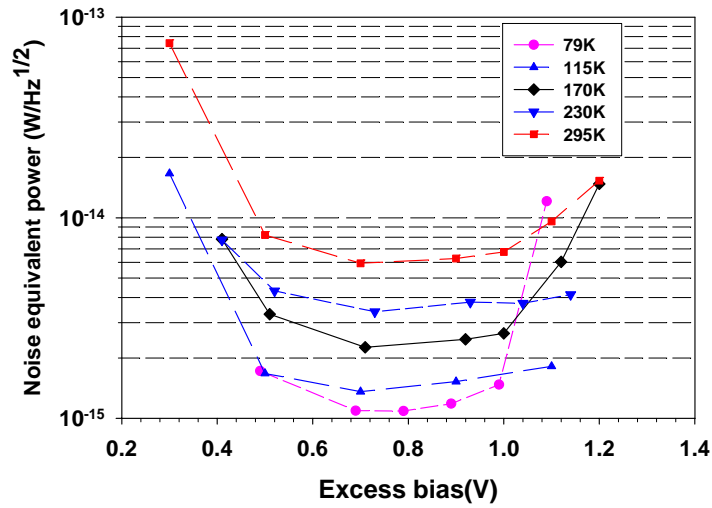
Figure 4.3: Noise equivalent power as a function of excess bias at various temperatures.

Figure 4.3 shows NEP versus excess bias for various operating temperatures. At any temperature, NEP increases at lower excess bias due to reduced detection efficiency.

At high excess bias it increases due to increasing dark count probability. The NEP was found to be low and unchanged for excess biases between 0.5 and 1V.

In the gated mode, a given excess voltage can be achieved by either using a small dc and a large pulse bias, or a high dc and a small pulse bias. The dc operating point determines the dark current passing through the detector between consecutive gates. Hence the use of a smaller dc bias and a larger pulse is expected to lower the dark count rate. On the other hand, it has been proposed that using dc bias close to the breakdown voltage empties traps faster [4-3], [4-4]. However, this trend was not observed in this study. SPDE and dark count probability were measured for two different pulse heights, 3.4V and 2V. No significant difference in the detector performance was observed between the two measurements.

During avalanche, the amount of charge flowing through the device is given by $Q = (C_d + C_s) \cdot V_{excess}$. Hence higher excess bias causes more charge flow through the device and thus increases the probability of trap related dark counts.

4.2   OPERATING TEMPERATURE
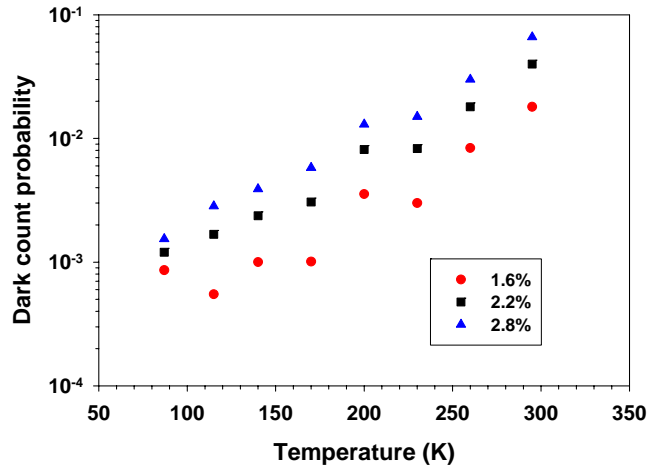
Figure 4.4:   Dark count probability versus temperature.

Operating temperature affects the device performance in many ways. It affects the breakdown voltage, dark count rate, lifetime of the traps, etc. Reduced operating temperature of the device reduces the dark current and thus the dark count rate. Figure 4.4 shows the dark count probability as a function of temperature for the $In_{0.53}Ga_{0.47}As/In_{0.52}Al_{0.48}As$ APD. The decrease in dark counts with temperature depends on the mechanism responsible for the dark count rate. A detailed discussion of temperature dependence of dark count rate is given in chapter 5. For junction breakdown caused by impact ionization, breakdown voltage decreases as temperature is lowered due to reduced phonon scattering. Hence the relative excess voltage is higher at lower temperatures. Since the breakdown probability in Geiger mode depends on relative excess bias above breakdown voltage, data at different temperatures should be compared at constant relative excess bias. As the temperature is reduced, the decrease in the detector quantum efficiency is slower than the decrease in its dark count probability.

Therefore the noise equivalent power of the detector improves with reduced temperature as shown in Figure 4.5.
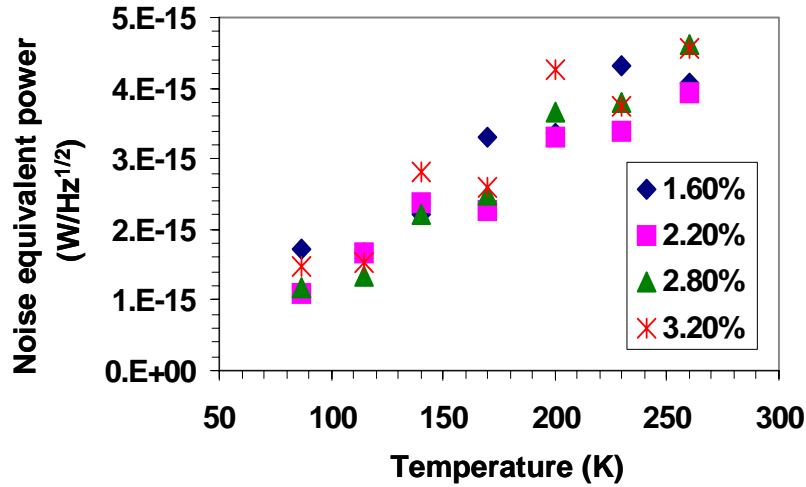
Figure 4.5:   Noise equivalent power as a function of operating temperature.

Figure 4.6 shows a plot of single photon detection efficiency versus dark count probability per bias pulse at various operating temperatures for this device. For a given detection efficiency, the dark count probability per bias pulse can be lowered by reducing the operating temperature. The best performance was obtained at 87K, where a detection efficiency of 13% was obtained at a dark count probability of 0.1%.
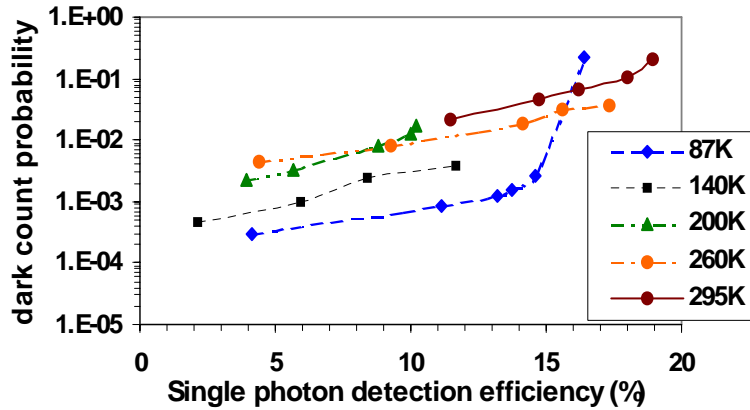
Figure 4.6:   Detection efficiency versus dark count probability for
In$_{0.53}$Ga$_{0.47}$As/In$_{0.52}$Al$_{0.48}$As APD.

Since the dark count rate decreases with reduced temperature for non-trap related dark counts, the device is generally cooled down to low temperatures. However, the performance of the detector also depends on the relative position of punchthrough voltage with respect to V_{br}. Punchthrough voltage is the bias at which the depletion layer starts to extend in the absorber. The detector must be operated above punchthrough to realize its best responsivity and speed. As temperature is reduced, the breakdown voltage of an APD decreases. However, the punchthrough voltage depends on integrated charge in the charge layer and is thus temperature independent. Hence the device will operate at a much reduced efficiency at lower temperature if it breaks down before the In$_{0.53}$Ga$_{0.47}$As absorber is fully depleted. This sets a lower limit to the operating temperature in some devices. For example, an In$_{0.53}$Ga$_{0.47}$As/InP APD from Fujitsu (FPD13W31RT) is found not to photon count below 150°C [4-2]. Reduction in temperature also increases the lifetime of trap centers thus worsening the afterpulsing effect. The after-pulsing effect is discussed in more detail later in section 4.4.
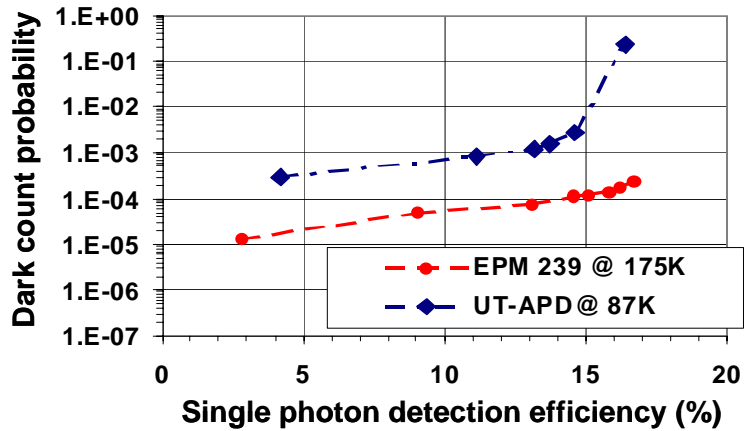
Figure 4.7:   Comparison between a commercial device and $In_{0.52}Al_{0.48}As/In_{0.53}Ga_{0.47}As$ APD.

Figure 4.7 shows the results of single photon counting using the $In_{0.53}Ga_{0.47}As/In_{0.52}Al_{0.48}As$ APD are compared with measurements for a commercial detector EPM239 from JDS Uniphase Inc. Both the devices have the same active area diameter of 40µm. The optimum temperature of operation for EPM 239 was determined to be 175K. Under optimum operating conditions, the dark count probability for the $In_{0.53}Ga_{0.47}As/In_{0.52}Al_{0.48}As$ device is an order of magnitude higher than that of EPM239. The dark count probability obtained with the $In_{0.53}Ga_{0.47}As/In_{0.52}Al_{0.48}As$ APD is very high for its use in applications. Improvements in the material quality and APD design are needed to improve its performance.

4.3   DISCRIMINATOR THRESHOLD

Discriminator threshold is an extremely important, but widely neglected parameter in single photon counting experiments. The discriminator level decides which current pulses at the output of an APD are counted as '1'. Setting it too high or too low

compromises the detector performance. For all the measurements in this study, the discriminator threshold was adjusted to minimize the noise equivalent power (NEP).

Figure 4.8 shows a plot of NEP as a function of discriminator threshold for a fixed operating temperature. At very low discriminator values, many noise pulses pass to the electronic counter thus increasing N_{dark} and the NEP. On the other hand, at very high discriminator threshold, not all signal pulses are counted and so SPDE reduces thus increasing NEP.
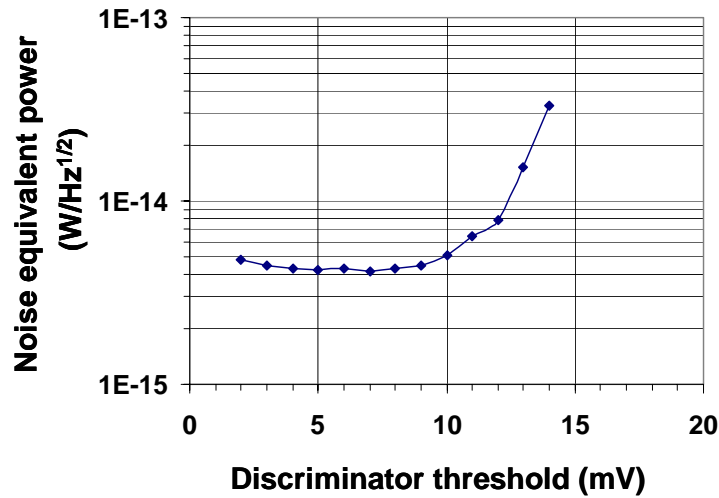
Figure 4.8:   Noise equivalent power versus discriminator threshold. T = 170K and V_{excess} = 0.7V.

4.4   REPETITION RATE

During the avalanche current flow, the trap centers in the depletion region capture some minority carriers that pass through the depletion layer. These trap centers are deep levels located between the mid gap and the band edges. The trapped charge is released

with a statistically fluctuating delay, which depends on the trap energy level and density. If this trapped charge is released during a subsequent gate pulse, it can lead to a self-sustaining avalanche and thus produce a dark count. These statistically correlated dark counts are called afterpulses.

During SPAD operation, the detector bias must be held below V_{br} for sufficient time (hold-off time) to allow the traps to discharge. One way to check if the hold-off time is long enough is to measure the dark count probability as a function of gate repetition rate. If the dark counts mainly arise from thermal generation-recombination, tunneling or diffusion, the dark count probability should not depend on the repetition frequency. Figure 4.9 is a plot of dark count probability as a function of repetition rate at 77K for a 75μm-diameter $In_{0.53}Ga_{0.47}As/In_{0.52}Al_{0.48}As$ APD. For a 2ns-wide pulse, the dark count rate in this device is independent of repetition rate up to 100kHz. As the pulse width increases, more charge flows through the device during the avalanche, which increases the probability of carrier capture by trap levels. Hence afterpulsing gets worse at lower repetition rates. The amount of charge flowing through the depletion layer also increases with excess bias. The dark count probability thus depends more strongly on gate repetition frequency for higher excess bias.
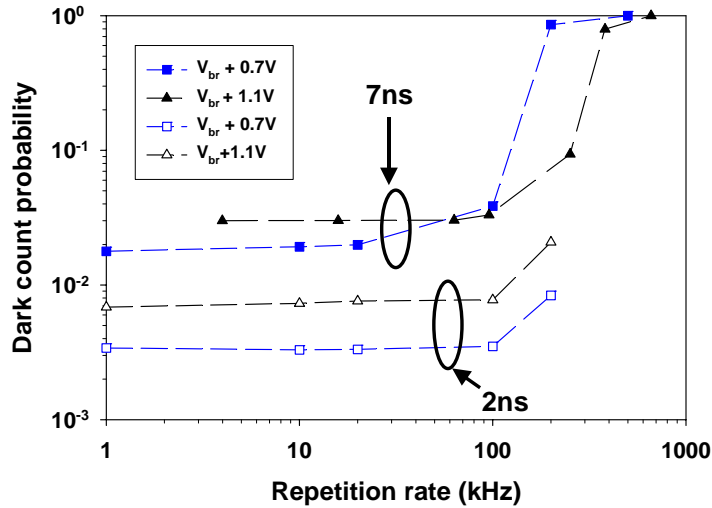
Figure 4.9: Dark count probability as a function of repetition frequency for ac pulse widths of 2ns and 7ns. T = 77K and device diameter = 75 μm.

Note that the deep levels involved in the afterpulsing effect are minority carrier traps. Capture of majority carriers in the depletion layer results in the shift of V_{br} [4-5].

4.5   PULSE WIDTH

In the gated mode operation, the avalanche current is quenched by the end of the gate pulse. Figure 4.10 shows the effect of gate width on dark counts for different excess biases. Dark counts increase with increasing pulse width due to following reasons:

1. For a long width of the pulse, more than one event may be detected at the output. For this to occur, after the first avalanche the APD bias must quench to a value below V_{br}, and then recharge back to $V_{applied}$ before the end of the gate pulse, as shown in Figure 4.11. With $R_L = 33k\Omega$ and $(C_s+C_d) \sim 2pf$, the recharge time is expected to be ~ 70 nanoseconds. This possibility is less likely in the current measurements since a maximum pulse width of 10ns was used.

62

2. For longer pulse width, the avalanche current flows through the device for a longer time before it is quenched. This increases the probability of some of this charge getting captured by the trap centers. Hence dark counts may increase with the pulse width due to increased afterpulsing. However, in this experiment, the repetition rate was kept at 500Hz. Afterpulsing was negligible at these frequencies as shown in Figure 4.12.

3. Let P' be the probability of dark carrier generation in the depletion layer per unit time at a given temperature and excess bias. During time τ_{ac} of the pulse width, the number of dark carriers passing through the depletion layer are P'τ_{ac}. For longer pulse width, the number of primary carriers crossing the depletion layer increases and so does the probability of dark counts. This is the most likely reason for the observed increase of dark counts with pulse width shown in Figure 4.10.

In the gated mode operation, where the APD bias is raised above breakdown only when a photon is expected at the input, it is better to keep the pulse width as narrow as possible.
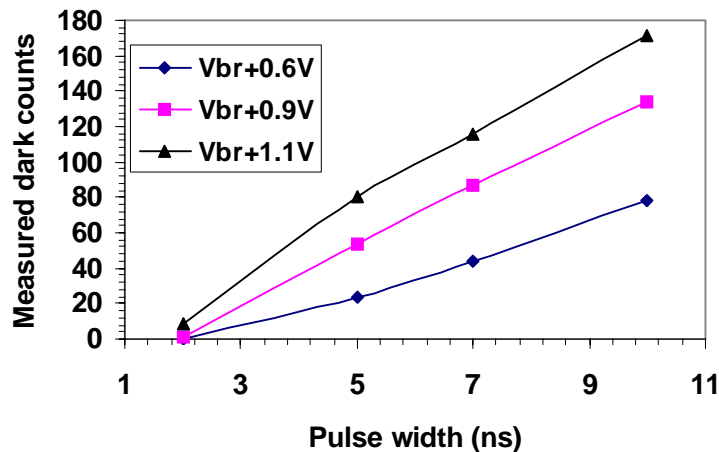
Figure 4.10: Effect of pulse width on dark counts. T = 295K, diameter = 40 μm and repetition rate = 500Hz.
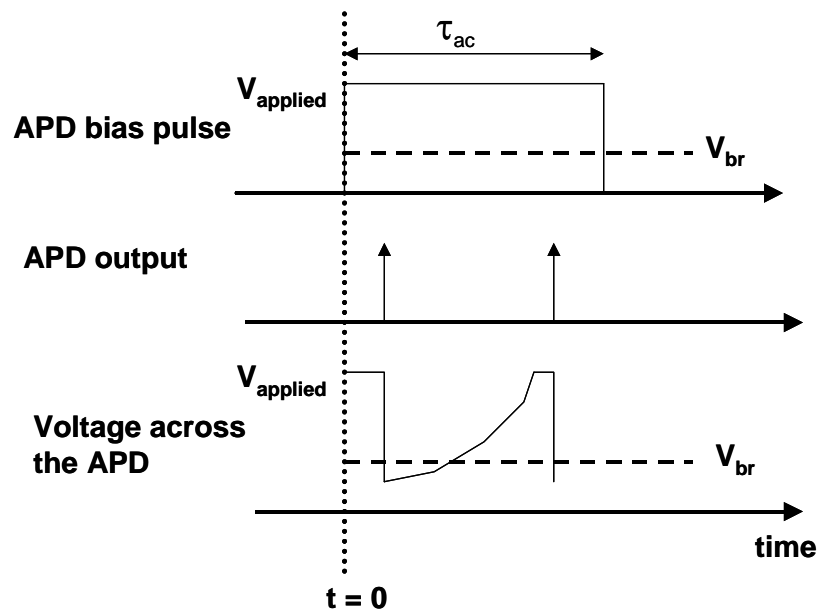
Figure 4.11: Detection of multiple events during a gate.
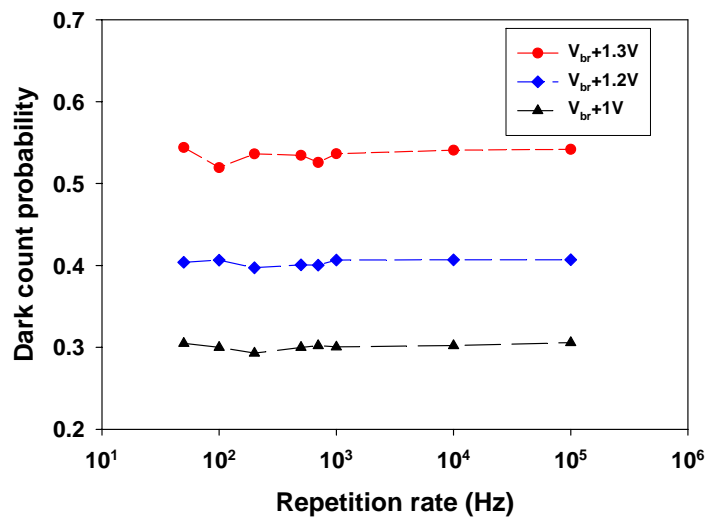
Figure 4.12: Dark count probability versus repetition rate for ac pulse width = 10ns. T = 295K.

In summary, operating parameters of a Geiger mode APD greatly influence its performance. The effect of parameters such as temperature, excess bias, repetition rate, bias pulse width and discriminator threshold were discussed in this chapter using photon counting measurements on an $In_{0.53}Ga_{0.47}As/In_{0.52}Al_{0.48}As$ APD. A set of optimum operating parameters was identified for this device. These parameters are: T = 80K, discriminator threshold = 10mV and excess bias = 0.7V. The highest single photon detection efficiency of 13% was obtained for a dark count probability of 10^{-3}. A similar series of experiments needs to be performed for each new detector to optimize the operation parameters.

References:

[4-1] Karve G., Zheng X., Zhang X., Li X., Li N., Wang S., Ma F., Holmes A. Jr., Campbell J.C., Kinsey G.S., Boisvert J.C., Isshiki T.D., Sudharsanan R., Bethune D.S., and Risk W.P., "Geiger mode operation of an $In_{0.53}Ga_{0.47}As$-$In_{0.52}Al_{0.48}As$ avalanche photodiode", *IEEE Journal of Quantum Electronics*, vol. 39, pp. 1281 (2003).

[4-2] D. Stucki, G. Ribordy, A. Stefanov, H. Zbinden, J. G. Rarity, and T. Wall, "Photon counting for quantum key distribution with Peltier cooled InGaAs/InP APDs," *J. Modern Optics*, vol. 48, no. 13, pp. 1967-1981 (2001).

[4-3] A. Lacaita, F. Zappa, S. Cova, and P. Lovati, "Single-photon detection beyond 1 µm: performance of commercially available InGaAs/lnP detectors", *Appl. Optics*, vol. 35, no. 16, pp. 2986-2996, (1996).

[4-4] G. Vincent, A. Chantre and D. Bois, "Electric field effect on the thermal emission of traps in semiconductor junctions", *J. Appl. Phys.*, vol. 50, no. 8, pp. 5484-5487 (1979).

[4-5] A. Lacaita, F. Zappa, S. Cova, P. Lovati, "Single-photon detection beyond 1 mu m: performance of commercially available InGaAs/InP detectors", *Appl. Optics*, vol. 35, no. 16, pp. 2986-2996 (1996).

Chapter 5   Temperature Characterization of $In_{0.53}Ga_{0.47}As/In_{0.52}Al_{0.48}As$ Avalanche Photodiodes

The operating temperature (T) of an avalanche photodiode (APD) affects its properties such as the breakdown voltage (V_{br}) and the dark current. Study of APD properties at different temperatures reveals very interesting physics. Studying these effects is also important for better understanding the low temperature operation of Geiger mode APDs. This chapter discusses the temperature dependence of some of the important APD parameters. Variation of the breakdown voltage with temperature is discussed in section 5.1. The dark current dependence on temperature is discussed in section 5.2. The temperature dependence of the punchthrough voltage, the excess noise factor and the gain-bandwidth product are described in section 5.3.

5.1   BREAKDOWN VOLTAGE

The breakdown in a pn junction can be explained by one of the three following mechanisms [5-1].

5.1.1   Thermal instability

At high reverse voltages, a large current passing through the junction increases the heat dissipation and thus the junction temperature. The reverse current through the junction increases in response to the increased temperature. This positive feedback effect, which destroys the junction, is referred to as thermal instability or thermal runaway.

5.1.2   Tunneling breakdown

At high electric fields, band to band tunneling in the semiconductors causes a large current flow through the device. The band gap of semiconductors decreases with

increasing temperature. At higher temperatures, a given value of tunneling current is achieved at smaller voltages. Hence tunneling V_{br} decreases with increasing temperature. The negative temperature coefficient of breakdown voltage is a signature of tunneling breakdown. Breakdown voltage due to impact ionization, on the other hand, has a positive coefficient of V_{br} change with T, as explained in section 5.1.3. The temperature dependence of V_{br} is generally used to distinguish the tunneling mechanism from avalanche breakdown.

Tunneling and impact ionization are two competing breakdown mechanisms in a pn junction. The dominant mechanism is determined by the doping, the thickness of active layers, and band gap energy, etc. A separate-absorption-charge-multiplication (SACM) structure must be carefully designed to avoid tunneling breakdown. As an example, consider the SACM structure shown in Figure 5.1. The charge layer doping ($4 \times 10^{17}/cm^3$) was chosen in the original design to achieve a punchthrough voltage close to 17V and a breakdown close to 30V by avalanche multiplication.

InGaAs, p^+ -1×10^{19}, 30nm Contact
InAlAs, p^+ -1×10^{19}, 200nm
InGaAlAs, un-doped, 50nm Transition
InGaAs, p-4×10^{17}, 50nm
InGaAs, p-2×10^{17}, 100nm
InGaAs, p-1×10^{17}, 300nm
InGaAlAs, un-doped, 50nm Transition
InAlAs, un-doped, 100nm
InAlAs, p-4×10^{17}, 55nm Charge
InAlAs, un-doped, 500nm Multiplication
InP, n-5×10^{18}, 800nm Buffer
InP, n+, Substrate

Absorber (InGaAs p-4×10¹⁷, p-2×10¹⁷, p-1×10¹⁷ layers)

Intended charge layer doping → InAlAs p-4×10¹⁷ Charge

Charge layer ← InAlAs, p-4×10¹⁷, 55nm Charge

Multiplication layer ← InAlAs, un-doped, 500nm Multiplication

Figure 5.1:   Schematic of an SACM APD design.

67
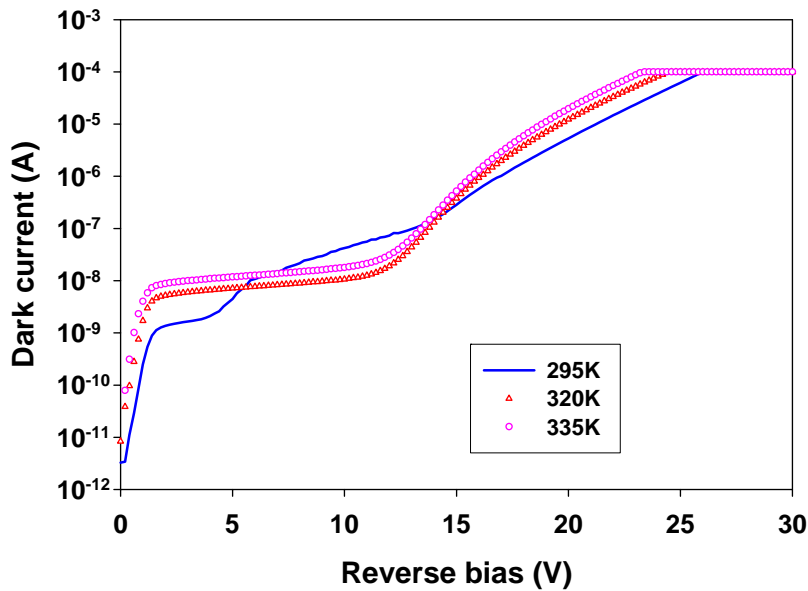
Figure 5.2: Dark current-voltage at different temperatures for the device shown in Figure 5.1.

The current-voltage characteristics for this device at different temperatures are shown in Figure 5.2. As the temperature increased, the breakdown voltage decreased, indicating tunneling related breakdown, which was unexpected according to the original design. At room temperature, the breakdown occurred at much smaller voltage than that expected for the avalanche breakdown. The room temperature dark current for this device was modeled using band-to-band tunneling in the InGaAs absorber. As shown in Figure 5.3, the observed dark current was explained well by this model. The fit was obtained using a background doping of $5.8 \times 10^{15}/cm^3$ in the absorber.

Secondary ion mass spectroscopy (SIMS) analysis of this device indicated the doping in the charge layer was $1.8 \times 10^{17}/cm^3$, as opposed to $4 \times 10^{17}/cm^3$ in the original design. Due to the smaller doping in the charge layer, the punchthrough occurred at very

68

low voltage of 2.5V, as shown in Figure 5.4, in the photo response of the device. After punchthrough, the depletion layer extended into the absorber thus increasing the electric field in the absorber. At 15V, the electric field in the absorber was 230kV/cm, which is higher than the field required for tunneling in InGaAs. Hence band-to-band tunneling occurred in InGaAs layer before avalanche multiplication could take place in the multiplication layer.
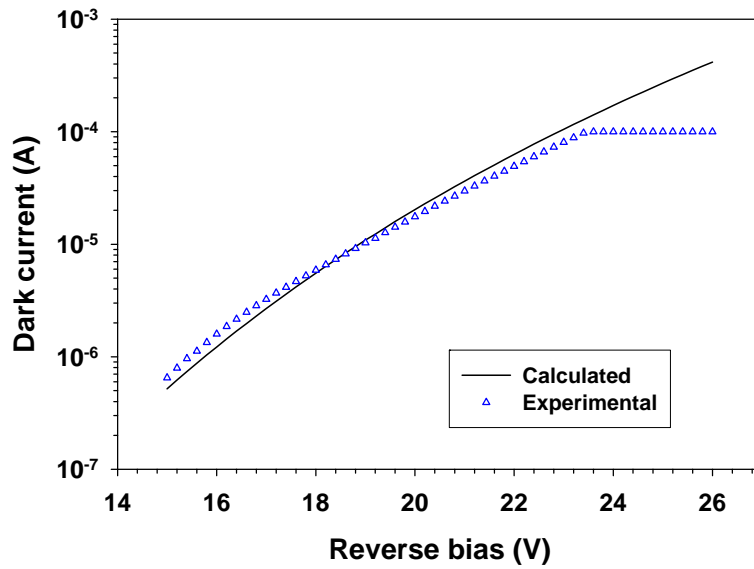
Figure 5.3:   Calculated tunneling current in InGaAs, for the device shown in Figure 5.1. Charge layer doping of $1.8 \times 10^{15}/cm^3$, obtained using SIMS analysis, was used in the calculation.
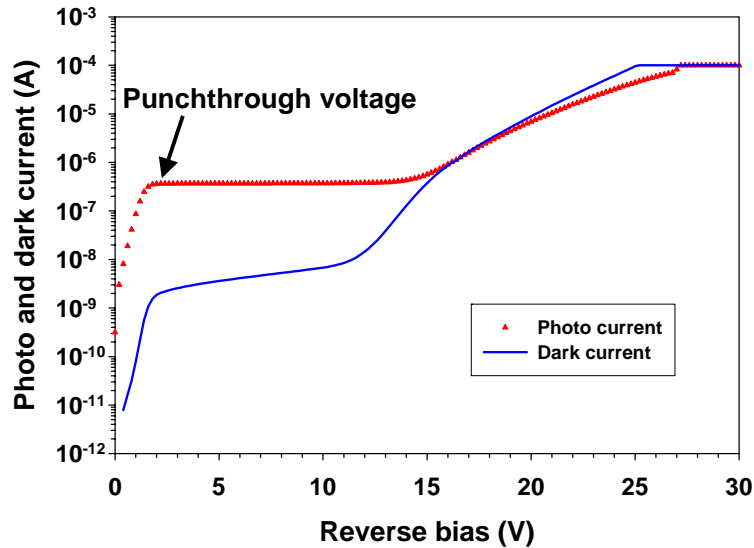
Figure 5.4:   Photo and dark current for the device shown in Figure 5.1.

5.1.3   Avalanche breakdown

The dependence of avalanche breakdown voltage on temperature is through that of the impact ionization coefficients. The impact ionization process depends on temperature primarily via scattering from optical phonons. The temperature dependence for the impact ionization coefficients has been thoroughly studied for a variety of materials such as AlGaAs, InGaAs, Si, Ge, etc [5-2, 5-3]. When a carrier moves through the depletion region under the action of an electric field, it gains energy from the field and can impact ionize. It also looses energy to phonons by scattering. A decrease in temperature reduces the phonon scattering rate. Therefore at lower temperature, a given value of multiplication is obtained at smaller biases and the breakdown voltage decreases. Thus the breakdown voltage due to avalanche multiplication exhibits a positive coefficient of V_{br} change with temperature.

70

For a correctly designed SACM structure, the breakdown should result from impact ionization in the multiplication layer. Figure 5.5 shows schematic of an APD structure. The structure and linear mode properties of this APD were discussed in detail in Chapter 2. The current-voltage characteristics (IVs) at different temperature for this device are shown in Figure 5.6. It can be seen that V_{br} increases with increasing temperature, thus indicating an avalanche breakdown. The plot of V_{br} as a function of temperature is shown in Figure 5.7. The coefficient of V_{br} change with temperature for this device is 15.5 mV/K. This coefficient depends on the material and the thickness of the depletion layer. The rate of change of V_{br} is smaller for thinner structures because a thinner device has higher breakdown field and so the carriers experience fewer phonon scattering events [5-4]. One advantage of a small change in V_{br} with temperature is that the difference between the punchthrough voltage and V_{br} is high even at lower temperatures, thus ensuring the complete depletion of the absorber at breakdown. Note that the change in breakdown voltage is slower at temperatures lower than 50K, as shown in Figure 5.7. The reason for this is as follows [5-2]. The average phonon number in a mode, $<n_q>$, depends strongly on temperature. The phonon absorption rate is proportional to $<n_q>$, where as the phonon emission rate is proportional to $<n_q>+1$. At low temperatures as $<n_q>$ approaches zero, both phonon absorption and stimulated emission rates approach zero and the dominant scattering mechanism is the spontaneous emission. Spontaneous emission does not depend explicitly on $<n_q>$ and on temperature, and hence the phonon scattering rate saturates at lower temperatures.

p+: InGaAs 9×10^{18}, 50nm
p+: InAlAs 5×10^{18}, 300nm
i: InGaAlAs Transition, 50nm
i: InGaAs, 1000nm ← Absorber
i: InGaAlAs Transition, 50nm
i: InAlAs Spacer, 50nm
p: InAlAs , , 3×10^{17}, 200nm ← Charge layer
i: InAlAs , 400nm ← Multiplication region
n+: InAlAs , 5×10^{18}, 100nm
n+: InP , 5×10^{18}, 500nm
n+ InP Substrate
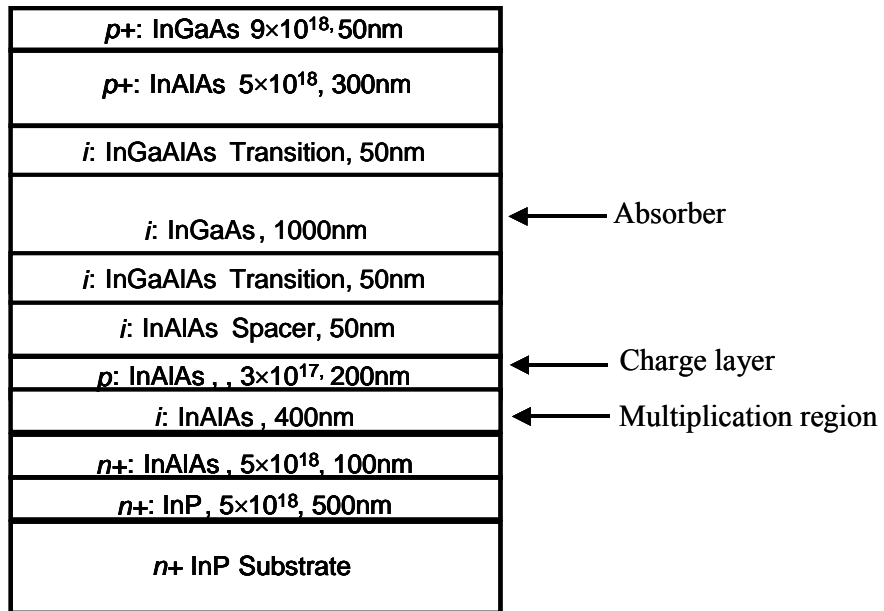
Figure 5.5:   Schematic of an SACM APD.
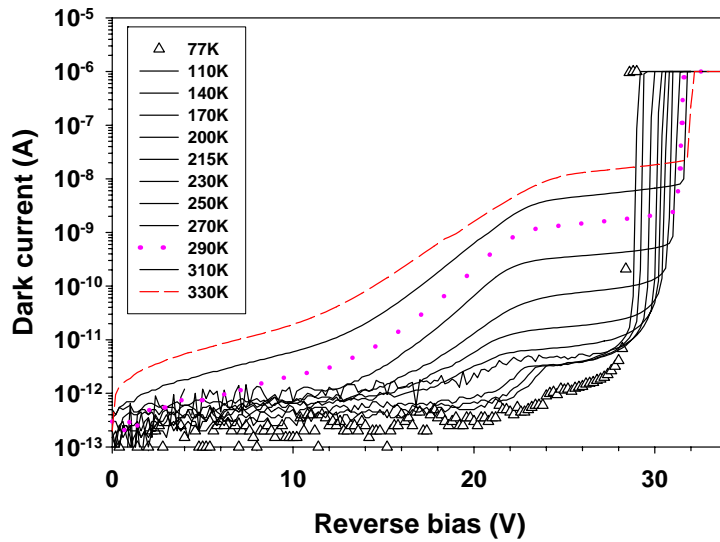
Figure 5.6:   Dark current-voltage for the SACM APD in Figure 5.5.
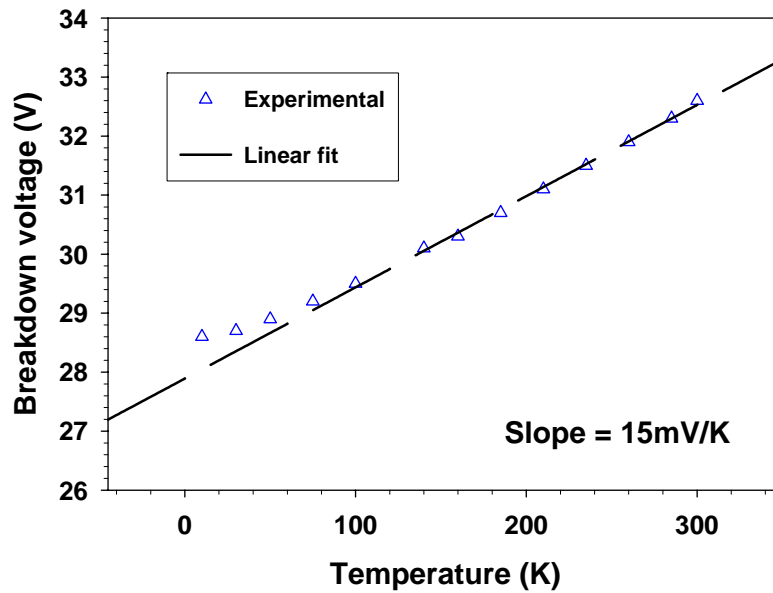
Figure 5.7: Breakdown voltage as a function of temperature for the SACM APD shown in Figure 5.5.

5.2   DARK CURRENT

5.2.1   Reverse bias operation

Dark current generation mechanisms in an APD have been studied thoroughly by various researchers [5-5]. A brief description of the primary dark current mechanisms in the reverse bias operation of the diode and their temperature dependences are described in the following sections.

5.2.1.1 Diffusion from the neutral region

The current due to diffusion from quasi-neutral p and n regions is proportional to n_i^2, where n_i is the intrinsic carrier density, which depends exponentially on E_g, where E_g is the band gap of the quasi-neutral layer.

73

$$I_{d,diffusion} \propto \exp\left(-E_g / kT\right) \tag{5.1}$$

where k is the Boltzman constant.

5.2.1.2 Generation-recombination in the depletion layer

The generation recombination current is given as $\dfrac{q \cdot n_i \cdot W}{\tau_{eff}}$. Here, W is the

depletion layer width and τ_{eff} is the minority carrier lifetime. Contributions from the absorber, the charge and the multiplication layer must be added, taking into account the gain in each layer. The temperature dependence of this component is exp(-E_g/2kT) for generation-recombination through traps close to the midgap [5-1].

$$I_{d,g-r} \propto \exp\left(-E_g / 2kT\right) \tag{5.2}$$

5.2.1.3 Tunneling current

The tunneling current contribution is given by

$$I_{d,tunneling} = \gamma \cdot \exp\left[\frac{-\pi \cdot \sqrt{m_0 \cdot m* \cdot E_g^{3/2}}}{4 \cdot \hbar \cdot e \cdot E}\right] \tag{5.3}$$

where, $\gamma = const \cdot E \cdot V$

E is the electric field, V is the applied bias, m* is the tunneling mass of the carriers, E_g is the bandgap and $\hbar$ = plank's constant/(2π). For trap assisted tunneling, E_g should be replaced by E_t, the tunneling barrier. The tunneling current depends on temperature primarily through the band gap of the material.

5.2.1.4 Surface leakage

Extraction of the surface leakage current was discussed in Chapter 2. The temperature dependence of surface leakage is similar to that of the generation-

recombination current [5-6]. The activation energy for this mechanism depends on the types of surface traps involved.

5.2.1.5 Shunt current

Shunt current occurs due to an effective resistance (R_s) of the diode. This component of current dominates at low temperature and low bias.

The experimental activation energy can be used to identify the dominant mechanism. The temperature dependence of the total dark current at a given voltage, V, can be written as

$$I_d(T) = A \cdot \exp(-\frac{E_a}{k \cdot T}) \tag{5.4}$$

where, $I_d(T)$ is dark current at temperature T, A is a temperature independent constant, and E_a is the activation energy. The slope of the natural logarithm of I_d versus $1/kT$ plot yields E_a, as shown in Figure 5.8.
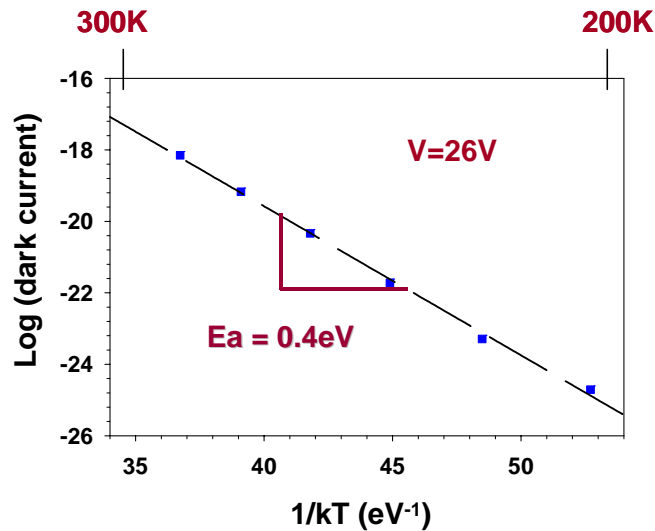
Figure 5.8: Extraction of activation energy from IV characteristics. APD structure is shown in Figure 5.5.

For the SACM APD shown in Figure 5.5, for a broad range of voltages above the punch through value, the activation energy was estimated to be 0.4eV. This points to generation-recombination in $In_{0.53}Ga_{0.47}As$ as the major mechanism for dark current. However, it is possible that other mechanism not considered here, such as, interfacial traps, surface leakage or deep traps could have contributions to the dark current as well.

5.2.2 Forward bias

The diode current in forward bias is given by the following expression,

$$I_{forward} = I_0 \cdot \left(\exp^{qV/nkT} - 1 \right) \qquad (5.5)$$

where q is the electronic charge, k is the Boltzman constant and n is the diode ideality factor. Figure 5.9 shows the diode forward IV characteristics at different temperatures. As temperature decreases the diode turns on at higher voltages due to the increased contact potential.
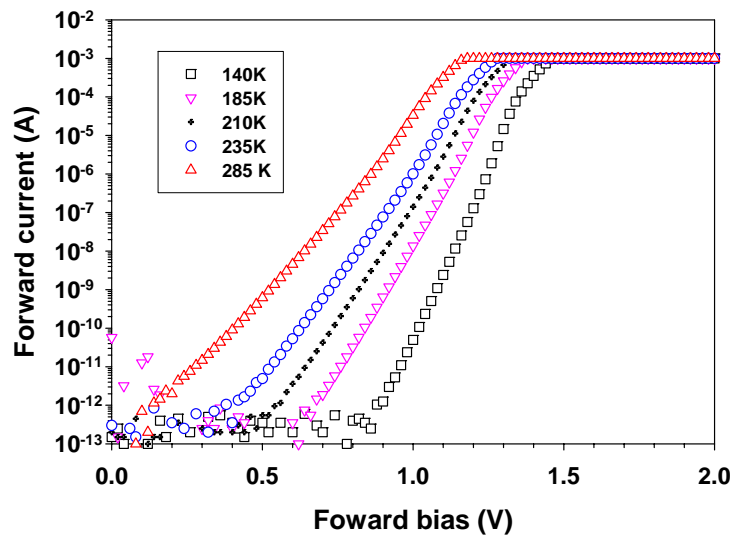
Figure 5.9:   Forward IV characteristics at different temperatures for an SACM APD.

76
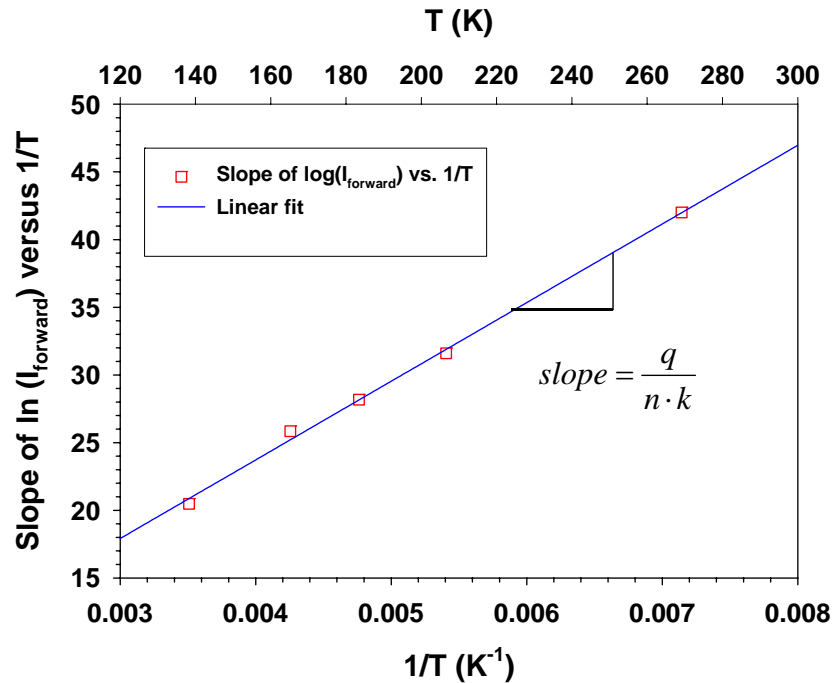
Figure 5.10: Dependence of slope of forward IV plot on temperature.

Taking the log of equation (5.5) yields the expression

$$\ln\left(I_{forward}\right) = \ln\left(I_o\right) + \frac{q}{n \cdot k \cdot T} \cdot V \tag{5.6}$$

At a given temperature, a plot of natural log of current versus voltage exhibits a slope of q/nkT (equation 5.6). As expected, the slope decreases linearly with temperature as shown in Figure 5.10.

5.3   PUNCHTHROUGH VOLTAGE, NOISE AND GAIN-BANDWIDTH PRODUCT

The punchthrough voltage of a diode depends only on the doping and thickness of the layers, both of which are not expected to change significantly with temperature in the range of temperatures considered here [5.1]. Even if we consider "dopant freezing" at low temperature as a possibility, a decrease in the doping should reduce the punchthrough voltage. However, the punchthrough voltage increases at lower T, as shown in Figure

5.11. The data plotted in Figure 5.11 is for the APD described in Figure 5.5. The reason for an increase of punchthrough voltage at low T could be the following. As the temperature decreases the carriers have less thermal energy and hence a slightly higher electric field is needed at the interface for punchthrough to occur [5.7].
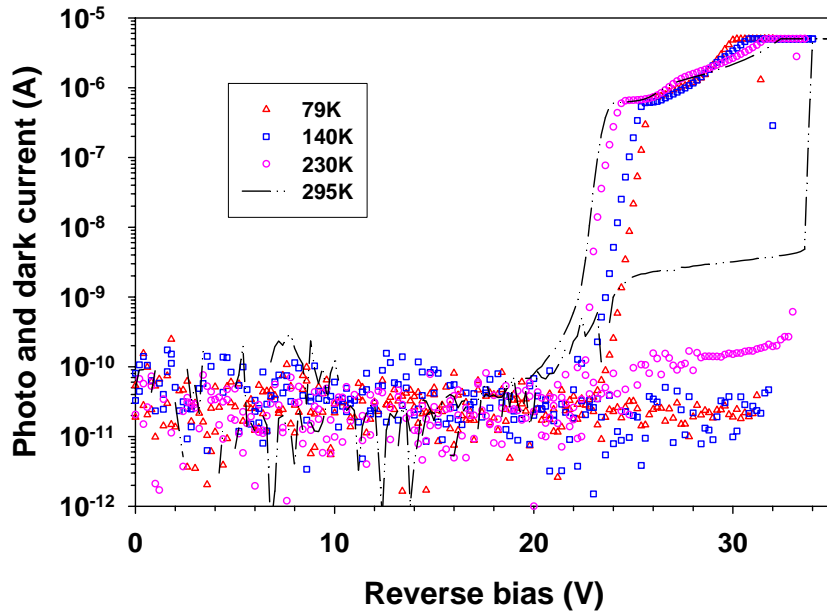
Figure 5.11: Photo and dark current as a function of voltage at different temperatures for the SACM APD shown in Figure 5.5.

The excess noise and the gain-bandwidth (GB) product of an APD also depend on temperature. Measurements of the excess noise factor at different temperatures have revealed that the noise decreases slightly at lower temperatures [5.8]. One possible explanation is that the electric field in the multiplication layer is higher at higher temperatures. At higher electric fields, the difference between ionization coefficient of electrons and holes is smaller thus resulting in higher noise. The gain-bandwidth product of an APD improves as the temperature is lowered [5.7].

78

In summary, in this the temperature dependence of various APD properties was discussed. The importance of proper design of the SACM APD was illustrated. The dark current, punchthrough voltage, noise and GB product dependence on temperature was also described.

References:

[5-1] S. M. Sze, *Physics of semiconductors*, Wiley-interscience publication, 2nd edition.

[5-2] F. Ma.; G. Karve, X. Zheng; X. Sun, A. L. Holmes, J. C. Campbell, "Low-temperature breakdown properties of $Al_xGa_{1-x}As$ avalanche photodiodes", *Appl. Phys. Lett.*, vol. 81, pp. 1908 (2002).

[5-3] M. Yee, W. K. Ng, J. P. R. David, P. A. Houston and C. N. Harrison, "Negative temperature dependence of electron multiplication in InGaAs", **",** *Appl. Phys. Lett.,* vol. 82,no. 8, pp.1224 (2003).

[5-4] J. P. R. David, S. A. Plimmer, G. J. Rees and R. Grey, "Temperature dependence of avalanche breakdown in GaAs p-i-n diodes", *Third European Conference on High Temperature Electronics, Abingdon, UK*, pp. 187-90 (1999).

[5-5] S.R. Forrest, O. K. Kim and R. G. Smith, "Analysis of the dark current and photoresponse of InGaAs/InP avalanche photodiodes", *Solid Sate Electron.*, vol. 26, no. 10, pp. 951-968 (1983).

[5-6] O. K. Kim, B. V. Dutt, R. J. Mccoy and J. R. Zubur, "A low dark-current, planar InGaAs p-i-n photodiode with a quaternary InGaAsP cap layer", *J. Quantum Electron.*, vol. QE-21, no. 2, pp. 138-143 (1985).

[5-7] J. Yu, L. E. Tarof, T. Baird, D. McGhan, R. Bruce and D. G. Knight, "Temperature characterization of separate absorption, grading, charge and multiplication InP/InGaAs avalanche photodiode", *Proc. SPIE*, vol. 2149, pp. 302-310 (1994).

[5-8] Y. Takanashi and Y. Horikoshi, "Noise performance of 1.3 μm InGaAsP avalanche photodiode at -190 degrees C", *Japanese Journal of Applied Physics*, vol.19, no.3, pp. L163-6 (1980).

Chapter 6   Origin Dark Counts in a Geiger mode Avalanche Photodiode

Avalanche photodiodes (APDs) operated above their breakdown voltage can achieve single photon detection sensitivity [6-1], [6-2]. Single photon avalanche detectors (SPADs) with an $In_{0.53}Ga_{0.47}As$ absorbing layer are of interest for photon counting at the telecommunication wavelengths [6-3], [6-4], [6-5]. However, operation at these wavelengths is severely limited by high dark count rate, i.e. the spurious counts that are registered at the output in the absence of light. Detection of such false counts results in an underestimation of the photon detection efficiency as well as higher noise of an SPAD. In order to minimize the dark counts it is necessary to identify the mechanisms that give rise to them. This chapter discusses the origin of dark counts in SPADs. The commonly considered dark count generation mechanisms are discussed in section 6.1. These mechanisms are diffusion from quasi-neutral regions, generation-recombination in the depletion layer, band-to-band tunneling, trap-assisted tunneling and surface generation-recombination. The distinctive dependence of each of these effects on temperature can be used as distinguishing signatures. Temperature dependence of the experimental dark count rate for an $In_{0.53}Ga_{0.47}As/In_{0.52}Al_{0.48}As$ Geiger mode APD is described in section 6.2. The observed experimental data was explained using band-to-band tunneling in the $In_{0.52}Al_{0.48}As$ multiplication layer. The modeling results are explained in section 6.3.

6.1   CONTRIBUTIONS TO THE DARK COUNT RATE IN AN SPAD

Figure 6.1 shows a simplified separate-absorption-charge-multiplication (SACM) structure. Let d_1, d_2 and d_3 be the thickness of the absorber, the charge layer and the multiplication layer, respectively. A practical SACM APD structure also contains

quaternary InAlGaAs grading layers and the n type buffer layer as explained in Chapter 3. For simplicity, these layers are ignored in the following discussion. The origin, x=0, is the interface between the p+ contact and the absorber layer. The electric field in the device was calculated by solving Poisson's equation with appropriate boundary conditions [6-6]. In single photon counting experiments, the APD is operated above its breakdown voltage (V_{br}). Above V_{br}, there is a finite probability, called the breakdown probability (P_{br}), that a carrier will cause a self-sustaining avalanche. P_{br} is a function of the electric field profile and the position, x, in the device. From the calculated electric field profile, P_{br} can be estimated as a function of x using McIntyre's model [6-7], [6-8]. Figure 6.2 shows P_{br} as a function of x for the simplified SACM APD structure.

n+: n contact, M: multiplication layer, C: charge layer
A: absorber, p+: p contact.
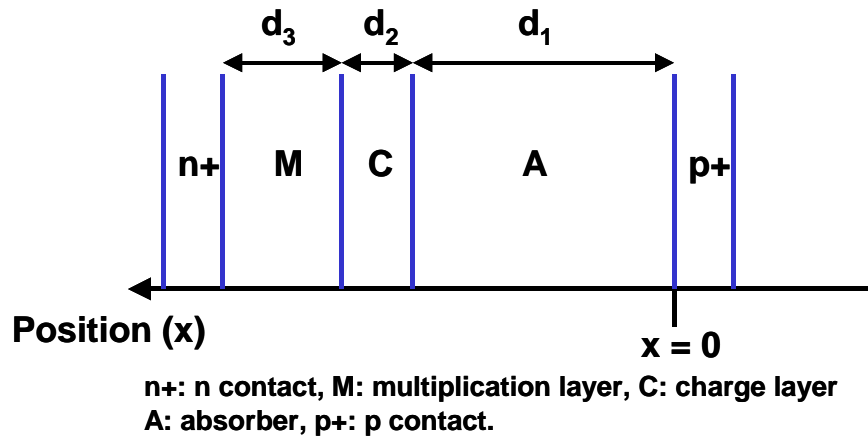
Figure 6.1: Simplified SACM APD structure. d_1, d_2 and d_3 are thickness of the absorber, the charge and multiplication layer respectively.
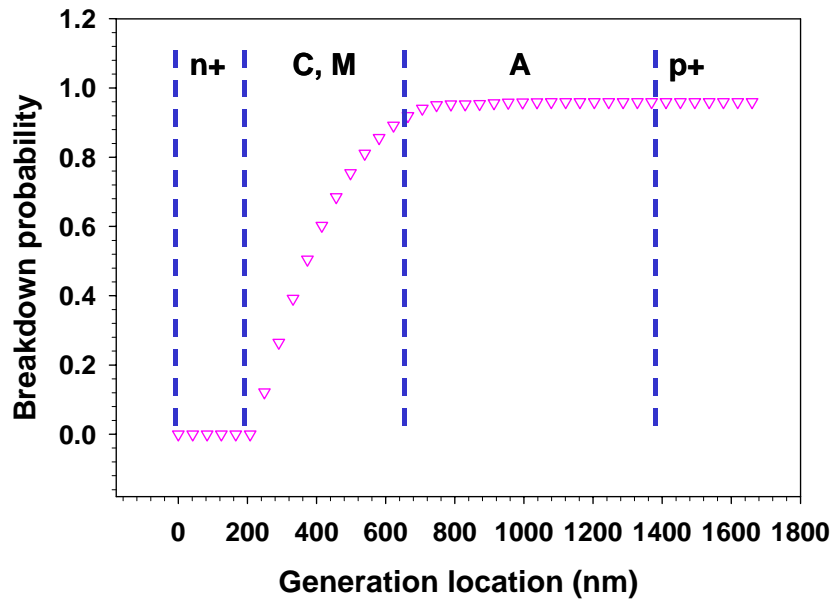
Figure 6.2:   Breakdown probability as a function of generation position for the simplified SACM APD structure. M: multiplication layer, C: charge layer and A: absorber layer.

The various dark count generation mechanisms in an SPAD are described in the subsequent sections.

6.1.1. Diffusion from the neutral region

Due to high doping levels, the electric field in the p+ and n+ quasi-neutral layers is very small. Any carriers generated in these layers can enter the multiplication or absorption layer only by diffusion. The diffusion component is usually very small and can be neglected. The temperature dependence of this component is $\exp(-E_g/kT)$, where E_g is the band gap of the quasi-neutral layer, k is the Boltzman's constant, and T is the absolute operating temperature.

6.1.2. Generation-recombination in the absorber layer

Carriers generated due to generation-recombination in InGaAs drift to the multiplication layer and give rise to the dark counts ($N_{d,abs}$)

$$N_{d,abs} = \int_{0}^{d_1} P_e(x)dx \cdot \frac{q.A \cdot n_{i,abs} \cdot d_1}{\tau_{eff,abs}}$$
(6.1)

where, $P_e(x)$ is the breakdown probability for an electron at position x, $n_{i,abs}$ is the intrinsic carrier concentration in InGaAs, $\tau_{eff,abs}$ is the minority carrier lifetime in the absorber, A is the cross-sectional area of the device and q is the electronic charge.

6.1.3. Generation-recombination in the charge layer

The contribution to dark counts from the charge layer is $N_{d,charge.}$

$$N_{d,charge} = \int_{d_1}^{d_1+d_2} P_e(x)dx \cdot \frac{q.A \cdot n_{i,charge} \cdot d_2}{\tau_{eff,charge}}$$
(6.2)

where, $P_e(x)$ is the breakdown probability for an electron at position x, $n_{i,charge}$ is the intrinsic carrier concentration in InAlAs, and $\tau_{eff,charge}$ is the minority carrier lifetime in the charge layer.

In equations (6.1) and (6.2), the breakdown probability for only electrons generated in the absorber and charge layer is considered since the holes generated in these layers move toward the p-contact, away from the multiplication layer.

6.1.4. Recombination in the multiplication layer

The dark counts arising from generation-recombination in the multiplication layer are given by the following expression.

$$N_{d,mul} = \int_{d_1+d_2}^{d_1+d_2+d_3} P_{eh}(x) \cdot \frac{q.A \cdot n_{i,mul}}{\tau_{eff,mul}} dx$$
(6.3)

where, $P_{eh}(x) = P_e(x) + P_h(x) - P_e(x)P_h(x)$
(6.4)

$P_{eh}(x)$ is the probability of breakdown by an electron-hole pair, $n_{i,mul}$ is the intrinsic carrier concentration in InAlAs, and $\tau_{eff,mul}$ is the minority carrier lifetime in the multiplication layer. The temperature dependence of generation-recombination components is mainly through that of the intrinsic carrier concentration, n_i. It depends exponentially on $E_g/2kT$.

6.1.5. Tunneling in the multiplication layer

Due to the high electric field in the multiplication layer, the electrons can tunnel from the valance band to the conduction band thus contributing to the dark count rate. The counts due to tunneling in the multiplication layer are given by $N_{d,tunneling}$.

$$N_{d,tunneling,mul} = \int_{d_1+d_2}^{d_1+d_2+d_3} P_{eh}(x)dx \cdot \gamma \cdot E(x) \cdot \exp[\frac{-\pi \cdot \sqrt{m_0 \cdot m_{InAlAs}}^* \cdot E_{g,InAlAs}^{3/2}}{4 \cdot \hbar \cdot e \cdot E(x)}] \qquad (6.5)$$

where, $\gamma = const \cdot V$

E is the electric field in the multiplication layer, m_{InAlAs}* is the electron effective mass, $E_{g,InAlAs}$ is the band gap of InAlAs, and $\hbar$ = Plank's constant/2π. The temperature dependence of tunneling is through that of the band gap of InAlAs.

Tunneling can also occur through energy states within the forbidden gap. The functional form of the tunneling expression is similar to equation (6.5). However the energy required for trap assisted tunneling is less than that of the band gap of the material.

6.1.6. Tunneling in the absorber

The dark counts due to tunneling in InGaAs are given by

$$N_{d,tunneling,abs} = \int_{0}^{d_1} dx P_e(x) \cdot \gamma \cdot \exp[\frac{-\pi \cdot \sqrt{m_0 \cdot m_{InGaAs}}^* \cdot E_{g,InGaAs}^{3/2}}{4 \cdot \hbar \cdot e \cdot E(x)}] \qquad (6.6)$$

where, $\gamma = const \cdot E \cdot V$

E is the electric field in the absorber, m_{InGaAs}^* is the electron effective mass, and $E_{g,InGaAs}$ is the bandgap of InGaAs.

6.1.7. Surface leakage

As explained in Chapter 3, the surface leakage of component of the dark current is not multiplied. At high multiplication factors above V_{br}, this component can be neglected if the electric field at the surface is small. Two dimensional electric field profiles could be calculated for a structure to confirm this.

6.2 EXPERIMENTAL INVESTIGATION OF ACTIVATION ENERGY FOR DARK COUNTS

The dark count rate obtained for an $In_{0.53}Ga_{0.47}As/In_{0.52}Al_{0.48}As$ SPAD is analyzed in this section. The structure consists of a 400nm thick multiplication layer, a 200nm thick charge layer and a 1000nm thick absorber. The structure and the photon counting results for this device can be found in Chapter 4. The absolute counts obtained in an experiment depend on the quenching method and experimental parameters, as explained in Chapter 2 and Chapter 4. However, the temperature dependence of dark counts obtained using any quenching method should still reflect the dominant mechanism. All the data discussed in this chapter was obtained by operating the APD in the gated mode. The details of the experimental set up can be found in Chapter 2. The dark count rate, which is expressed in number/second is the number of dark counts measured when the detector has a cumulative bias above breakdown voltage for 1 second. For a detector operated in the gated mode, the measured dark counts, $M_{d,measured}$, were converted into the

dark count rate, N_d, by dividing the measured dark counts by the fraction of time for which the detector was above breakdown voltage. The expression for N_d is

$$N_d = \frac{M_{d,measured}}{\tau \cdot n_s} \tag{6.7}$$

where τ is the pulse width and n_s is the number of bias pulses in one second.

Each contribution to the dark count rate has a distinguishing dependence on temperature. The temperature dependence of the total dark count rate can be expressed as

$$N_d(T) = A \cdot \exp(-\frac{E_a}{k \cdot T}) \tag{6.8}$$

where, $N_d(T)$ is dark count rate at temperature T, A is a temperature independent constant, E_a is the activation energy and k is the Boltzman's constant. The slope of the plot of natural logarithm of N_d versus $1/kT$ is E_a. The value of the activation energy can be used to identify the responsible mechanism.
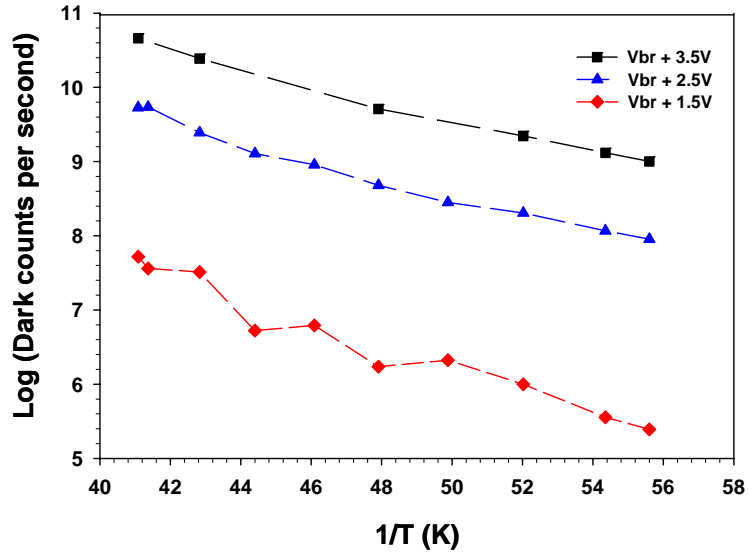
Figure 6.3:   Dark count rate as a function of 1/kT for different excess voltages for $In_{0.53}Ga_{0.47}As$ / $In_{0.52}Al_{0.48}As$ APD.

Figure 6.3 shows an Arrhenius plot of dark count rate at different excess voltages for an $In_{0.53}Ga_{0.47}As$ / $In_{0.52}Al_{0.48}As$ Geiger mode APD. These values of excess bias yield

single photon detection efficiencies in the range ~ 10-15%. Since the dark counts exhibit an exponential dependence on temperature, the activation energy can be extracted from the slope of the above plot. The activation energies obtained from the plots range from 0.12 to 0.15eV for excess bias of 3.5V to 1.5V. Figure 6.4 shows the estimated temperature dependence of various mechanisms.
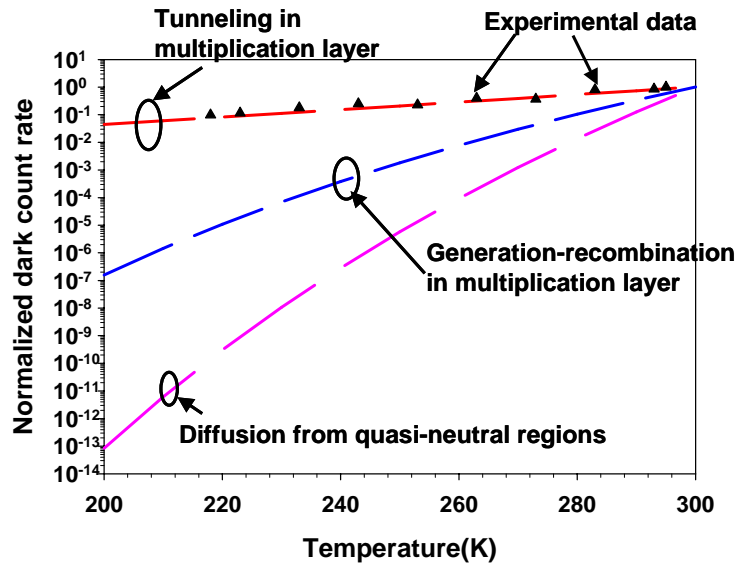
Figure 6.4: Estimated temperature dependence of various dark count generation
             mechanisms.

The dark counts resulting from diffusion of carriers from quasi-neutral n and p regions to the multiplication layer have an exponential dependence on temperature through the band gap. Hence the activation energy is expected to be equal to the band gap of the quasi-neutral regions. For dark counts resulting from generation-recombination in the $In_{0.53}Ga_{0.47}As$ absorber layer, the activation energy is expected to be ~ ½ the band gap of $In_{0.53}Ga_{0.47}As$, which is 0.37eV. For generation-recombination in the multiplication layer, the activation energy should be ~ ½ band gap of $In_{0.52}Al_{0.48}As$, which is 0.72eV.

87

The experimentally observed activation energy is much lower than the value expected from any of the above-mentioned mechanisms. Surface recombination is not expected to dominate at high gains observed in the Geiger mode operation of an APD. The estimated maximum electric field in the absorber was < 1kV/cm. Hence tunneling in the absorber is not expected to be dominant. The temperature dependence of dark count rate could be explained by invoking band-to-band tunneling in the multiplication layer. Band profile simulations of the device above breakdown voltage indicate a triangular barrier for tunneling.

6.3   DARK COUNTS DUE TO TUNNELING IN THE MULTIPLICATION REGION

6.3.1   Modeling of Tunneling

The concept of tunneling was initially invoked for describing the field ionization of atomic hydrogen. This phenomena was put to practical use in tunnel diodes by Esaki, et. al. in 1958 [6-9]. The tunneling in semiconductors can be either direct or indirect. During tunneling, the momentum of the system must be conserved. In direct band gap materials, such as, GaAs and $In_{0.52}Al_{0.48}As$, the conduction band minima (Γ point) and the valance band maximum (Γ point) have the same momentum and thus the conservation condition is satisfied. In case of indirect band gap materials such as Si or Ge, the momentum is conserved with participation from phonons or impurities. Direct tunneling in the $In_{0.52}Al_{0.48}As$ multiplication layer was modeled to understand the origin of dark counts from tunneling.

A thorough analysis of tunneling related dark counts should use equation (6.5). It involves integrating the product of the generation rate due to band-to-band tunneling and

position dependent breakdown probability over the depletion layer width. In the simple analytical model used here, the breakdown probability was treated as a constant, P_{eh}(junction). Dark counts due to tunneling ($N_{d,tunneling}$) were estimated by dividing the tunneling dark current, $I_{tunneling}$, by the electronic charge, q, and multiplying by the breakdown probability, P_{eh}(junction), which yields the expression

$$N_{d,tunneling} = \frac{I_{tunneling}}{q} \cdot P_{eh}(junction) \tag{6.9}$$

P_{eh}(junction) is the electron-hole pair breakdown initiation probability at the junction, where the electric field is maximum [6-10]. The dark counts per second due to tunneling can be written as [6-11]

$$N_{d,tunneling} = P_{eh}(junction) \cdot C_1 \cdot V_a \cdot E_m \cdot \exp\left(\frac{-C_2}{E_m}\right). \tag{6.10}$$

C_1 can be expressed as

$$C_1 = \sqrt{\frac{2 \cdot m_r^*}{E_g}} \cdot \frac{q^2}{4 \cdot \pi^3 \cdot \hbar^2}. \tag{6.11}$$

The form of C_2 depends on the type of tunneling barrier. For a triangular barrier,

$$C_2 = \left(-\frac{4 \cdot \sqrt{2 \cdot m_r^*} \cdot E_g^{3/2}}{3 \cdot q \cdot \hbar}\right) \tag{6.12}$$

The various terms in equations (6.10)-(6.12) are described below. E_m is the electric field in the multiplication region. Equation (6.10) is derived assuming a constant electric field in the depletion layer [6-12]. Since the electric field in the multiplication layer of an SACM APD is not constant, the average electric field obtained by solving Poison's equation for the SACM APD with appropriate boundary conditions was used in the calculation. V_a is the voltage drop across the junction, E_g is the band gap of $In_{0.52}Al_{0.48}As$, $\hbar$ = plank's constant/(2π), and m_r^* is the tunneling effective mass.

The effective mass involved in tunneling calculations should be derived from the complex band structure of the material. In this calculation, its value was taken to be the reduced effective mass defined as follows [6-13],

$$\frac{1}{m_r{}^*} = \frac{1}{m_e{}^*} + \frac{1}{m_{lh}{}^*} \quad . \tag{6.13}$$

where, $m_e{}^* = 0.079 \, m_0$ is the Γ valley electron effective mass and $m_{lh}{}^* = 0.086 \, m_0$ is the light hole effective mass for $In_{0.52}Al_{0.48}As$. The effective mass of heavy holes, 0.5 m_0, being much higher than the electron or light hole effective masses, it was neglected in the reduced mass calculation.
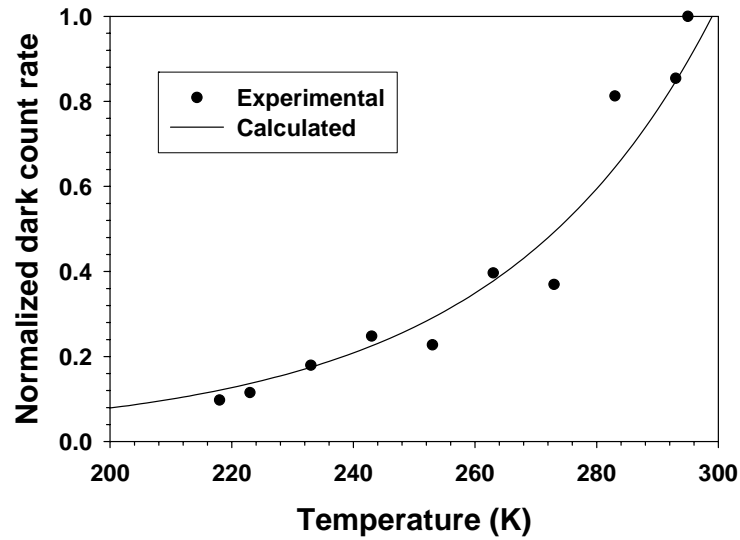
Figure 6.5:   Normalized dark count rate as a function temperature at excess bias of 1.5V for $In_{0.53}Ga_{0.47}As$ / $In_{0.52}Al_{0.48}As$ APD.

Figure 6.5 shows the calculated dark count rate as a function of temperature, normalized to the value at room temperature. It should be noted that the absolute value of dark count rate depends on the experimental details, for example the discriminator threshold, the quenching technique, and the repetition rate. Also the simple tunneling model does not take into account non-uniformities in the active area. However, regardless

of the absolute value of the dark counts, for a given excess voltage their temperature dependence is unique. A good fit to the experimental data was obtained for temperature ranging from 77K to room temperature, for all the excess biases.

6.3.2 Note on the electric field calculation

Due to the small coefficient of V_{br} change with temperature in $In_{0.52}Al_{0.48}As$, the difference between the absolute excess biases at different temperatures is small. Since V_{br} reduces with decreasing temperature, the total bias and thus the electric field is lower at lower temperatures. The electric field at various temperatures was estimated using the room temperature electric field equations. Doing so assumes that the dielectric constant, the doping and the layer thickness do not vary with temperature, which is a reasonable assumption for the temperature range considered here.

6.3.3 Activation energy estimation

The activation energy (E_a) is the slope of log (N_d) versus $1/kT$ plot. To estimate the value of E_a theoretically, the following equation was considered

$$N_{d,tunneling} = P_{eh}(junction) \cdot C_1 \cdot V_a \cdot E_m \cdot \exp\left(\frac{-C_2}{E_m}\right). \tag{6.10}$$

Taking the natural logarithm of both sides, one obtains

$$\ln\left(N_{d,tunneling}\right) = C_3 - \frac{C_2}{E_m} \tag{6.13}$$

where, $C_3 = \ln\left(P_{eh}(junction) \cdot C_1 \cdot V_a \cdot E_m\right).$ $\tag{6.14}$

The temperature dependence of the dark count rate is primarily due to the temperature dependence of the band gap of $In_{0.52}Al_{0.48}As$, which appears in C_2.

$$C_2 = \left(-\frac{4 \cdot \sqrt{2 \cdot m_r{}^* \cdot E_g(T)^{3/2}}}{3 \cdot q \cdot \hbar}\right) \tag{6.12}$$

91

The band gap of In$_{0.52}$Al$_{0.48}$As was calculated using the band gaps of InAs and AlAs and the bowing parameter for In$_{0.52}$Al$_{0.48}$As [6.14]. Figure 6.6 shows the band gap of In$_{0.52}$Al$_{0.48}$As as a function of temperature from 77K to room temperature.
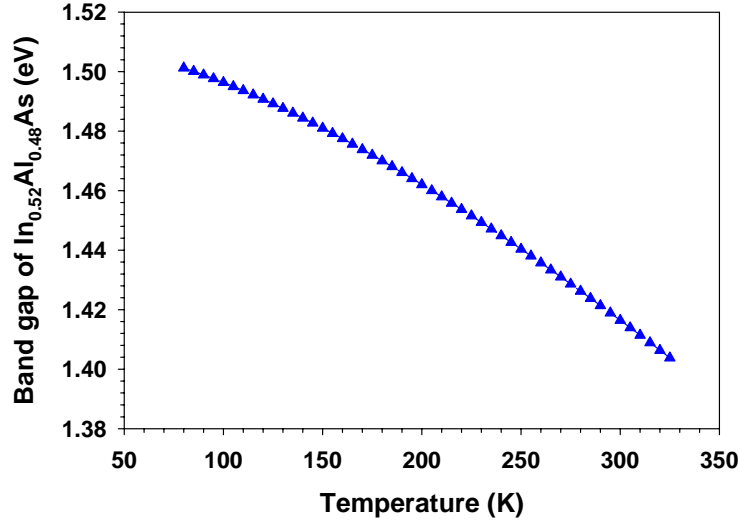
Figure 6.6:   Band gap of In$_{0.52}$Al$_{0.48}$As as a function of temperature.

In the temperature range from 200K to 300K, E$_g$$^{3/2}$ has an almost linear dependence on 1/kT and can be expressed as

$$E_g(T)^{3/2} = \alpha \cdot \frac{1}{k \cdot T} + \beta \qquad (6.15)$$

where, E$_g$(T) is the band gap of In$_{0.52}$Al$_{0.48}$As at temperature T, k is the Boltzman's constant, and α are β the slope and the intercept of E$_g$(T)$^{3/2}$ versus 1/kT plot, respectively. A linear fit results in = 4.8*10^{-3} eV$^{5/2}$ as shown in Figure 6.7.

Figure 6.7: Dependence of $E_g^{3/2}$ on $1/kT$ for $In_{0.52}Al_{0.48}As$.

Substituting equation (6.15) in (6.13), we obtain

$$\ln\left(N_{d,tunneling}\right) = C_3 - \frac{C_2 \cdot \beta + C_2 \cdot \alpha \cdot \dfrac{1}{k \cdot T}}{E_m} \tag{6.16}$$
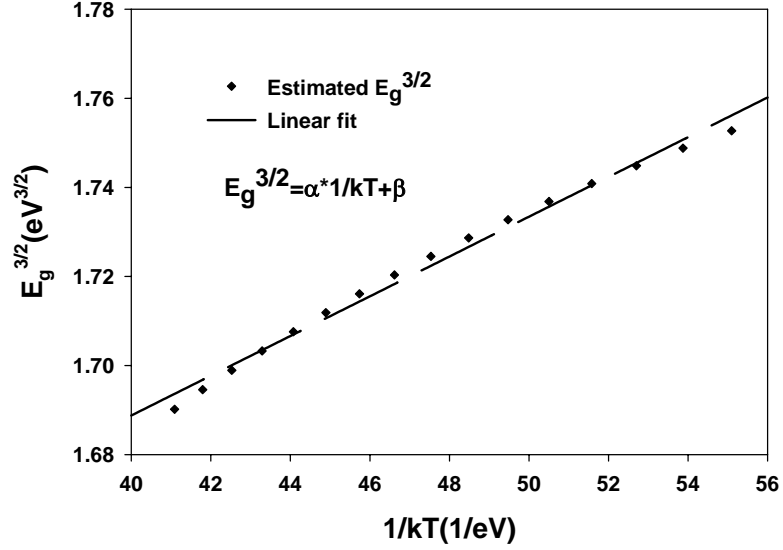
Hence a plot of the $\ln(N_{d,tunneling})$ versus $1/kT$ is expected to exhibit a slope of $C_2 \cdot \dfrac{\alpha}{k \cdot E_m}$

$= \left(-\dfrac{4 \cdot \sqrt{2 \cdot m_r{}^* \cdot \alpha}}{3 \cdot q \cdot \hbar \cdot E_m}\right)$. The slope, which is the activation energy calculated from this

expression at an excess bias of 3.5V, is 0.14eV. This matches reasonably well with the

experimentally observed value of 0.11eV. The activation energy depends inversely on

electric field in the multiplication layer, which was also observed experimentally.

The dominance of band-to-band tunneling in Geiger mode operation for this

device is attributed to the high electric field in its 400nm thin multiplication layer.

However, such a thin multiplication layer results in very good timing performance. A

75µm diameter device exhibits timing jitter of only 60ps at 200K when operated at 3.5V above breakdown voltage [6-15]. Thus there is a trade off between the timing performance of a Geiger mode APD and tunneling in its multiplication layer. Since tunneling current is very sensitive to electric field, we estimate that increasing the multiplication layer thickness by a factor of 2 will reduce the tunneling induced dark counts by 3 orders of magnitude. The increased thickness of the multiplication layer is also expected to give a steeper increase in breakdown probability with excess voltage, and hence improved single photon counting performance [6-16]. Ultimately generation-recombination in the multiplication layer and avalanche build up time will determine the optimum multiplication layer thickness.

In summary, a study of the origin of dark counts in an $In_{0.53}Ga_{0.47}As/In_{0.52}Al_{0.48}As$ SACM APD using the temperature dependence of the dark count rate was described in this chapter. Various dark count generation mechanisms were considered. The dark count rate in this device was found to be dominated by band-to-band tunneling in its multiplication layer.

References:

[6-1] A. karlsson, M. Bourennane, G. Ribordy, H. Zbinden, J. Brendel, J. Rarity and P. Tapster, "A single-photon counter for long-haul telecom", *Circuits and devices*, vol. , pp. 34-40, 1999.

[6-2] D. Stucki, G. Ribordy, A. Stefanov, H. Zbinden, J. G. Rarity, and T. Wall, "Photon counting for quantum key distribution with Peltier cooled InGaAs/InP APDs," *J. Modern Optics*, vol. 48, no. 13, pp. 1967-1981 (2001).

[6-3] W. P. Risk, and D. S. Bethune, "Quantum cryptography using autocompensating fiber-optic interferometers," *Optics and Photonics news*, vol. 13, no. 7, pp.26 (2002).

[6-4] B. F. Levine, C. G. Bethea, J. Campbell, "1.52 μm room temperature photon counting optical time domain reflectometer," *Electron. Lett.*, vol. 21, pp. 194-196 (1985).

[6-5] M. Bourennane, A. Karlsson, J.P.Ciscar, and M. Mathes, "Single-photon counters in the telecom wavelength region of 1550 nm for quantum information processing", *J. Mod. Optics*, vol. 48**,** no**.** 13, pp. 1983-1995 (2001).

[6-6] K-S. Hyun and C-Y. Park, "Breakdown characteristics in INP/InGaAs avalanche photodiode with p-i-n multiplication layer structure", *J. Appl. Phys.*, vol. 81, no. 2, pp. 974-984 (1997).

[6-7] Shuling Wang; Feng Ma; Xiaowei Li; Karve, G.; Xiaoguang Zheng; Campbell, J.C., "Analysis of breakdown probabilities in avalanche photodiodes using a history-dependent analytical model", *Appl. Phy. Lett.*, vol. 82, pp. 1971 (2003).

[6-8] R. J. McIntyre, "A new look at impact ionization-Part I: A theory of gain, noise, breakdown probability, and frequency response," *IEEE Trans. Electron. Devices*, vol. 46, no. 8, pp. 1623-1631, (1999).

[6-9] L. Esaki, "Discovery of the tunnel diode", *IEEE Trans. Electron. Devices*, vol. ED-23, pp. 644 (1976).

[6-10] W.J.Kindt, Geiger mode avalanche photodiode arrays for spatially resolved single photon counting, (Delft University press, Netherlands, Nov. 1999).

[6-11] R.H.Haitz, "Mechanisms contributing to the noise pulse rate of avalanche diodes", *J. Appl. Phys.*, vol. 36**,** no. 10, pp. 3123-3131 (1965).

[6-12] E. O. Kane, "Theory of tunneling", *J. Appl. Phys.*, vol. 32, no. 1, pp. 83 (1961).

[6-13] H. Ando, H. Kanbe, M. Ito and T. Kaneda, "Tunneling current in InGaAs and optimum design for InGaAs/InP avalanche photodiode", *Jap. J. Appl. Phys.*, vol. 19, no. 6, pp. L277-L280 (1980).

[6-14] I. Vurgaftman, J. R. Meyer and L. R. Ram-Mohan, "Band parameters for III-V compound semiconductors and their alloys", *J. Appl. Phys.*, vol.89, no.11, pp. 5815-75 (2001).

[6-15] R. Ispasoiu, private communication.

[6-16] Shuling Wang, Feng Ma, Xiaowei Li, Karve G., Xiaoguang Zheng, and Campbell J.C., "Analysis of breakdown probabilities in avalanche photodiodes using a history-dependent analytical model", *Appl. Phy. Lett.*, vol. 82, pp. 1971 (2003).

Chapter 7   Photon Counting in Ultraviolet and Near Infrared Regions

SiC and GaAs/AlGaAs material systems have the potential for photon counting in the ultraviolet (UV) and near infrared (NIR) wavelengths, respectively. This chapter discusses the photon detection experiments in the UV and NIR regions. Section 7.1 describes single photon detection at 325nm using SiC avalanche photodiodes. The work presented in this section was done in collaboration with a fellow graduate student Ariane Beck. GaAs/AlGaAs based avalanche photodiodes as photon detectors at 830nm are discussed in section 7.2.

7.1   UV PHOTON COUNTING

A variety of applications in medical, military, and environmental areas require ultra-sensitive, low noise and compact photodetectors in the UV range of wavelengths [7-1], [7-2]. Photomultiplier tubes with high gains and low dark currents are available for wavelengths as short as 150nm [7-3]. However, due to their limitations such as high operating voltages, bulkiness, etc., alternative solutions are sought. Wide band gap materials such as GaN and SiC have been studied as UV photodetectors. Their material growth and process technology has matured significantly over the past few years [7-4]. Demonstrations of avalanche photodiodes with these wide band gap materials confirms their potential as Geiger mode APDs. SiC is more attractive since it has lower defect density than GaN [7-5]. It also exhibits a high ratio of hole to electron ionization coefficients, low dark current, good thermal conductivity and visible-blind performance. SiC APDs with gains of 10^6 and low excess noise have been demonstrated [7-6]. Recently, single photon detection using SiC APDs has also been demonstrated [7-7]. SiC exhibits over 200 polytypes. The polytypes are differentiated by the stacking sequence of

each tetrahedrally bonded Si-C bilayer [7-8]. 4H-SiC exhibiting hexagonal symmetry is preferable due to its large band gap of 3.26eV compared to the other polytypes. Its wavelength cut-off of 380nm makes it suitable for the visible-blind applications. All the data discussed in this chapter used 4H-SiC APDs. The schematic of the SiC APD is shown in Figure 7.1. Mesa photodiodes were processed using reactive ion etching (RIE), PECVD deposition of SiO_2 as passivation layer and contact deposition using e-beam evaporation. Ni and Ti/Al/Ti were used as n and p contacts, respectively. Details of the growth and the device processing can be found in reference [7-9]. The devices used for photon counting experiments were processed with Ti/Au contact pads for wire bonding. The ring contact geometry was used for p metal in the photon counting devices to ensure a uniform electric field distribution across the mesa [7-10]. The devices were also processed with a positive bevel to reduce the electric field at the edges [7-11]. Figure 7.2 shows the current-voltage and the gain-voltage characteristics for a 160 μm diameter device. The slight difference in the breakdown voltage with and without illumination is probably due to the gain non-uniformities across the mesa.
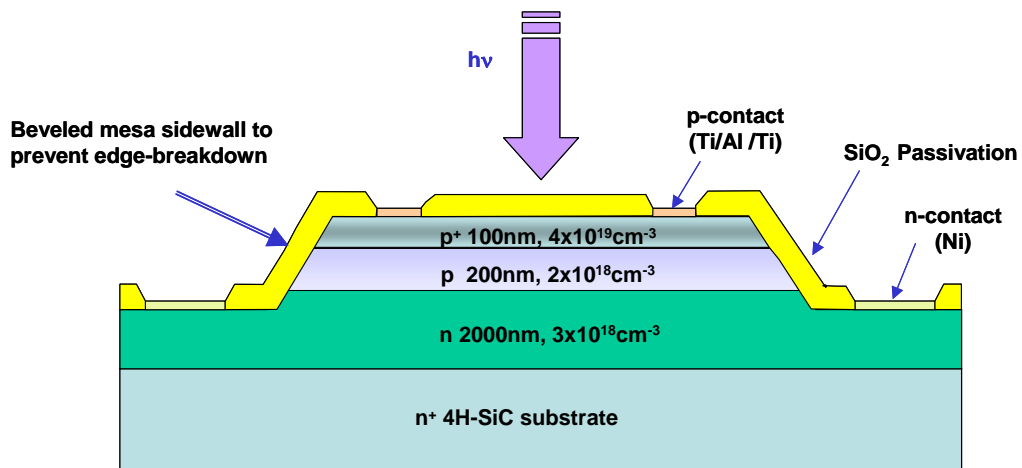
Figure 7.1:   Schematic of the SiC APD.
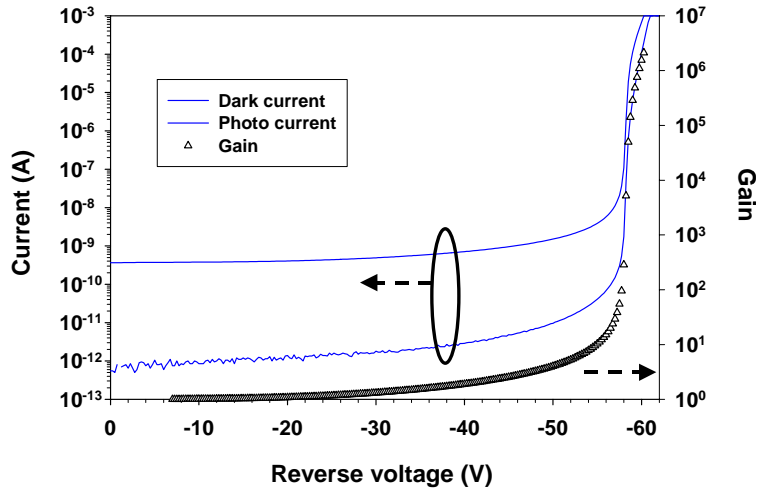
Figure 7.2:   Photo and dark current at room temperature for a 160 μm SiC APD.

Photon counting experiments with both passive and gated mode quenching were performed using SiC APDs. The results are presented in the following sections.

7.1.1   Passive quenching

The operating principle of the passive quenching mode is explained in Chapter 2. A 150kΩ resistor was used as the quenching resistor. This value of quenching resistor allowed the use of excess voltages as high as 1.5V. A 266 nm pulsed laser was used as the source of light. The linear mode quantum efficiency of the detector was 36% at 266nm. At room temperature, the dark count rate for the device was hundreds of kHz. Due to the high dark count rate, the difference between the single photon count rate and the dark count rate was less than 3 times the standard deviation in the measurements. The dark current in this device was dominated by tunneling and so reducing the operating temperature had little effect on the dark count rate [7-9]. The system dead time was another important issue in the experiments. For a 160 μm diameter APD, the device

capacitance was 8pF. The total capacitance including the stray capacitance was ~ 10pF in these experiments. For the quenching resistor of 150kΩ, the estimated dead time of the system was ~ 0.75 μs with the discriminator threshold set to half the output pulse height. This long dead time limited the maximum counts that could be accumulated without significant error to < 13 kcps. With the high dark count rate, it was difficult to collect accurate data in the passive quenching mode. The single photon detection was achieved with gated mode quenching, where the dark counts were reduced.

7.1.2   Gated quenching

The experimental set up for gated mode quenching is described in Chapter 2. The device was dc biased below breakdown voltage (V_{br}) and ac biased above V_{br} for 4ns at a repetition rate of 10kHz. The bias pulse width of 4ns was chosen instead of 2ns, which was used for the IR photon counting experiments. The reason being that the response of SiC APDs was not as fast as the InGaAs/InAlAs APDs. Hence a longer width of bias pulse was necessary to ensure that the APD recharged to the applied voltage in the duration of the bias pulse [7-10]. While using a 266nm pulsed laser source, the optical pulse had to be synchronized with the bias pulse. In the IR photon counting experiments, the laser source was triggered externally using a pulse generator. Thus the delay in optical path could be adjusted by tuning the laser trigger delay. The 266nm pulsed laser source, however, was internally triggered. It produced 500ps pulses at a repetition rate of 7.5kHz. Hence a part of the laser beam was coupled in a fast photodiode to create the system clock. Figure 7.3 shows the schematic of the experimental set-up.

99
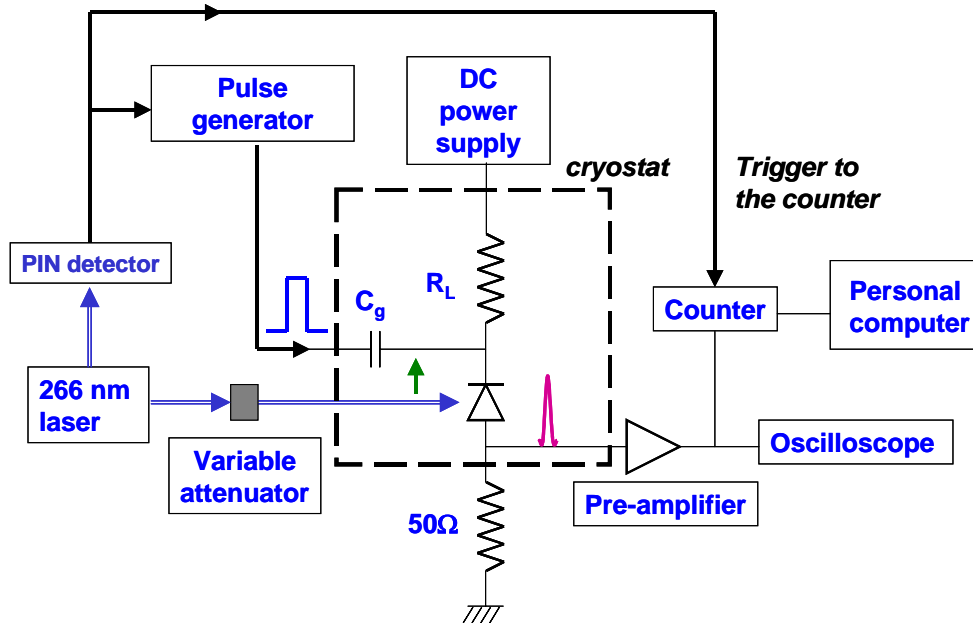
Figure 7.3:   Gated mode quenching set up for single photon detection at 266nm.

The bias pulse generator exhibited an internal delay of ~ 85ns between its trigger input and the output. This made it necessary to delay the optical signal by ~ 80ns. The optical signal was delayed by introducing an optical fiber in the laser path. The length of fiber required for the desired delay was > 9 meter. The loss of laser power due to the long fiber length made it impossible to achieve the sufficient intensity at the APD to perform optical coupling.

Alternately, 325nm He-Cd cw laser was used for the experiments. Use of a cw light source eliminated the need for elaborate synchronization in the optical and the electrical path. However, the linear mode quantum efficiency of the detector at 325nm was only 10%. The single photon detection efficiency was hence sacrificed. The laser power was attenuated using free space attenuators so that on average less than one photon fell on the APD in each bias pulse. The estimation of average photon number is explained

in appendix II. The photon counting performance of the APD is shown in Figure 7.4. At room temperature, a detection efficiency of ~3% was obtained for a dark count probability of 10^{-2}. The APD exhibited no sign of afterpulsing for repetition rates as high as 100kHz. Hence afterpulsing was ignored while estimating the detection efficiency at 10kHz.
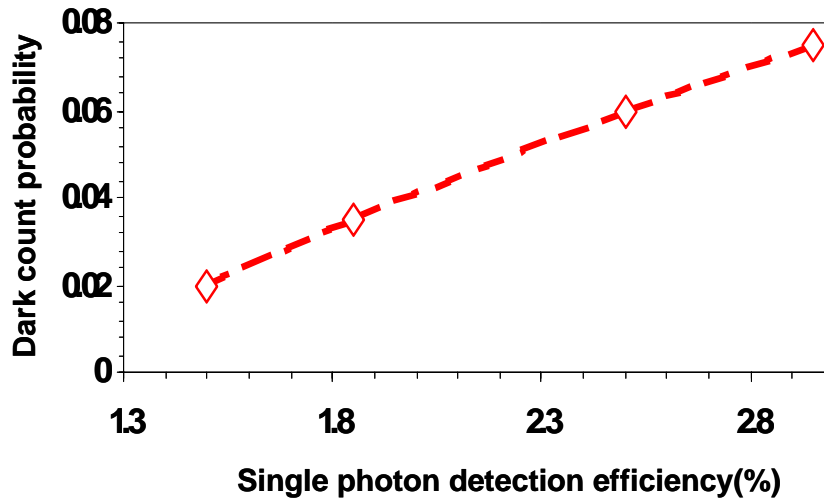
Figure 7.4:   Dark count probability versus single photon detection efficiency for SiC APD at room temperature.

The low dark current obtained below V_{br} in the SiC APDs implies that a lower dark count rate should be also be achievable. One possible reason for very high dark count rate may be the high gain at the dc bias operating point [7-12]. Use of a smaller dc voltage and larger ac pulse bias is expected to reduce the dark count rate. Use of a smaller diameter device is also expected to decrease the dark counts. The dark count rate can also be reduced by lowering the operating temperature. In order to use temperature as an effective parameter for reducing dark counts, tunneling related dark counts should be minimized. This can be achieved using a structure with thicker depletion layer so that the tunneling in the i layer is suppressed. A thicker depletion layer means that the breakdown

voltage may exceed 100V. In order to still achieve high excess bias ratio, a larger bias pulse must be used. Further, use of a shorter wavelength source will increase the detection efficiency.

7.2 NEAR IR PHOTON COUNTING

GaAs-based materials are attractive choices for photodetector applications in the 650-870nm range. For all compositions of Al, $Al_xGa_{1-x}As$ is lattice matched to GaAs. This has opened up the possibilities of using GaAs-AlGaAs based heterostructures for numerous optoelectronic applications [7-13]. Ultra low noise and low dark current photodiodes based on GaAs and AlGaAs heterostructures have been demonstrated [7-14]. GaAs based material systems have also been studied for photon counting in the near IR region. Timing resolution and dark count rate comparable to the Si SPADs has been demonstrated with Geiger mode GaAs APDs [7-15]. The growth and process technology for GaAs is most mature among III-V compound semiconductors. Hence the GaAs material system offers an ideal platform for performing controlled experiments to understand the physics of Geiger mode APDs. We have attempted single photon counting with $GaAs/Al_{0.6}Ga_{0.4}As$ APDs grown by MBE.

The structure of a GaAs based APD is shown in Figure 7.5. The structure was grown using Molecular Beam Epitaxy (MBE). It used a GaAs absorber and $Al_{0.6}Ga_{0.4}As$ multiplication and charge layers. Be and Si were used as p and n dopants, respectively.

p+ GaAs; 50 nm
p: AlGaAs; 400 nm
i: GaAs; 1000 nm
i: AlGaAs/GaAs ; 26 nm
p: AlGaAs; 80 nm, ~2.5e17
i: AlGaAs; 800 nm
n AlGaAs; 486 nm
n GaAs; 486 nm
i GaAs; 200 nm
i GaAs substrate

i: GaAs; 1000 nm ← Absorber

p: AlGaAs; 80 nm, ~2.5e17 ← Charge layer

i: AlGaAs; 800 nm ← Multiplication layer
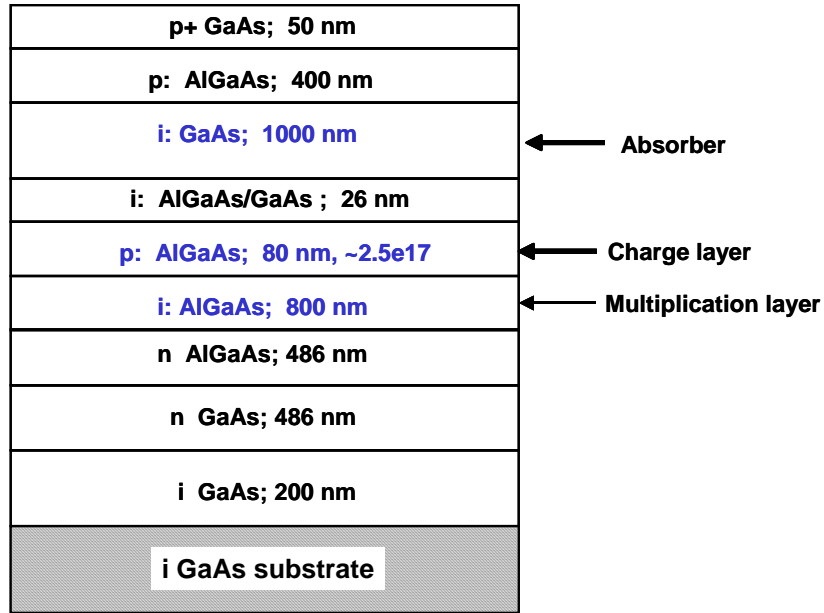
Figure 7.5: Schematic of the GaAs based APD.

Top-illuminated mesa structures with diameters ranging from 36 μm to 160 μm were fabricated using standard photolithography and lift off, wet chemical etching, and SiO_2 passivation. Cr/Au and Ni/AuGe/Au were used as the p-contact and n-contact, respectively. The details of the processing can be found in Chapter 3. Room temperature photo current, dark current and gain for the device as a function of applied reverse bias are shown in Figure 7.6. The dark current in the device was ~0.098 pA/μm^2 at 90% of V_{br}. The low temperature photo and dark current characteristics for the device are shown in Figure 7.7. The breakdown voltage of the device decreased with decreasing temperature at a rate of 5 mV/K. The measured quantum efficiency is shown in Figure 7.8. At unity gain above the punchthrough voltage, an efficiency of 46 % was obtained at 830nm. The sharp decrease in the quantum efficiency at 900nm is a characteristic of the absorption spectrum of GaAs.
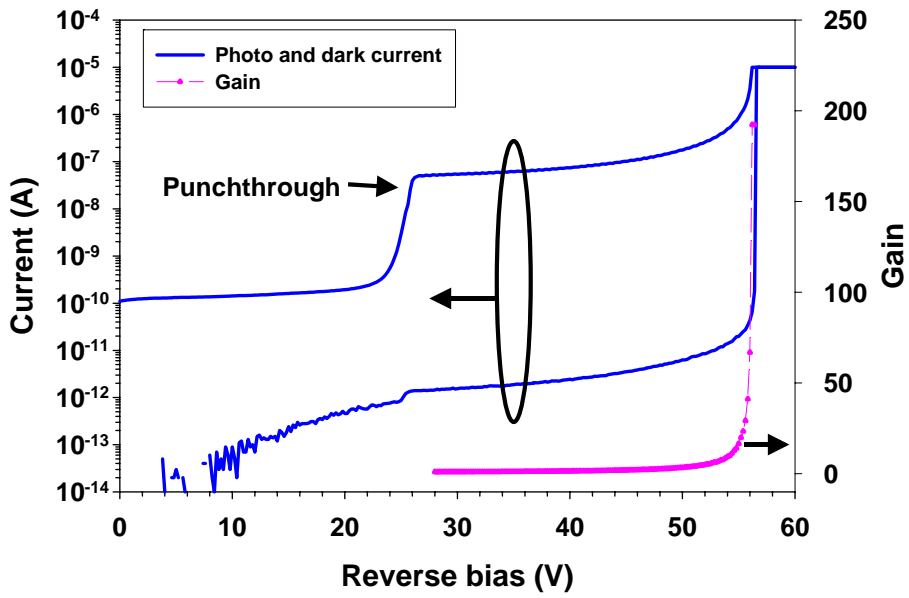
Figure 7.6:   Photo and dark current-voltage and gain-voltage characteristics of GaAs APD. T = 295K, device diameter = 158 μm.
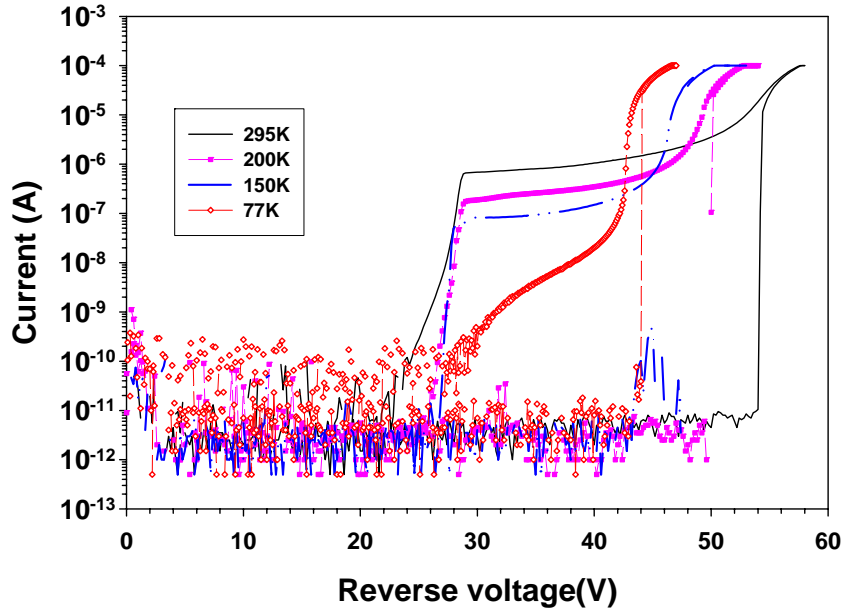
Figure 7.7:   Photo and dark current versus voltage at different temperatures for GaAs APD shown in Figure 7.5.
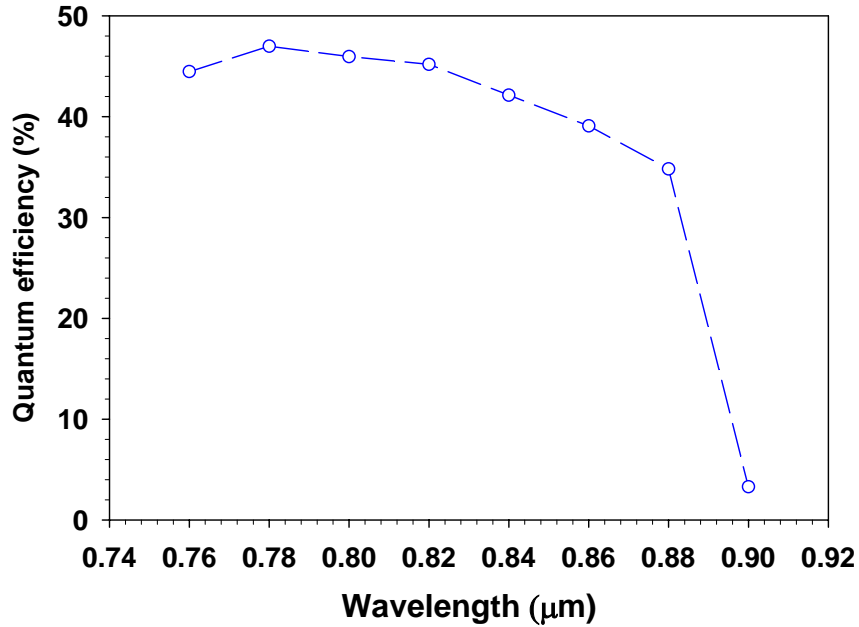
Figure 7.8: Measured quantum efficiency as a function of wavelength for GaAs APD.

The edge breakdown in the GaAs APD was investigated using a two-dimensional raster scan. Light from a 361nm Argon ion laser was tightly focused on the mesa top. The beam position was scanned using computer-controller micropositioners to generate a two-dimensional photoresponse profile. Experimental gain as a function of beam position is shown in Figure 7.9. It can be seen that at 1V below breakdown, no evidence of edge breakdown or electric field crowding under the contacts was observed. The gain is quite uniform across the entire mesa region.
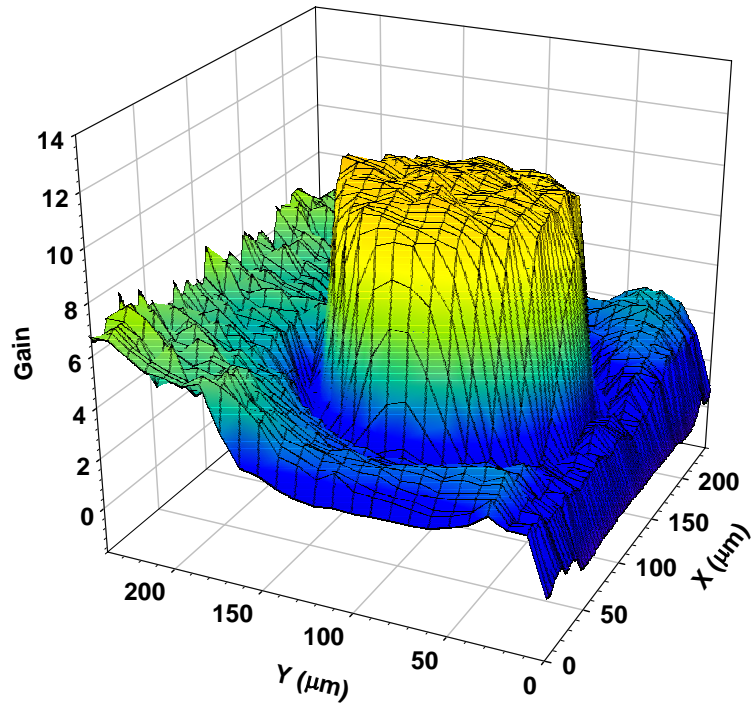
Figure 7.9: Two-dimensional gain profile for GaAs APD. The device was biased 1V below its breakdown voltage.

This device demonstrated the potential to be a good photon counter as evidenced by its low dark current, good quantum efficiency and uniform gain in the linear mode. However, Geiger-mode single photon detection was not observed with this device. The reason for this is not completely understood. In the photon counting experiments, a cw laser at 830nm was used as the optical source. No difference was observed between the photo and the dark count probability. Further, the dark counts obtained under fixed operating conditions were not repeatable. The dark count rate also exhibited a very peculiar behavior. Figure 7.10 shows a plot of the measured dark count probability sampled at different times. The data was accumulated at room temperature, at a repetition rate of 1kHz. Under the fixed operating conditions, the dark counts sampled at different times are expected to exhibit statistical fluctuations about some average value (See Figure

2.6). However, for this APD, a systematic increase was observed in the measured dark counts with successive data points. The time interval between successive measurements is referred to as the dwell time of the electronic counter. The APD bias remains on during the dwell time. The systematic increase in the dark counts was independent of the dwell time, for dwell times between 0.5 second to 5 seconds. The amount of increase also did not depend on the pulse repetition rate. Heat dissipation in the diode is not expected to cause this behavior. The junction temperature and hence the junction breakdown voltage increase due to diode heating. Hence, if heating is significant, the dark count rate would be expected to decrease during subsequent sampling. Afterpulsing or reignition have not yet been confirmed to be the cause for this behavior.
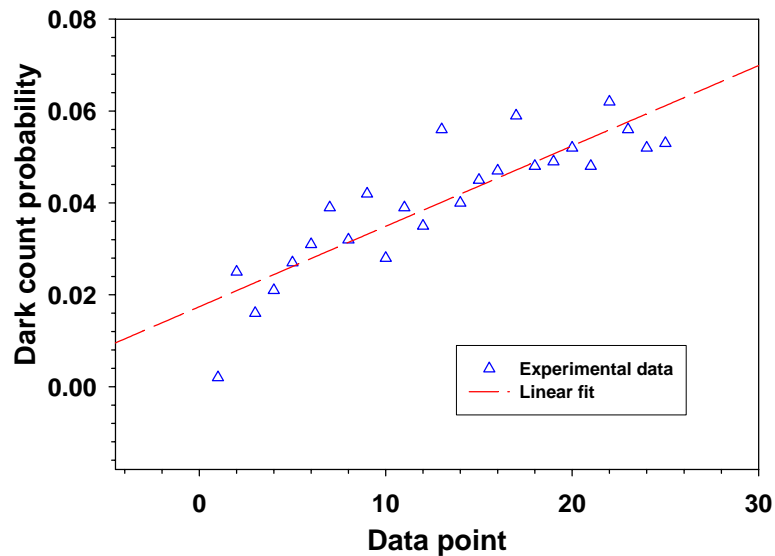
Figure 7.10: Dark count probability sampled at different time intervals. The operating conditions were fixed during the measurements.

Such systematic increase in the measured dark count rate under fixed operating conditions was also observed for other APDs grown by MBE. These APDs were designed for photon counting at 1.5 μm. None of the APDs grown using metal-organic

107

vapor phase epitaxy (MOVPE) exhibit this effect. It is not clear whether this is due to some fundamental difference in the defects between the MBE and the MOVPE material. Controlled experiments to understand the trap levels present in the materials are necessary to further understand this phenomenon. Such experiments include deep level transient spectroscopy (DLTS) and time correlated carrier counting [7-16].

In summary, photon counting in the UV and near IR range using SiC and GaAs APDs were discussed in this chapter. Single photon detection at 325nm using SiC was described. Study of GaAs/AlGaAs as a potential material system for photon counting at 830nm was also discussed.

References:

[7-1] R. Korde and J. Geist, *State Electron.,* vol. 30, no. 1, pp. 89 (1987).

[7-2] L. R. Confiled, J.Kerner and R. Korde, *SPIE*, vol. 1344, pp. 372 (1990).

[7-3] Hamamatsu Optoelectronics; 360 Foothill Rd, Bridgewater, NJ 08807. (http://www.hamamatsu.com).

[7-4] A. R. Powekk and L. B. Rowland, "SiC materials-progress, status and potential roadblocks", *Proc. IEEE.*, vol.90, pp. 942-955 (2002).

[7-5] P. G. Neudeck, "Electrical impact of SiC structural crystal defects on high field devices", *Material Science Forum*, vol. 338-342, pp. 1161-1166 (2000).

[7-6] B. K. Ng, F. Yan, J. P. R. David, R. C. Tozer, G. J. Rees, C. Qin and J. H. Zhao, "Multiplication and excess noise characteristics of thin 4H-SiC UV avalanche photodiodes", *IEEE Photonics Tech. Lett*., vol 14, no. 9, pp.1342-1344 (2002).

[7-7] X. Xin, F. Yan, X. Sun, P. Alexandrove, C. M. Stahle, J. Hu, M. Matsumura, X. Li, M. Weiner and H. J. Zhao, "Demonstration of 4H-SiC UV single photon counting avalanche photodiode", *Electron. Lett.*, vol. 41, no. 4, pp. 67-68 (2005).

[7-8] G. B. Dubrovskii, *Sov. Phys. Solid State*, vol. 13, pp. 2107 (1972).

[7-9] X. Guo, A. L. Beck, X. Li, J. C. Campbell, D. Emerson and J. Sumakeris, "Study of dark current in 4H-SiC avalanche photodiodes", *J. Quantum Electron.*, vol. 41, no. 4, pp. 562-567 (2005).

[7-10] A.L. Beck, G. Karve, S. Wang, J. Ming, X. Guo, and J.C. Campbell, "Geiger Mode Operation of Ultraviolet 4H-SiC Avalanche Photodiodes", *Electron. Lett.,* accepted for publication.

[7-11] A. L. Beck, B. Yang, X. Guo and J. C. Campbell, "Edge breakdown in 4H-SiC avalanche photodiodes", *J. Quantum. Electron.*, vol. 40, no. 3, pp. 321-324 (2004).

[7-12] Y. Kang, H. X. Lu, Y. H. Lo, and D. S. Bethune, **"**Dark count probability and quantum efficiency of avalanche photodiodes for single-photon detection**",** *Appl. Phys. Lett.*, vol. 83, no. 14, pp. 2955-2957 (2003).

[7-13] D. G. Esaev, M. M. Rinzan, S. G. Matsik, and A. G. U. Perera," Design and optimization of GaAs/AlGaAs heterojunction infrared detectors", *J. Applied Physics*, vol. 96, no. 8, 15, pp. 4588-97 (2004).

[7-14] J. C. Campbell, S. Wang, X. G. Zheng, G. S. Kinsey, A. L. Holmes Jr., X. Sun, R. Sidhu and P. Yuan, "Ultra-low-noise avalanche photodiodes", *Proc. SPIE*, vol. 4283, pp. 480-488 (2001).

[7-15] G. Kirchner, F. Koidl, I. Prochazka and K. Hamal, "SPAD on GaAs for SLR", *Proc. 12th International Workshop on Laser Ranging, Matera, Italy* (2000). (Full text available at http://geodaf.mt.asi.it/html/news/iwlr/Kirchner_et_al_GaAs.pdf.)

[7-16] S. Cova, A. Lacaita and G. Ripamonti, "Trapping phenomena in avalanche photodiodes on nanosecond scale", *Electron. Device Lett.*, vol. 12, no. 12, pp. 685-687 (1991).

Chapter 8   Conclusions and Future Work

8.1   CONCLUSIONS

Efficient detection of single photons is achievable using avalanche photodiodes (APDs) operated above their breakdown voltage. Several APDs based on InP, GaAs and SiC were fabricated and characterized as single photon counters. Linear mode characterization experiments such as current-voltage, capacitance-voltage, quantum efficiency, and contact resistance were performed to determine viability of detectors as photon counters. An experimental set-up to study and characterize photodiodes as single photon counting detectors was established. The set up was calibrated using a commercial $In_{0.53}Ga_{0.47}As/InP$ APD, whose single photon counting performance has been studied by other research groups. The detection of a single incoming photon involves precise timing of the incident photon, the bias to the detector, and the detection gate. A number of parameters have to be optimized in order to reduce the noise from the detection electronics and achieve such weak light sensitivity. The effects of various experimental parameters such as the excess bias, operating temperature, the discriminator threshold, the repetition rate, and the bias pulse width were studied. A procedure was outlined for optimizing these parameters for a single photon counting avalanche photodiode. Single photon detection was demonstrated at 1.55 μm using separate-absorption-charge-multiplication $In_{0.53}Ga_{0.47}As/In_{0.52}Al_{0.48}As$ avalanche detectors. This was the first demonstration of $In_{0.52}Al_{0.48}As$ multiplication layer APDs as photon counters. A detection efficiency of 13% was obtained for dark count probability of 0.1% at 80K.

Dark count rate in a single photon detector increases noise and results in underestimation of the quantum efficiency. The distinctive dependence of various dark count generation mechanisms on temperature can be used as distinguishing signatures.

Various dark current and dark count generation mechanisms were modeled to understand the temperature dependence of dark counts in separate absorption-charge-multiplication $In_{0.53}Ga_{0.47}As/In_{0.52}Al_{0.48}As$ APDs. The observed dark count rates for $In_{0.53}Ga_{0.47}As/In_{0.52}Al_{0.48}As$ single photon counting detector were successfully explained with band-to-band tunneling in the multiplication layer. With the help of the experimental and the modeling results, design criteria for single photon counting APDs was developed. A single photon counting APD should use a thicker multiplication layer in order to minimize tunneling in the depletion layer. Further, the integrated charge in the charge layer should be adjusted such that the punchthrough voltage is very close to the breakdown voltage. This ensures a low electric field and thus reduced tunneling at the $In_{0.53}Ga_{0.47}As/In_{0.52}Al_{0.48}As$ heterointerface.

SiC and GaAs based APDs were studied for single photon counting at ultraviolet and near infrared wavelengths, respectively. Single photon detection at 325nm was demonstrated using 4H-SiC APDs. A detection efficiency of 3% at dark count probability of 10^{-2} was obtained at room temperature. This is the first demonstration of Geiger mode operation of SiC APDs. GaAs based APDs were studied for photon counting at 830nm.

8.2   FUTURE DIRECTIONS

The field of single photon detection offers numerous opportunities for experimental and theoretical study. Some promising ideas to extend the understanding of Geiger mode APDs are described in this section.

Use of APDs with thicker multiplication layers has potential to lower tunneling related dark counts. Timing resolution of the single photon avalanche diodes for a thicker multiplication layer may be sacrificed, unless lateral avalanche spreading delay dominates. Recently, theoretical work on the use of heterostructure multiplication layers

111

for single photon counting has been reported [8-1]. Experiments on such structures have promise in helping us understand the physics of Geiger mode APD operation. An undepleted absorber APD is a potential candidate for single photon detection in the IR. APDs with undepleted InGaAs absorber with high gain, high bandwidth and low noise have been demonstrated [8-2]. An undepleted absorber implies very low, almost zero electric field in the absorber and thus complete suppression of tunneling at the InGaAs/InAlAs heterointerface.

For single photon counting at 1.06 μm, a resonant cavity APD has been developed [8-3]. Photon counting performance of these devices needs to be characterized in more detail.

The single element photon counting could further be extended to integrate the detection circuit with the detection element. This will not only make the module compact, but will also facilitate formation of single photon counting arrays. Work is needed on integrating detector electronics with the detector.

The detection efficiencies in the UV can be enhanced by use of a thicker depletion layer. The concept of separate-absorption-charge (SAM) APDs can be extended in the UV region for photon counting.

More work is needed in order to fully understand the role of the growth method and associated traps on the detector's photon counting performance. Use of MBE grown material for single photon counting has not been demonstrated yet. In order to understand this completely, experiments to identify the trap densities, energy levels, and lifetimes in the depletion layer of APDs are needed. Experimental techniques such as time-correlated carrier counting and deep level transient spectroscopy should be developed in our lab.

References:

112

[8-1] O. H. Kwon, M. M. Hayat, J. C. Campbell, B. A. E. Saleh and M. C. Teich, "Optimized breakdown probabilities in AlGaAs-GaAs heterojunction avalanche photodiodes", *Electron Device Lett.*, vol. 25, no. 9, pp. 599-601 (2004).

[8-2] Li N., Sidhu, R., Li X., Ma F., Zheng X., Wang S., Karve, G., Demiguel, S., Holmes A.L., and Campbell, J.C., "InGaAs/InAlAs avalanche photodiode with undepleted absorber", *Applied Physics Letters*, vol. 82, pp. 2175 (2003).

[8-3] Sidhu R., Chen, H., Yuan N., Karve G.V., A.L.Holmes, and J.C.Campbell; "GaAsSb resonant cavity avalanche photodiode operating at 1.06 μm", *Electronics Letters*, vol.40, no.20, pp. 1296 (2004).

Appendix I Working Principle of the Transient Cancellation Cables

In gated mode operation of a single photon avalanche detector (SPAD), short bias pulses passing through the differentiator formed by the capacitors (C_g+C_s+C_d) and the resistor R_L produce large transients at the output. C_g is the input capacitor, C_d is the APD capacitance, C_s is the stray capacitance, and R_L is the load resistance. These transients can be stronger than the photon-induced avalanche pulse thus making detection of the incident photon difficult. The technique described in this appendix uses a pair of matched transient cancellation cables (TC cables) to separate the transients from the APD signal in the time domain. This method was conceived and developed by Dr. Bethune and co-workers at IBM [I-1].

Figure I.1 shows the transient cancellation circuit implemented in the gated mode. The cathode of the APD, K, is connected to the pulse bias source and a shorted coaxial cable using an SMA "T" connector at node N_1. A similar connector is also used to connect the anode of the APD, A, to a coaxial cable, which is open at the opposite end. This SMA "T" connector splits the output at the anode, one part of which is traced on the oscilloscope as V_{out}. The cathode of the APD is also connected to a dc source through a resistor R_L, which is used to dc bias the APD below breakdown.
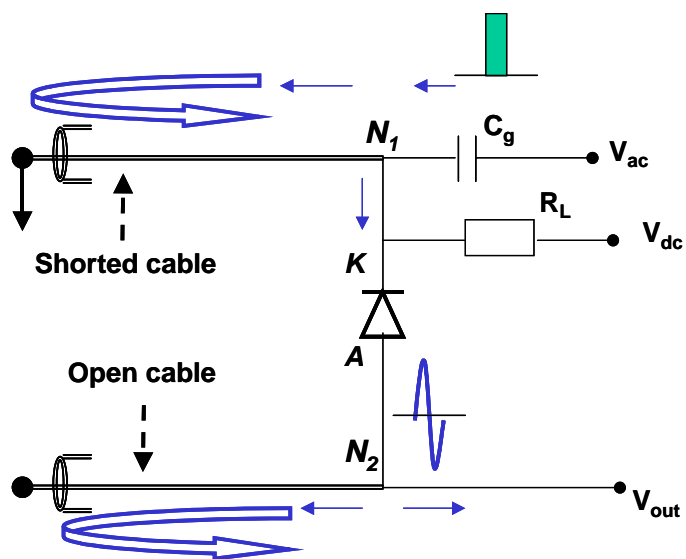
Figure I.1: Transient cancellation circuit implemented in the gated mode quenching set-up.
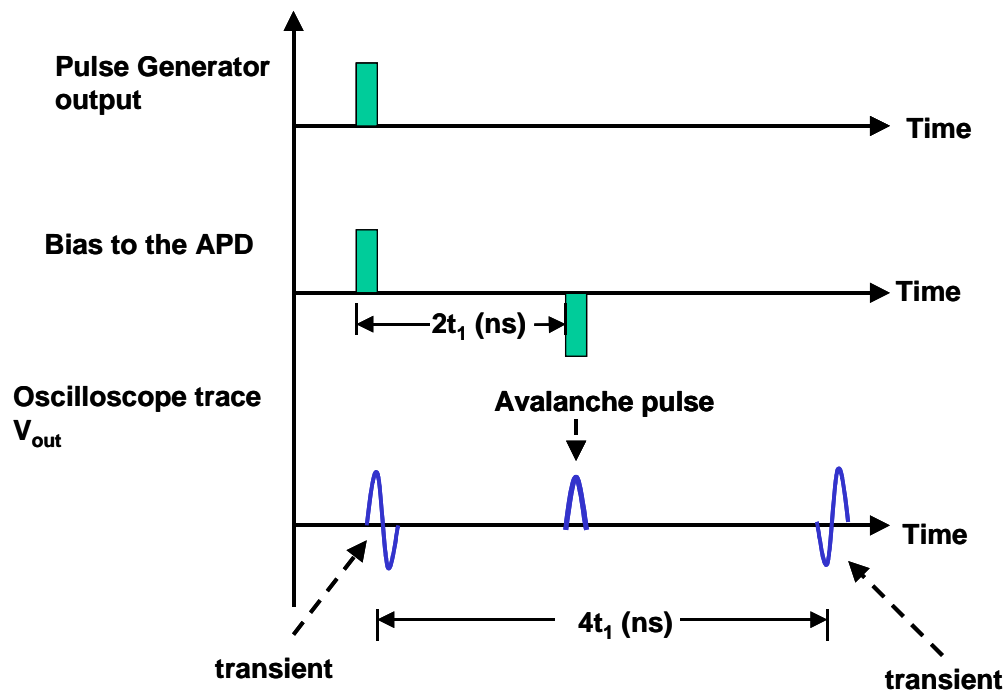
Figure I.2: Timing diagram for the transient cancellation circuit.

Let L_1 and t_1 be the length and delay of each of the TC cables. The pulse bias applied to the cathode of the APD splits at node N_1. One part passes through the APD and produces transient + the avalanche output at the anode. The other part travels down the shorted coaxial cable and gets reflected. The inverted reflection of the ac pulse returns at N_1 at time $2t_1$. The output produced by the 1st pulse is split at N_2. One part is coupled at the output and the second part travels through the open delay line and returns at N_2 non-inverted, after time $2t_1$. This non-inverted part of the output is cancelled by the transient produced by the inverted reflection of the bias pulse passing through the APD. Figure I.2 shows the timing diagram of the signal at V_{out}. The APD is biased twice, at t=0 and at t=$2t_1$. The output V_{out} in Figure I.2 shows the first and the last un-cancelled transient separated by $4t_1$, and the avalanche signal at $2t_1$ on a flat background. The detection gate of the electronic counter is placed at the center pulse to collect the avalanche signal on a noise-less background. Note that in this configuration, the APD is biased above breakdown voltage only during the first ac pulse passing through it. The incoming photon must be synchronized to arrive at the detector during the first pulse. This cancellation method works as long as the cables are matched and respond linearly.

A configuration of the TC cables where, the TC cable to the anode is shorted and the cable connected to the cathode is open; is also possible. In this case, however, the reflection at the N_1 is non-inverted and the APD is reverse biased twice above breakdown voltage. This can lead to an increased probability of after-pulsing related dark counts and hence is not preferred.

References:

[I-1]   W. P. Risk, and D. S. Bethune, "Quantum cryptography using autocompensating fiber-optic interferometers," *Optics and Photonics news*, vol. 13, no. 7, pp. 26 (2002).

Appendix II   Estimation of Number of Photons per Pulse

The single photon source used in the laboratory experiments was an attenuated pulsed or cw laser. It is a pseudo-single photon source and the number of photons in a pulse are distributed by Poisson statistics, as explained in Chapter 2. This appendix describes the estimation of average number of photons per pulse for a pulsed and a cw laser.

Consider a laser source at optical frequency ν, peak power P_{peak}, and a repetition rate of f_s. The average number of photons per second is given by,

$$\overline{N'} = \frac{P_{peak}}{h \cdot \nu}. \tag{II.1}$$

The number of photons in a pulse is given by

$$\overline{N} = \overline{N'} \cdot \tau_{laser}. \tag{II.2}$$

where, τ_{laser} is the pulse width of the laser.

Hence the number of photons per pulse is given by,

$$\overline{N} = \frac{P_{peak}}{h \cdot \nu} \cdot \tau_{laser}. \tag{II.3}$$

Experimentally, it is easier to measure average power from a laser instead of the peak power. The peak power and the average power are related by

$$P_{average} = P_{peak} \cdot f_s \cdot \tau_{laser}. \tag{II.4}$$

Hence the number of photons per pulse can be calculated from the average power using

$$\overline{N} = \frac{P_{average}}{h \cdot \nu} \cdot \frac{1}{f_s \cdot \tau_{laser}} \cdot \tau_{laser} = \frac{P_{average}}{h \cdot \nu \cdot f_s}. \tag{II.5}$$

In case of a cw laser, the number of photons per second ($\overline{N'}$) can be estimated by substituting P_{peak} with $P_{average}$ in equation (II.1). The average number of photons incident on the detector per bias pulse ($\overline{N}$) is given by,

$$\overline{N'} = \frac{P_{average}}{h \cdot v} .$$

(II.6)

$$\overline{N} = \overline{N'} \cdot \tau_{ac} .$$

(II.7)

where, τ_{ac} is the bias pulse width.

Sources Cited

H. Ando, H. Kanbe, M. Ito and T. Kaneda, "Tunneling current in InGaAs and optimum design for InGaAs/InP avalanche photodiode", *Jap. J. Appl. Phys.*, vol. 19, no. 6, pp. L277-L280 (1980).

S. Banerjee, B. Streetman, *Solid state electronic devices*, Prentice-Hall, Englewood Cliffs, NJ, 3rd edition 1990.

A.L. Beck, G. Karve, S. Wang, J. Ming, X. Guo, and J.C. Campbell, "Geiger Mode Operation of Ultraviolet 4H-SiC Avalanche Photodiodes," *IEEE Electron. Lett.*, accepted for publication.

A. L. Beck, B. Yang, X. Guo and J. C. Campbell, "Edge breakdown in 4H-SiC avalanche photodiodes", *J. Quantum. Electron.*, vol. 40, no. 3, pp. 321-324 (2004).

D. S. Bethune, and W. P. Risk, "An autocompensating fiber-optic quantum cryptography system based on polarization splitting of light," *IEEE J. Quantum Electron.*, vol. 36, no. 3, pp. 340-347 (2000).

D. S. Bethune, W. P. Risk and G. W. Pabst, "A high performance integrated single-photon detector for telecom wavelengths," *J. Modern Optics,* vol. 51, no. 9-10, pp. 1359-1368 (2004).

J. Boisvert, G. S. Kinsey, D. McAlister, T. Isshiki, R. Sudharsanan, and M. Krainak, "Large area InAlAs/InGaAs single photon counting avalanche photodiodes", *Proc. SPIE*, vol. 5412, pp.126-136 (2004).

M. Bourennane, A. Karlsson, J.P.Ciscar, and M. Mathes, "Single-photon counters in the telecom wavelength region of 1550 nm for quantum information processing", *J. Mod. Optics*, vol. 48**,** no**.** 13, pp. 1983-1995 (2001).

J. C. Campbell, S. Wang, X. G. Zheng, G. S. Kinsey, A. L. Holmes Jr., X. Sun, R. Sidhu and P. Yuan, "Ultra-low-noise avalanche photodiodes", *Proc. SPIE*, vol. 4283, pp. 480-488 (2001).

L. R. Confiled, J.Kerner and R. Korde, *SPIE*, vol. 1344, pp. 372 (1990).

S. Cova, M. Ghioni, A. Lacaita, C. Samori, and F. Zappa, "Avalanche photodiodes and quenching circuits for single-photon detection," *Appl. Optics*, vol. 35, no. 12, pp. 1956-1976 (1996).

S. Cova, A.Longoni and A. Andreoni, "Towards picosecond resolution with single-photon avalanche diodes", *Rev. of Sc. Instrum.*, vol. 52, pp. 408-412 (1981).

S. Cova, A. Lacaita and G. Ripamonti, "Trapping phenomena in avalanche photodiodes on nanosecond scale", *Electron. Device Lett.*, vol. 12, no. 12, pp. 685-687 (1991).

S. Cova, M. Ghioni and I. Rech, "Photon counting and timing detector modules for single-molecule spectroscopy and DNA analysis", *Proceedings of IEEE LEOS Annual Conference*, vol. 1, pp. 70-72 (2004).

Credence Systems Co.; 1421 California Circle Milpitas, CA 95035. (www.credence.com).

J. P. R. David, S. A. Plimmer, G. J. Rees and R. Grey, "Temperature dependence of avalanche breakdown in GaAs p-i-n diodes", *Third European Conference on High Temperature Electronics, Abingdon, UK*, pp. 187-90 (1999).

H. Dautet, P. Deschamps, B. Dion, A. D. MacGregor, D. MacSween, R. J. McIntyre, C. Trottier, and P. W. Webb, "Photon counting techniques with silicon avalanche photodiodes," *Appl. Optics*, vol. 32, no. 21, pp. 3894 (1993).

G. B. Dubrovskii, *Sov. Phys. Solid State*, vol. 13, pp. 2107 (1972).

L. Duraffourg, J. M. Merolla, J. P. Goedgebuer, N. Butterlin, and W. T. Rhodes, "Photon counting in the 1540-nm wavelength region with a germanium avalanche photodiode," *IEEE J. Quantum Electron.*, vol. 37, no. 1, pp. 75-79, (2001).

L. Esaki, "Discovery of the tunnel diode", *IEEE Trans. Electron. Devices*, vol. ED-23, pp. 644 (1976).

D. G. Esaev, M. M. Rinzan, S. G. Matsik, and A. G. U. Perera," Design and optimization of GaAs/AlGaAs heterojunction infrared detectors", *J. Applied Physics*, vol. 96, no. 8, 15, pp. 4588-97 (2004).

S. Fancey, "Single photon avalanche diodes for time resolved photoluminescence measurements in the near infra-red", Ph.D. dissertation (Heriot-Watt University, Edinburgh, UK, 1996).

S. R. Forrest, O. K. Kim and R. G. Smith, "Optical response time of $In_{0.47}Ga_{0.53}As$/InP avalanche photodiodes", *Appl. Phys. Lett.*, vol. 41, pp. 91-95 (1982).

S.R. Forrest, O. K. Kim and R. G. Smith, "Analysis of the dark current and photoresponse of InGaAs/InP avalanche photodiodes", *Solid Sate Electron.*, vol. 26, no. 10, pp. 951-968 (1983).

S. R. Forrest, R. G. Smith and O. K. Kim, "Performance of $In_{0.47}Ga_{0.53}As$/InP avalanche photodiodes", *J. Quantum Electron.*, vol. QE-18, no. 12, pp. 2040-2047 (1982).

K. K. Forsyth, and J. C. Dries, "Variations in the photon-counting performance of InGaAs/InP avalanche photodiodes"**,** *Proceedings of IEEE LEOS Annual Conference*, vol. 2, pp. 777 (2003).

X. Guo, A. L. Beck, X. Li, J. C. Campbell, D. Emerson and J. Sumakeris, "Study of dark current in 4H-SiC avalanche photodiodes", *J. Quantum Electron.*, vol. 41, no. 4, pp. 562-567 (2005).

R.H.Haitz, "Mechanisms contributing to the noise pulse rate of avalanche diodes", *J. Appl. Phys.*, vol. 36**,** no. 10, pp. 3123-3131 (1965).

D. Halliday and R. Resnick, *Physics: Part II*, Willey Eastern Limited, 1995.

Hamamtsu Co., 360 Foothill Rd, Bridgewater, NJ 08807. (www.hamamatsu.com).

M. M. Hayat, U. Sakoglu, O-H Kwon, S. Wang, J. C. Campbell, B. E. A. Saleh, and M. C. Teich, "Breakdown probabilities for thin heterostructure avalanche photodiodes," *IEEE J. Quantum Electron.*, vol. 39, no. 1, pp. 179-185 (2003).

R. M. Heinrichs, B. F. Aull, R. M. Marino, D. G. Fouche, A. K. McIntosh, J. J. Zayhowski, T. Stephens, M. E. O'Brian and M. A. Albota, "Three-dimensional laser radar with APD arrays", *Proc. SPIE*, vol. 4377, pp. 106-116 (2001).

P. A. Hiskett, G. S. Buller, A. Y. Loudon, J. M. Smith, I. Gontjo, A. C. Walker, P. D. Townsend, and M. J. Robertson, "Performance and design of InGaAs/InP photodiodes for single photon counting at 1.55 μm," *Appl. Optics*, vol. 39, no. 36, pp. 6818-6829 (2000).

K-S. Hyun and C-Y. Park, "Breakdown characteristics in INP/InGaAs avalanche photodiode with p-i-n multiplication layer structure", *J. Appl. Phys.*, vol. 81, no. 2, pp. 974-984 (1997).

R. Ispasoiu, private communication.

J.C. Jackson, D. Phelan, A. P. Morrison, R. M. Redfern and A. Mathewson, "Toward integrated single photon counting microarrays", *Opt. Engn*. Vol. 42, no. 1, pp. 112-118 (2003).

E. O. Kane, "Theory of tunneling", *J. Appl. Phys.*, vol. 32, no. 1, pp. 83 (1961).

Y. Kang, Y-H. Lo, M. Bitter, S. Kristjansson, Z. Pan and A. Puchard, "InGaAs-on-Si single photon avalanche photodetectors", *Appl. Phys. Lett.*, vol. 85, no. 10, pp.1668-1670, 2004.

Y. Kang, H. X. Lu, Y. H. Lo, and D. S. Bethune, "Dark count probability and quantum efficiency of avalanche photodiodes for single-photon detection", *Appl. Phys. Lett.*, vol. 83, no. 14, pp. 2955-2957 (2003).

O. K. Kim, B. V. Dutt, R. J. Mccoy and J. R. Zubur, "A low dark-current, planar InGaAs p-i-n photodiode with a quaternary InGaAsP cap layer", *J. Quantum Electron.*, vol. QE-21, no. 2, pp. 138-143 (1985).

Karve G., Zheng X., Zhang X., Li X., Li N., Wang S., Ma F., Holmes A. Jr., Campbell J.C., Kinsey G.S., Boisvert J.C., Isshiki T.D., Sudharsanan R., Bethune D.S., and Risk W.P., "Geiger mode operation of an $In_{0.53}Ga_{0.47}As$-$In_{0.52}Al_{0.48}As$ avalanche photodiode", *IEEE Journal of Quantum Electronics*, vol. 39, pp. 1281 (2003).

A. karlsson, M. Bourennane, G. Ribordy, H. Zbinden, J. Brendel, J. Rarity and P. Tapster, "A single-photon counter for long-haul telecom", *Circuits and devices*, vol. , pp. 34-40, 1999.

H. S. Kim, J. H. Choi, H. M. Bang, Y. Jee, S.W. Yun, J.Bur, M. D. Kim and A. G. Choo, "Dark current reduction in APD with BCB passivation", *Electron. Lett.,* vol. 37, no. 7, pp. 455-457 (2001).

W.J.Kindt, Geiger mode avalanche photodiode arrays for spatially resolved single photon counting, (Delft University press, Netherlands, Nov. 1999).

G.S. Kinsey, J. C. Campbell, and A. G. Dentai, "Waveguide avalanche photodiode operating at 1.55 µm with a gain-bandwidth product of 320 GHz," *IEEE Photon. Tech. Lett.*, vol. 13,no. 8, pp. 842-844 (2001).

G. Kirchner, F. Koidl, I. Prochazka and K. Hamal, "SPAD on GaAs for SLR", *Proc. 12th International Workshop on Laser Ranging, Matera, Italy* (2000). (Full text available at http://geodaf.mt.asi.it/html/news/iwlr/Kirchner_et_al_GaAs.pdf.)

R. Korde and J. Geist, *State Electron.,* vol. 30, no. 1, pp. 89 (1987).

O. H. Kwon, M. M. Hayat, J. C. Campbell, B. A. E. Saleh and M. C. Teich, "Optimized breakdown probabilities in AlGaAs-GaAs heterojunction avalanche photodiodes", *Electron Device Lett.*, vol. 25, no. 9, pp. 599-601 (2004).

A. Lacaita, M. Ghioni, and S. Cova, "Double epitaxy improves single-photon avalanche diode performance," *Electron. Lett.*, vol. 25, pp. 841-843, (1989).

A. Lacaita, F. Zappa, S. Cova, and P. Lovati, "Single-photon detection beyond 1 µm: performance of commercially available InGaAs/InP detectors," *Appl. Optics*, vol. 35, no. 16, pp. 2986-2996 (1996).

A. Lacaita, P. A. Francese, F. Zappa and S. Cova, "Single-photon detection beyond 1 μm: performance of commercially available germanium photodiodes," *Appl. Optics*, vol. 33, no. 30, pp. 6902-6918 (1994).

A. Lacaita, F. Zappa, S. Cova, and P. Lovati, "Single-photon detection beyond 1 μm: performance of commercially available InGaAs/lnP detectors", *Appl. Optics*, vol. 35, no. 16, pp. 2986-2996, (1996).

Sang Lee, H., Hwang, I.H., Spinhirne, J.D., and Scott, V.S**, "**Micro pulse lidar for aerosol and cloud measurement**",** *Advances in* Atmospheric *Remote Sensing with Lidar. Selected Papers of the 18th International Laser Radar Conference (ILRC). Berlin, Germany: Springer-Verlag*, pp. 7-10 (1996).

B.F. Levine, C. G. Bethea, and J. C. Campbell, "Near room temperature 1.3 μm single photon counting with a InGaAs avalanche photodiode," *Electron. Lett.*, vol. 20, no. 14, pp. 596-597, (1984).

B. F. Levine and C. C. Bethea, "10-MHz single photon counting at 1.3 μm", *Appl. Phys. Lett.*, vol. 44, pp. 581-583 (1984).

C. Lenox, H. Nie, P. Yuan, G. Kinsey, A. L. Holmes Jr., B. G. Streetman, and J. C. Campbell, "Resonant-cavity InGaAs-InAlAs avalanche photodiodes with gain-bandwidth product of 290 GHz," *IEEE Photon. Tech. Lett.*, vol. 11, no. 9, pp. 1162-1164 (1999).

Y. Liu, S. R. Forrest, J. Hladky, M. J. Lange, G. H. Olsen and D. E.Ackley, "A planar InP/InGaAs avalanche photodiode with floating guard ring and double diffused junction", *J. of lightwave tech.*, vol. 10, no. 2, pp. 182-193 (1992).

L-Q. Li and L. M. Davis, "Single photon avalanche diode foe single molecule detection", *Rev. Sci. Instrum.*, vol. 64, no. 6, pp. 1524-1529 (1993).

Ting Li, "Gallium Nitride and Aluminum Nitride based ultraviolet photodetectors" Ph.D. dissertation (University of Texas at Austin, Austin, TX, 2000).

Li N., Sidhu, R., Li X., Ma F., Zheng X., Wang S., Karve, G., Demiguel, S., Holmes A.L., and Campbell, J.C., "InGaAs/InAlAs avalanche photodiode with undepleted absorber", *Applied Physics Letters*, vol. 82, pp. 2175 (2003).

A. Y. Loudon, P. A. Hiskett, and G. S. Buller," Enhancement of the infrared detection efficiency of silicon photon-counting avalanche photodiodes by use of silicon germanium absorbing layers"**,** *Optics Letters*, vol.27, no.4, pp. 219-21 (2002).

124

C. L. F. Ma, M. J. Deen, L. E. Tarof and J. Yu, "Modelling breakdown voltage and its temperature dependence in SAGCM InP/InGaAs avalanche photodiode", *IEDM*, pp. 583-586 (1994).

F. Ma.; G. Karve, X. Zheng; X. Sun, A. L. Holmes, J. C. Campbell, "Low-temperature breakdown properties of $Al_xGa_{1-x}As$ avalanche photodiodes", *Appl. Phys. Lett.*, vol. 81, pp. 1908 (2002).

K. A. McIntosh, J. P. Donnelly, D. C. Oakley, and A. Napoleone, "Development of Geiger-mode APD arrays for 1.06 μm", *Proceedings of IEEE LEOS Annual Conference*, vol. 2, pp. 760-761 (2002).

K. A. McIntosh, J. P. Donnelly, D. C. Oakley, A. Napoleon, S. D. Calawa, L. J. Mahoney, K. M. Molvar, E. K. Duerr, S. H. Groves, and D. C. Shaver, "InGaAsP/InP avalanche photodiodes for photon counting at 1.06 μm," *Appl. Phys. Lett.*, vol. 81, no. 14, pp. 2505-2507, Sep. 2002.

R. J. McIntyre, "A new look at impact ionization-Part I: A theory of gain, noise, breakdown probability, and frequency response," *IEEE Trans. Electron. Devices*, vol. 46, no. 8, pp. 1623-1631 (1999).

R. J. McIntyre, "A new look at impact ionization-Part I: A theory of gain, noise, breakdown probability, and frequency response," *IEEE Trans. Electron. Devices*, vol. 46, no. 8, pp. 1623-1631, (1999).

P. G. Neudeck, "Electrical impact of SiC structural crystal defects on high field devices", *Material Science Forum*, vol. 338-342, pp. 1161-1166 (2000).

B. K. Ng, F. Yan, J. P. R. David, R. C. Tozer, G. J. Rees, C. Qin and J. H. Zhao, "Multiplication and excess noise characteristics of thin 4H-SiC UV avalanche photodiodes", *IEEE Photonics Tech. Lett.*, vol 14, no. 9, pp.1342-1344 (2002).

H. Nie, K. A. Anselm, C. Lenox, P. Yuan, C. Hu, G. Kinsey, B. G. Streetman, and J. C. Campbell, "Resonant-cavity separate absorption, charge and multiplication avalanche photodiodes with high-speed and high gain-bandwidth product, " *IEEE Photon. Tech. Lett*, vol. 10, no. 3, pp. 409-411 (1998).

K. Nishida, K. Taguchi and Y. Matsumoto, "InGaAsP heterostructure avalanche photodiode with high avalanche gain," *Appl. Phys. Lett.*, vol. 35, pp. 251-253 (1979).

Optoelectronic components; 28 Des Lilas, Kirkland, QC H9J 4A7.

Perkin Elmer Optoelectronics; 44370 Christy Street, Fremont, CA 94538-3180, USA (http://perkinelmer.com).

A. R. Powekk and L. B. Rowland, "SiC materials-progress, status and potential roadblocks", *Proc. IEEE*., vol.90, pp. 942-955 (2002).

I. Prochazka, K. Hamal and B. Soplo, "Achievements in single photon detector and their applications", .*J. Modern Optics*, vol. 51, no. 9-10, pp. 1289-1312 (2004).

J. G. Rarity, T. E. Wall, K. D. Ridley, P. C. M. Owens, and P. R. Tapster, "Single-photon counting for the 1300-1600-nm range by use of Peltier-cooled and passively quenched InGaAs avalanche photodiodes," *Appl. Optics*, vol. 39, no. 36, pp. 6746-6753 (2000).

W. P. Risk, and D. S. Bethune, "Quantum cryptography using autocompensating fiber-optic interferometers," *Optics and Photonics news*, vol. 13, no. 7, pp. 26 (2002).

A. Rochas, M. Gosch, A. Serov, and P. A. Besse, "First fully integrated 2-D array of single-photon detectors in standard CMOS technology", *IEEE Photonics Technology Letters*, vol.15, no.7, pp. 963-965 (2003).

A. Rochas, M. Gani, B. Furrer, P. A. Besse and R. S. Popovic, "Single photon detector fabricated in a complimentary metal-oxide-semiconductor high voltage technology", *Review of Sc. Intrum*., Vol. 74, no. 7, pp. 3263-3270 (2003).

A. M. Saad, "High quantum efficiency of uv-enhanced silicon photodiodes", *Can. J. Phys.,* vol. 80, pp. 1601-1608 (2002).

B A. E. Saleh and M. C. Teich, *Fundamentals of photonics*, Wiley Interscience publication, 1991.

M. A. Saleh, M. M. Hayat, P. P. Sotirelis, A. L. Holmes, J. C. Campbell, B. A. E. Saleh, and M. C. Teich, "Impact-ionization and noise characteristics of thin III-V avalanche photodiodes", *Trans. Electron. Devices*, vol. 48, no. 12, pp. 2722-2731 (2001).

Sensors unlimited Inc.; 3490 Route 1, Building 12, Princeton, NJ 08540 USA (www.sensorsinc.com).

Sidhu R., Chen, H., Yuan N., Karve G.V., A.L.Holmes, and J.C.Campbell; "GaAsSb resonant cavity avalanche photodiode operating at 1.06 μm", *Electronics Letters*, vol.40, no.20, pp. 1296 (2004).

Siegmund, O.H.W, "Advances in microchannel plate detectors for UV/visible astronomy", *Nuclear Instruments & Methods in Physics Research, Section A (Accelerators, Spectrometers, Detectors and Associated Equipment)*, vol. 525, no.1-2, pp. 12-16 (2004).

J. M. Smith, P. A. Hiskett, I. Gontijo, L. Purves and G. S. Buller, "A picosecond time-resolved photoluminescence microscope with detection at wavelength greater than 1500nm", *Review Sci. Intrum.*, vol. 72, no. 5, pp. 2325-2329 (2001).

D. Stucki, G. Ribordy, A. Stefanov, H. Zbinden, J. G. Rarity, and T. Wall, "Photon counting for quantum key distribution with Peltier cooled InGaAs/InP APDs," *J. Modern Optics*, vol. 48, no. 13, pp. 1967-1981 (2001).

X. Sun and F. M. Davidson, "Photon counting with silicon avalanche photodiodes", *J. Lightwave Tech.*, vol. 10, no. 8, pp. 1023-1032 (1992).

S. M. Sze, *Physics of semiconductors*, Wiley-interscience publication, 2nd edition.

Y. Takanashi and Y. Horikoshi, "Noise performance of 1.3 µm InGaAsP avalanche photodiode at -190 degrees C", *Japanese Journal of Applied Physics*, vol.19, no.3, pp. L163-6 (1980).

S. Verghese, K.A. McIntosh, R.J. Molnar, L.J. Mahoney, R.L. Aggarwal, M.W. Geis, K.M. Molvar, E.K. Duerr, and I. MeIngailis, "GaN Avalanche Photodiodes Operating in Linear-Gain Mode and Geiger Mode," *IEEE Trans. Electron Devices*, vol. 48 n.3, pp.502-511 (2001).

G. Vincent, A. Chantre and D. Bois, "Electric field effect on the thermal emission of traps in semiconductor junctions", *J. Appl. Phys.*, vol. 50, no. 8, pp. 5484-5487 (1979).

I. Vurgaftman, J. R. Meyer and L. R. Ram-Mohan, "Band parameters for III-V compound semiconductors and their alloys", *J. Appl. Phys.*, vol.89, no.11, pp. 5815-75 (2001).

E. Waks, K. Inoue, W. D. Oliver, E. Diamanti and Y. Yamamoto, "High-efficiency photon-number detection for quantum information processing", *IEEE J. of selected topics in Quan. Electron.*, vol. 9, no. 6, pp. 1502-1511 (2003).

S. Wang, "Low Noise Avalanche Photodiodes with An Impact-Ionization-Engineered Multiplication Region", Ph.D. dissertation, (University of Texas at Austin, Austin, TX, 2002).

Wang S., Ma F., Li X., Karve G., Zheng X., and Campbell, J.C., "Analysis of breakdown probabilities in avalanche photodiodes using a history-dependent analytical model", *Applied Physics Letters*, vol. 82, pp. 1971 (2003).

Westbond Inc.; 1551 Gene Autry Way, Anaheim, CA 92805 (www.westbond.com).

X. Xin, F. Yan, X. Sun, P. Alexandrove, C. M. Stahle, J. Hu, M. Matsumura, X. Li, M. Weiner and H. J. Zhao, "Demonstration of 4H-SiC UV single photon counting avalanche photodiode", *Electron. Lett.*, vol. 41, no. 4, pp. 67-68 (2005).

F.Yan, C.Qin, J.H.Zhao, M.Weiner, B.K.Ng, J.P.R.David, and R.C.Tozer, "Low-noise visible-blind UV avalanche photodiodes with edge terminated by 2° positive bevel," *Electon. Lett*., vol. 38, pp. 335-336 (2002).

M. Yee, W. K. Ng, J. P. R. David, P. A. Houston and C. N. Harrison, "Negative temperature dependence of electron multiplication in InGaAs", **",** *Appl. Phys. Lett.,* vol. 82,no. 8, pp.1224 (2003).

J. Yu, L. E. Tarof, T. Baird, D. McGhan, R. Bruce and D. G. Knight, "Temperature characterization of separate absorption, grading, charge and multiplication InP/InGaAs avalanche photodiode", *Proc. SPIE*, vol. 2149, pp. 302-310 (1994).

F. Zappa, S. Tisa, S. Cova, P. Maccagnani, D. Bonaccini, G. Bonanno, M. Belluso and R. Ronacella, "Pulsing technologies: Single-photon avalanche photodiode arrays", *SPIE*, vol. 5490 (2004).

F. Zappa, A. Lacaita, S. Cova and P. Webb, "Nanosecond single-photon timing with InGaAs/InP photodiodes", *Optics Lett*., vol. 19, no. 11, pp. 846-848 (1994).

X. Zheng, "Long-wavelength, high-speed avalanche photodiodes and APD arrays", Ph.D. dissertation (University of Texas at Austin, Austin, TX, 2004).

E. Zielinski, H. Schweizer, K. Streubel, H. Eisele and G. Weimann, *J. Appl. Phys.*, vol. 59, no. 6, pp. 2196-2204 (1986).

Vita

Gauri Vibhakar Karve was born in Kalyan, Maharashtra, India on June 17 1976, to her parents, Mrs. Manisha Karve and Mr. Vibhakar Karve. After graduating from Captain R. M. Oak high school in Kalyan, she entered R. K. Talreja college, affiliated to Mumbai University, where she received her B.S. in Physics in 1996. She completed an M.S. in Physics with specialization in spectroscopy from Indian Institute of Technology, Mumbai in 1998. She joined the graduate program in Physics at the University of Texas at Austin in 1998. In 1999, she transferred to the Microelectronics Research Center and received her M.S. in Electrical Engineering from University of Texas, Austin, in 2001. She started research on avalanche photodiodes for single photon counting applications under Dr. Campbell's supervision in 2001.

Permanent address: 2913 Bernardino Cove, Austin, TX 78728

This dissertation was typed by the author.